Solar RRL
www.solar-rrl.com

Check for updates

Efficient and Stable All-Inorganic Perovskite Solar Cells

Jiangzhao Chen and Wallace C. H. Choy**

The large-scale commercial application of organic–inorganic hybrid perovskite solar cells (PSCs) based on organic hole transport material (HTM) is still hindered by poor long-term operational stability, although a certified record power conversion efficiency (PCE) as high as 25.2% can be achieved. In the recent several years, all-inorganic PSCs have received tremendous attention due to their superb thermal and moisture stability and considerable progresses have been witnessed. Herein, the recent advancements of all-inorganic PSCs are reviewed comprehensively. First, the recent progresses of the strategies for stabilizing the black phase of inorganic perovskites through either increasing tolerance factor or enhancing the energy barrier of phase transition from black to yellow phase are summarized and discussed. Second, the deposition and growth techniques of inorganic perovskite films are discussed. Third, the effective inorganic HTMs in normal all-inorganic PSCs are described. Fourth, HTM-free normal all-inorganic PSCs are discussed. Afterward, the effective inorganic electron transport materials in inverted all-inorganic PSCs are discussed. Subsequently, the advancements of interface engineering for increasing the PCE and stability of all-inorganic PSCs are reviewed. Finally, a brief summary and outlook are presented to push up the PCE of all-inorganic PSCs to over 20% in the near future.

1. Introduction

Since the pioneering report on unstable liquid perovskite solar cells (PSCs) with a power conversion efficiency (PCE) of 3.8% based on the liquid-state electrolyte[1] and the first report on all-solid-state PSCs with a PCE as high as 9.7% based on solid hole transport material (HTM) Spiro-OMeTAD,[2] PSCs have attracted tremendous attention[3–12] and have achieved a certified record PCE of 25.2% up to now,[13] which has approached that of monocrystalline silicon solar cells and has been regarded as one of the promising next-generation photovoltaic technologies.

Prof. J. Chen
Key Laboratory of Optoelectronic Technology & Systems (Ministry of Education)
College of Optoelectronic Engineering
Chongqing University
Chongqing 400044, China
E-mail: jiangzhaochen@cqu.edu.cn

Prof. W. C. H. Choy
Department of Electrical and Electronic Engineering
University of Hong Kong
Pok Fu Lam Road, Hong Kong, SAR, China
E-mail: chchoy@eee.hku.hk

The ORCID identification number(s) for the author(s) of this article can be found under https://doi.org/10.1002/solr.202000408.

DOI: 10.1002/solr.202000408

The organic–inorganic hybrid perovskite absorbers usually possess a chemical formula of ABX_3, where A is a monovalent cation (e.g., methylammonium [MA^+], formamidinium [FA^+], Cs^+, Rb^+, etc.), B is a divalent metal cation (e.g., Pb^{2+} and Sn^{2+}), and X is a monovalent anion such as I^-, Br^-, Cl^-, SCN^-, and BF_4^-. Presently, all high-efficiency PSCs with PCEs exceeding 20% were fabricated based on organic–inorganic hybrid perovskite compositions. However, the organic–inorganic hybrid perovskites often suffer from poor thermal stability because of volatilization of organic cations (like MA^+ and FA^+) in perovskite compositions.[14,15] It was reported that CH_3NH_2 can be released from MA-based perovskite films at 80 °C,[16] which can't meet the fundamental stability requirements of international photovoltaics. To address the problem of the organic cation-induced instability, other monovalent inorganic cations have been attempted. The partial incorporation of Cs^+ at A-site has been demonstrated to be able to significantly improve light, moisture, and thermal stability of perovskite films.[17–20] Nevertheless, partial substitution of organic cations with Cs^+ still can't completely solve the poor long-term operational stability problem induced by volatilization of organic cations. Consequently, it is imperative to develop all-inorganic perovskite compositions for the fabrication of efficient and stable PSCs.

To date, various Cs-based all-inorganic perovskite compositions have been developed and applied into PSCs, such as $CsPbI_3$, $CsPbI_2Br$, $CsPbIBr_2$, $CsPbBr_3$, etc.[14,21] In the past few years, extensive attention has been focused on $CsPbI_3$ due to its appropriate bandgap ($E_g = 1.73$ eV). High temperature is usually necessary to sustain its cubic α-phase, which is easy to convert into a yellow orthorhombic (δ) nonperovskite phase with E_g of 2.82 eV at room temperature (RT) and in humid environment.[21] Meanwhile, several methods have been developed to stabilize the phase of $CsPbI_3$, mainly including additive engineering, quantum dots (QDs), dimension engineering, and composition engineering. Regarding additive engineering, it is worth noting that Wang et al. obtained a stable tetragonal β-$CsPbI_3$ phase with a E_g of 1.68 eV instead of α-phase and γ-phase through incorporating dimethylammonium iodide (DMAI) into the perovskite precursor solution. In combination with choline iodide surface treatment, the best-performing device achieved a high PCE of 18.4%.[12] Subsequently, the same group achieved a PCE of 19.03% using DMAI as an additive and phenyltrimethylammonium chloride (PTACl) as a surface

 © 2020 Wiley-VCH GmbH

passivator. To the best of our knowledge, this efficiency is the highest PCE reported for PSCs based on inorganic perovskites (**Figure 1**).[22] They revealed that DMAI additive was released from perovskite films instead of being incorporated into the perovskite crystal lattice. The earlier work indicates that synergistic engineering of additive and surface passivation molecules is crucial to prepare high-quality inorganic $CsPbI_3$ films and thus realize efficient and stable $CsPbI_3$-based all-inorganic PSCs. In addition, the reduction of grain size by preparing QDs has been demonstrated to be an effective approach to stabilize the black phase of $CsPbI_3$. For example, Luther and coworkers found that $CsPbI_3$ QD films can be stable for several months in ambient conditions, which shows that the phase transition temperature of QD films is much lower than that of bulk counterpart.[23] The same group developed an A-site cation halide salt (AX) treatment method to tune the surface chemistry of $CsPbI_3$ QD films and coupling between QDs. By this method, the carrier mobility of perovskite films increased twice. As a result, a record certified efficiency of 13.43% was achieved for the AX-treated device.[24] Although great progresses have been achieved in stabilizing the black phase of $CsPbI_3$ by additive engineering and reducing grain sizes, the realization of long-term phase-stable $CsPbI_3$ remains a huge challenge. It is well known that grain boundary (GB) density would increase as grain sizes reduce, which leads to serious nonradiative charge recombination losses. Except for the additive strategy and QD film, dimension engineering also shows great potentials in stabilizing α-phase of $CsPbI_3$. Zhao et al. demonstrated that a small amount of 2D $EDAPbI_4$ (ethylenediamine (EDA)) can effectively stabilize the α-phase of $CsPbI_3$.[25] The PSCs delivered a PCE of 11.8% upon the incorporation of $EDAPbI_4$. It was revealed that 2D $EDAPbI_4$ can significantly enhance the phase stability of α-$CsPbI_3$, improve electron transfer, and passivate surface defects. Finally, composition engineering is also an effective and important strategy used for stabilizing the black phase of $CsPbI_3$ film and improving its crystallization and morphology. To stabilize black phase and improve optoelectronic properties of $CsPbI_3$, A-site, B-site, and X-site in $CsPbI_3$ were substituted partially by other alkali metal ions (i.e., Li^+, Na^+, K^+, and Rb^+),[26,27] other divalent metal ions (e.g., Sn^{2+},[28] Ge^{2+},[29] Sr^{2+},[30] Ca^{2+},[31] etc.), and other halide anions (like I^- and Cl^-),[32] respectively. Among them, substitution of Br is very successful in stabilizing α-phase of $CsPbI_3$. Widely used inorganic perovskite absorbers ($CsPbI_2Br$, $CsPbIBr_2$, and $CsPbBr_3$), which are much more stable than $CsPbI_3$ at ambient conditions, can be obtained by introducing an appropriate amount of Br in $CsPbI_3$. You and coworkers introduced a small amount of Br into $CsPbI_3$ to fabricate $CsPbI_{3-x}Br_x$-based PSCs. Combining with the LiF surface modification of SnO_2, the champion device achieved a PCE of 18.64%.[33] Although these inorganic compositions ($CsPbI_2Br$, $CsPbIBr_2$, and $CsPbBr_3$) containing a large amount of Br are much more stable than $CsPbI_3$, the corresponding PSCs based on these Br-containing inorganic compositions showed much lower PCEs than $CsPbI_3$-based PSCs because of enlarged E_g.[34] Consequently, a good balance between phase stability and light-harvesting ability is key to achieve both high efficiency and excellent stability. Despite great advancements that have been obtained for inorganic PSCs, currently, its PCE is far behind that of hybrid PSCs. It is highly desirable to increase PCE and stability through stabilizing the black photoactive phase of inorganic perovskites and systematically optimizing the device.

It is well known that the long-term operational stability of PSCs is closely associated with each functional layer and interface. Presently, all high-efficiency inorganic PSCs were fabricated based on unstable organic HTMs (like Spiro-OMeTAD), which still suffer from poor long-term operational stability.[12,22,33] Therefore, developing all-inorganic PSCs is critical to completely address the poor long-term operational stability of inorganic PSCs based on organic HTMs. Here it should be stressed that each functional layer instead of only the perovskite layer in all-inorganic PSCs mentioned in this Review is inorganic material. All-inorganic PSCs generally can be classified into normal all-inorganic PSCs and inverted all-inorganic PSCs. As for the normal all-inorganic PSCs, the development of high-performance solution-processable inorganic HTMs is a huge challenge. To date, some inorganic HTMs have been attempted, such as CuI,[35] Cu_2ZnSnS_4 QDs,[36] $Cu(Cr,M)O_2$ (M = Ba^{2+}, Ca^{2+}, or Ni^{2+}) nanoparticles,[37] Co_3O_4,[38] MnS,[39] PbS

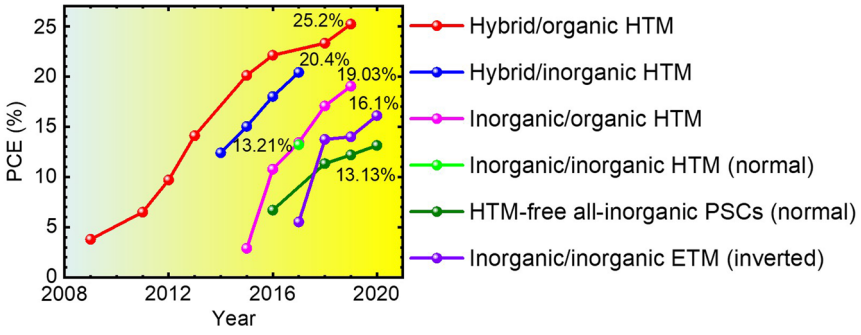


Figure 1. Representative efficiency advancements of various PSCs. Hybrid/organic HTM stands for the device with a structure of TCO/inorganic ETM/organic inorganic hybrid perovskites/organic HTM/Au or Ag. Hybrid/inorganic HTM stands for the device with a structure of TCO/inorganic ETM/organic inorganic hybrid perovskites/inorganic HTM/Au or Ag. Inorganic/organic HTM stands for the device with a structure of TCO/inorganic ETM/inorganic perovskites/organic HTM/Au or Ag. Inorganic/inorganic (normal) stands for the device with a structure of TCO/inorganic ETM/inorganic perovskites/inorganic HTM/Au, Ag or carbon. HTM-free all-inorganic PSCs (normal) stand for the device with a structure of TCO/inorganic ETM/inorganic perovskites/carbon. Inorganic/inorganic ETM (inverted) stands for the device with a structure of TCO/inorganic HTM/inorganic perovskites/inorganic ETM/metal electrode. TCO represents a transparent conductive metal oxide.

© 2020 Wiley-VCH GmbH

QDs,[40] CuPc,[41] etc. Hu et al. demonstrated a PCE of 13.21% based on the normal all-inorganic PSCs with the structure of FTO/c-TiO_2/$CsPb_{0.96}Bi_{0.04}I_3$/CuI/Au (Figure 1).[35] After that, no further improvement in PCE was obtained. To reduce cost and simplify the procedure of device fabrication, numerous efforts have been dedicated to develop hole-conductor-free all-inorganic PSCs especially for the carbon electrode (CE) and optimize its performance.[28,42] It is worth noting that Liang et al. achieved a PCE of 12.04% based on the device configuration of FTO/c-TiO_2/m-TiO_2/$CsPbI_3$:Br:InI_3/CE.[42] In addition, Liu et al. achieved a PCE of 12.19% based on the structure of FTO/SnO_2/$CsPbI_2Br$/CE where excess PbI_2 was incorporated into perovskite precursor solution.[43] Recently, Yang and coworkers demonstrated a promising PCE as high as 13.13% based on hole-conductor-free all-inorganic PSCs (Figure 1).[44] Consequently, hole-conductor-free all-inorganic PSCs exhibit great potentials in achieving a high PCE and high stability relative to all-inorganic PSCs with HTMs (Figure 1). Regarding inverted all-inorganic PSCs, the development of effective inorganic electron transport materials (ETMs) plays a key role in realizing high efficiency and long-term stability. To this end, the applications of various inorganic ETMs in inverted all-inorganic PSCs have been explored, such as MoO_x,[45] C_{60},[46] ZnO/C_{60} bilayer,[47–49] CeO_x,[50] carbide-TiO_2 (C-TiO_2),[51] etc. A PCE as high as 16.1% was reported for inverted all-inorganic PSCs with the structure of ITO/NiO_x/$CsPbI_xBr_{3-x}$/ZnO/C_{60}/Ag.[49] To the best of our knowledge, this efficiency is the reported highest efficiency in normal and inverted all-inorganic PSCs up to now (Figure 1). The earlier obtained achievements confirm the great potentials of all-inorganic PSCs in achieving a high PCE and excellent operational stability simultaneously. However, the PCEs of all-inorganic PSCs are still much lower than those of hybrid PSCs and those of inorganic PSCs with organic HTMs. Consequently, it is of great significance and urgent to further improve PCEs of all-inorganic PSCs.

In the recent two years, several reviews have been reported to summarize the research advancements of inorganic PSCs instead of all-inorganic PSCs. In view of the rapid development in the field of all-inorganic PSCs, a timely review is urgently needed. This Review aims at providing a guide for readers to further improve the PCE and stability of all-inorganic PSCs. In the present Review, we first summarize and discuss the progresses of strategies used for stabilizing the black phase of inorganic perovskites and improving their crystallization. Subsequently, we summarize and discuss effective inorganic HTMs in normal all-inorganic PSCs and HTM-free normal all-inorganic PSCs. After that, effective inorganic ETMs in inverted all-inorganic PSCs are summarized and discussed. Then, we summarize and discuss the advancements of interface engineering strategies for optimizing the PCEs of all-inorganic PSCs. Finally, an outlook of challenges and possible solutions for all-inorganic PSCs is proposed.

2. Strategies for Improving Phase Stability of Inorganic Perovskites

It is well known that inorganic perovskites usually possess several phases. Taking $CsPbI_3$ as an example, four phases were reported, including cubic (α), tetragonal (β), and two orthorhombic phases (a non-perovskite yellow phase [δ] and a black phase [γ]).[52] Among them, α, β, and γ phases are black phases and photoactive. In contrast, δ phase is yellow phase and nonphotoactive. Consequently, the stabilization of black phase is key to achieve efficient and stable all-inorganic PSCs. The phase and structural stability can be predicted and evaluated by Goldschmidt's tolerance factor value (t), which can be described as $t = (r_A + r_B)/[2^{1/2}(r_B + r_X)]$, where r_A, r_B, and r_X are radii of A, B, and X ions, respectively.[53,54] It is widely recognized that ABX_3 perovskites can be stabilized when t is located in the range of 0.8–1.[15,21,54] According to the ionic radii of alkali metal ions, as shown in **Table 1**, t of $APbI_3$ (A is alkali metal ion) is calculated to be 0.62 for Li^+, 0.67 for Na^+, 0.75 for K^+, 0.78 for Rb^+, and 0.81 for Cs^+, respectively.[20] Therefore, t of only Cs^+ is in the range of 0.8–1 among all alkali metal ions but still a little small, which is the origin of unstable black phases of $CsPbI_3$. Subsequently, we will summarize and discuss strategies used for stabilizing the black phase of inorganic perovskites from the perspective of B-site substitution, X-site substitution, intermediate with hydroiodic acid (HI), organic cations, additive engineering, and QDs, respectively. In a word, black phases of inorganic perovskites can be stabilized by either increasing the Goldschmidt tolerance factor value or enhancing the activation energy barrier of phase transition (black phase to yellow phase) (**Table 2**).

2.1. B-Site Substitution

As the ionic radius of Cs^+ is the largest among all alkali metal ions, it is a big challenge to further enhance t of inorganic perovskites through increasing the size of A-site cation. Consequently, it is expected to increase t and thus phase stability by substitutional doping for B- and X-sites with other metal and halide ions, respectively. It is well known that decreasing the radii of B-site cations can effectively increase the t of $CsPbI_3$ from 0.81 to 0.9–1.0. Considering that Sn and Pb belong to the same group in the periodic table of elements, Sn as a promising metal element was attempted by Liang et al.[28] to partially take place of Pb^{2+} in $CsPbIBr_2$ to obtain $CsPb_{0.9}Sn_{0.1}IBr_2$. The corresponding all-inorganic PSC based on CE showed much improvement in PCE from 8.25% for control device to 11.33%. The incorporation of Sn not only improved the phase stability of $CsPbIBr_2$ but also reduced bandgap from 2.05 to 1.79 eV, which resulted in improved stability and PCE. In addition, improved band alignment also should be responsible for enhanced PCE. In addition, Li et al.[56] used Sn to partially substitute Pb to prepare

Table 1. Radii of possible elements for A-, B-, and X-sites in ABX_3 inorganic perovskites.[20,34,55]

A-site [Å]		B-site [Å]				X-site [Å]	
Cs^+	1.69	Pb^{2+}	1.20	Mn^{2+}	0.66	I^-	2.16
Rb^+	1.48	Sr^{2+}	1.13	Bi^{3+}	1.08	Br^-	1.95
K^+	1.33	Ca^{2+}	0.99	Eu^{3+}	0.95	Cl^-	1.81
Na^+	0.95	Sn^{2+}	0.93	Sb^{3+}	0.92		
Li^+	0.76	Ge^{2+}	0.73	In^{3+}	0.81		

© 2020 Wiley-VCH GmbH

Table 2. Summary of progresses on strategies for stabilizing black phases in inorganic PSCs.

Strategies	Device configuration	J_{sc} [mA cm^{-2}]	V_{oc} [V]	FF	PCE [%]	Stability condition	Ref.
B-site substitution	FTO/c-TiO_2/m-TiO_2/$CsPb_{0.9}Sn_{0.1}IBr_2$/carbon	14.30	1.26	0.63	11.33	>2 weeks, at 100 °C, Encapsulated	[28]
	ITO/SnO_2/C_{60}/$CsPb_{0.75}Sn_{0.25}IBr_2$/Spiro-OMeTAD/Au	12.57	1.21	0.758	11.53	Under illumination, ≈50–60% RH RT, unencapsulated	[56]
	FTO/SnO_2/$CsPb_{0.8}Ge_{0.2}I_2Br$/P3HT/Spiro-OMeTAD/Au	12.15	1.27	0.701	10.8	7 h, 50–60% RH	[29]
	FTO/c-TiO_2/m-TiO_2/$CsPb_{0.9}Bi_{0.067}I_3$/Spiro-OMeTAD/Au	16.66	1.05	0.680	11.90	28 days under 40% RH	[57]
	FTO/c-TiO_2/$CsPb_{0.96}Bi_{0.04}I_3$/CuI/Au	18.76	0.97	0.726	13.21	Maintained 68%, 55% average RH at 25 °C	[35]
	FTO/c-TiO_2/m-TiO_2/$CsPb_{0.96}Sb_{0.04}I_3$/carbon	14.65	0.73	0.500	5.31	37 days, stored in ambient condition	[58]
	FTO/c-TiO_2/$CsPb_{0.9}Zn_{0.1}I_2Br$/Spiro-OMeTAD/Ag	15.8	1.18	0.727	13.6	65 °C, 400 h in N_2	[59]
	FTO/TiO_2/$CsPb_{0.98}Mn_{0.02}I_2Br$/PTAA/Au	14.37	1.172	0.80	13.47	25–35% RH and RT, unencapsulated	[60]
	FTO/c-TiO_2/m-TiO_2/$CsPb_{0.995}Mn_{0.005}I_{1.01}Br_{1.99}$/Spiro-OMeTAD/Au	13.15	0.99	0.57	7.36	Over 300 h, ambient atmosphere, encapsulated	[61]
	FTO/c-TiO_2/mp-TiO_2/$CsPb_{0.95}Ca_{0.05}I_3$/P3HT/Au	17.9	0.945	0.80	13.5	2 months, encapsulated	[31]
	FTO/c-TiO_2/mp-TiO_2/$CsPb_{0.98}Sr_{0.02}I_2Br$/P3HT/Au	15.3	1.04	0.699	11.2	30 days, encapsulated	[30]
	FTO/c-TiO_2/mp-TiO_2/$CsPb_{0.97}Sr_{0.03}Br_3$/carbon	7.71	1.54	0.811	9.63	800 h, 80% RH, RT, unencapsulated	[62]
	FTO/c-TiO_2/mp-TiO_2/BaI_2:$CsPbI_2Br$/P3HT/Au	15.45	1.210	0.795	14.85	Over 400 h, 85 °C, unencapsulated	[63]
	FTO/c-TiO_2/mp-TiO_2/$CsPb_{0.97}Sm_{0.03}Br_3$/carbon	7.48	1.594	0.851	10.14	110 days under 80% RH or 60 days at 80 °C, unencapsulated	[64]
	FTO/c-TiO_2/$CsPbI_2Br(Eu(Ac)_3)$/Spiro-OMeTAD/Au	15.44	1.25	0.79	15.25	30 days, 35–40% RH, unencapsulated	[65]
	FTO/c-TiO_2/m-TiO_2/$CsPb_{0.95}Eu_{0.05}I_2Br$/Spiro-OMeTAD/Au	14.63	1.22	0.766	13.7	370 h in N_2	[66]
X-site substitution	ITO/c-TiO_2/$CsPbI_2Br$-GTA-ATS-IPA/Spiro-OMeTAD/Au	16.79	1.23	0.778	16.07	100 mW cm^{-2} UV irradiation, N_2, unencapsulated	[67]
	ITO/SnO_2/PN4N/$CsPbI_2Br$/PDCBT/MoO_3/Ag	15.3	1.30	0.815	16.2	Continuous one sun equivalent illumination	[68]
	FTO/TiO_2/$SmBr_3$/$CsPbIBr_2$/PTAA/Au	12.75	1.17	0.73	10.88	–	[69]
	ITO/SnO_2QD/$CsPbBr_3$/$CsSnBr_3$/carbon	7.80	1.610	0.844	10.60	80 °C and N_2	[70]
	FTO/c-TiO_2/m-TiO_2/$CsPbBr_3$/$CuInS_2$/ZnS QDs/LPP-carbon	7.73	1.626	0.863	10.85	80% RH, or 80 °C, or solar irradiation	[71]
	FTO/TiO_2/$CsPbBr_3$/Spiro-OMeTAD/Ag	9.78	1.498	0.745	10.91	≈45% RH or 100 °C	[72]
	ITO/SnO_2/LiF/$CsPbI_{3-x}Br_x$+10%$PbCl_2$/Spiro-OMeTAD/Au	18.3	1.234	0.826	18.64	Over 1000 h under 100 mW cm^{-2} illumination, N_2, unencapsulated	[33]
Intermediate with hydroiodic acid	FTO/TiO_2/$CsPbI_3$-PTABr/Spiro-OMeTAD/Ag	19.15	1.104	0.806	17.06	Continuous illumination in N_2	[73]
	ITO/SnO_2/$CsPbI_{3-x}Br_x$+10%$PbCl_2$/Spiro-OMeTAD/Au	18.3	1.234	0.826	18.64	Over 1000 h under 100 mW cm^{-2} illumination, N_2, unencapsulated	[33]
Organic cations	ITO/PTAA/$CsPbI_{2.94}Cl_{0.06}$-NDSB201/PCBM/C_{60}/BCP/Cu	14.9	1.08	0.70	11.4	Ambient condition, unencapsulated	[32]
	FTO/TiO_2/$CsPbI_3$·0.025EDAPbI_4/Spiro-OMeTAD/Ag	14.53	1.15	0.71	11.86	Dark and dry box	[25]
	ITO/SnO_2/$PEA_2Cs_{59}Pb_{60}X_{181}$/Spiro-OMeTAD/Au	16.59	1.07	0.70	12.4	Ambient atmosphere without sealing	[74]
	ITO/SnO_2/LiF/$CsPbI_xBr_{3-x}$-GA_2PbI_4/Spiro-OMeTAD/Au	18.01	1.27	0.79	18.06	40% RH	[75]
	FTO/TiO_2/$CsPbI_3$-PEAI/PTAA/Au	18.95	1.059	0.749	15.07	20–30% RH	[76]
	FTO/TiO_2/$CsPbI_3$-PTABr/Spiro-OMeTAD/Ag	19.15	1.104	0.806	17.06	Continuous illumination in N_2	[73]
	FTO/c-TiO_2/m-TiO_2/$DMA_{0.15}Cs_{0.85}PbI_3$/Spiro-OMeTAD/Ag	19.4	1.05	0.75	15.3	–	[77]
	FTO/TiO_2/DMAI-$CsPbI_3$-CHI/Spiro-OMeTAD/Ag	20.23	1.11	0.82	18.4	Continuous illumination under 100 mW cm^{-2}	[12]
	FTO/TiO_2/DMAI-$CsPbI_3$-PTACl/Spiro-OMeTAD/Ag	20.23	1.137	0.827	19.03	10 ± 5% RH and 20–25 °C	[22]
Additive engineering	FTO/TiO_2/$CsPbI_{3-x}Br_x$+CsBr/Spiro-OMeTAD/Au	15.52	1.10	0.765	13.09	–	[78]
	FTO/TiO_2/$CsPbI_2Br$+Pb(II)propionate/poly(DTSTPD-r-BThTPD)/Au	15.66	1.15	0.81	14.58	–	[79]
	FTO/PTAA/$CsPbI_3$+OTG3/PCBM/BCP/Ag	15.81	1.121	0.752	13.32	Less than 10% RH	[80]

© 2020 Wiley-VCH GmbH

Table 2. Continued.

Strategies	Device configuration	J_{sc} [mA cm^{-2}]	V_{oc} [V]	FF	PCE [%]	Stability condition	Ref.
QDs	FTO/TiO_2/$CsPbI_3$ QD/Spiro-OMeTAD/MoO_3/Al	13.47	1.23	0.65	10.77	Months in ambient air	[23]
	FTO/TiO_2/AX-coated $CsPbI_3$ QD/Spiro-OMeTAD/MoO_3/Al	14.37	1.20	0.78	13.4	–	[24]
	FTO/TiO_2/$CsPbI_3$ QD/PTB7/MoO_3/Ag	12.39	1.27	0.80	12.55	–	[81]
	FTO/TiO_2/$CsPbI_3$ QD-cesium salts/PTAA/MoO_3/Ag	14.96	1.248	0.756	14.10	–	[82]
	FTO/TiO_2/$CsPbI_3$ QD /PTAA/MoO_3/Ag	15.84	1.243	0.76	14.90	–	[83]

$CsPb_{1-x}Sn_xIBr_2$ perovskite alloys by the one-step antisolvent (ATS) method. As shown by steady-state photoluminescence (PL) spectra in Figure 1a, the PL emission peak gradually red-shifted as the increase in the substitution amount of Sn occurred. After systematic optimization of Sn content, the optimal device performance was achieved when x in $CsPb_{1-x}Sn_xIBr_2$ was equal to 0.25, as shown in Figure 1b. The optimized device based on $CsPb_{0.75}Sn_{0.25}IBr_2$ exhibited a PCE of 11.53%, which was much higher than 7.34% of device without doping. In addition, significantly reduced hysteresis was demonstrated upon Sn doping. The moisture stability under illumination at about 50–60% relative humidity (RH) showed that the unencapsulated $CsPb_{0.75}Sn_{0.25}IBr_2$-based device degraded less than 10% after 120 min illumination whereas $CsPbIBr_2$-based device decayed completely just after 40 min (Figure 1c). Improved stability was ascribed to improved phase stability due to enhanced t induced by incorporation of smaller Sn. The earlier works indicate that Sn is an ideal candidate to replace Pb in inorganic perovskites because the introduction of Sn can improve film quality, narrow bandgap, and conquer phase instability. However, instability originating from the oxidation of Sn^{2+} to Sn^{4+} by oxygen should be investigated carefully in inorganic perovskite alloys in the future research work. In the hybrid PSCs, various strategies have been made to conquer the above instability through suppressing the oxidation reaction of Sn^{2+} to Sn^{4+}.[84] It is highly desirable to overcome the instability of Sn-containing inorganic perovskites by either learning from hybrid PSCs or developing novel and effective strategies. Similar with Sn, Yang et al.[29] reported doping of germanium (Ge) for inorganic perovskite $CsPbI_2Br$ and demonstrated that Ge (0.73 Å) with a much smaller radius than Pb^{2+} (1.20 Å) can stabilize the cubic phase, which was confirmed by the disappeared diffraction peak at 10.0° corresponding to an orthorhombic phase (**Figure 2**d). After optimization, $CsPb_{0.8}Ge_{0.2}I_2Br$-based PSCs produced the highest PCE of 10.8% among all the investigated doping ratios, which is much higher than 5.3% of

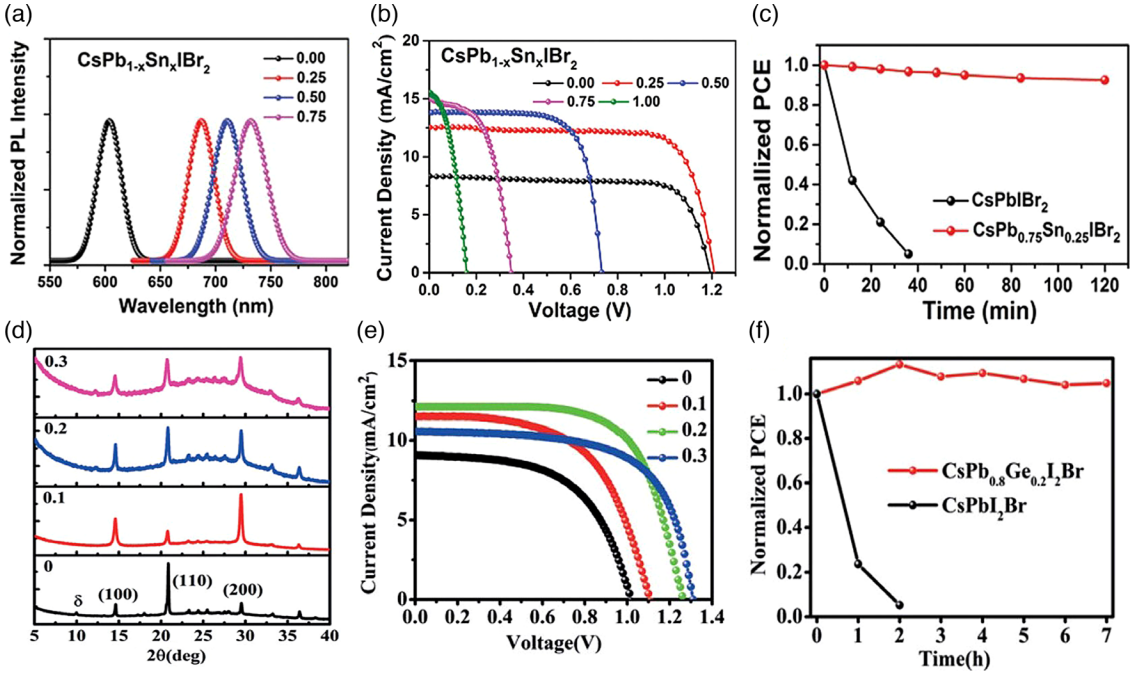


Figure 2. a) Steady-state PL spectra of $CsPb_{1-x}Sn_xIBr_2$ films. b) J–V curves of champion devices based on $CsPb_{1-x}Sn_xIBr_2$ films. c) Stability of unencapsulated devices based on $CsPbIBr_2$ and $CsPb_{0.75}Sn_{0.25}IBr_2$ under illumination measured in the ambient condition with a RH of around 50–60%. Reproduced with permission.[56] Copyright 2018, Wiley-VCH. d) XRD spectra of $CsPb_{1-x}Ge_xI_2Br$ perovskite films. e) J–V curves of champion devices based on $CsPb_{1-x}Ge_xI_2Br$. f) Stability of unencapsulated devices based on $CsPbI_2Br$ and $CsPb_{0.8}Ge_{0.2}I_2Br$ at 50–60% RH ambient atmosphere. Reproduced with permission.[29] Copyright 2018, Wiley-VCH.

© 2020 Wiley-VCH GmbH

the device based on pristine $CsPbI_2Br$, as shown in Figure 2e. As a result of improved phase stability of perovskite films, a remarkably enhanced stability was observed for $CsPb_{0.8}Ge_{0.2}I_2Br$-based PSCs as compared with a control device under 50–60% RH ambient atmosphere without encapsulation. This work suggests that the ambient fabrication of inorganic perovskites can be realized by improving phase stability via adopting chemical doping. Considering that bismuth (Bi) is close to Pb in the same period, Bi^{3+} could be an effective candidate to replace Pb^{2+} in inorganic perovskites. Hu et al.[35] for the first time demonstrated that partial substitution of Pb^{2+} by Bi^{3+} (1.08 Å) can stabilize the α-phase of $CsPbI_3$ at RT. X-ray diffraction (XRD) results showed that the black phase of $CsPbI_3$ can be stabilized when a suitable amount of Bi^{3+} is incorporated into $CsPbI_3$. The δ-phase thoroughly disappeared upon the incorporation of 4 mol% Bi^{3+}. As shown in **Figure 3**a, they proposed a possible mechanism of improved phase stability of α-$CsPbI_3$. The doping of the proper amount of Bi^{3+} (4 mol%) can lead to strong microstrain in the crystal of $CsPbI_3$ and accordingly slight distortion of the cubic structure as well as improved phase stability. After 4 mol% Bi^{3+} doping, the PCE of the device based on CuI as HTM was increased from 8.07% to 13.21% (Figure 3b). The $CsPb_{0.96}Bi_{0.04}I_3$-based device exhibited a much improved ambient stability compared with the control device based on pristine $CsPbI_3$ (Figure **3**c). In addition, Huang et al.[57] revealed that Bi^{3+} doping not only can stabilize the black phase of $CsPbI_3$ but also improve its film quality by reducing trap states. The PCE was improved from 10.09% for the control device to 11.90% for the doped device, which was mainly as a consequence of significantly increased V_{oc}. The synergistic strategy of nonstoichiometry and antimony Sb doping for $CsPbI_3$ was developed by Xiang et al.[58] to improve the phase stability and film morphology. The $CsPb_{0.96}Sb_{0.04}I_3$-based device achieved a PCE of 5.18% based on CE and maintained 93% of its initial PCE after 37 days of storage in ambient condition. Sun et al.[59] introduced Zn^{2+} to partially substitute Pb^{2+} in $CsPbI_2Br$ inorganic perovskites and achieved a PCE improvement from 11.8% for the $CsPbI_2Br$-based device to 13.6% for $CsPb_{0.9}Zn_{0.1}I_2Br$-based device, which was put down to improved crystallization and markedly enlarged grain sizes along with the highly orientated crystallites. The stronger interaction of Zn^{2+} with Br^- and I^- anions due to its higher chemical activity than Pb^{2+} resulted in the suppressed crystallization process of inorganic perovskites. In addition, this work proposed that Cs–Zn–Br/I compound could effectively passivate GBs. A slightly widened absorption spectrum was because of

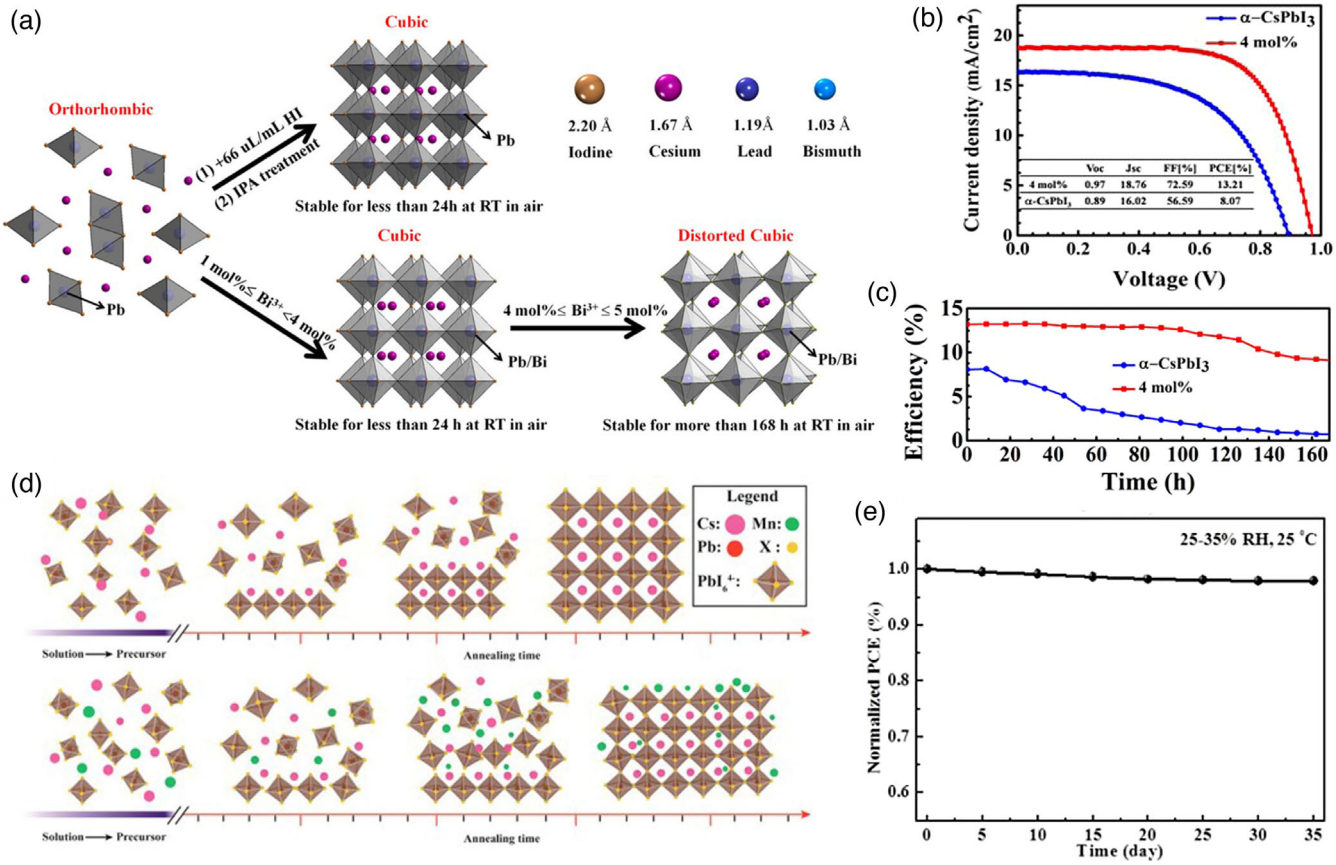


Figure 3. a) Possible mechanisms for stabilizing α-$CsPbI_3$ by introducing HI or Bi^{3+} in the precursor solution. b) *J–V* curves of the best-performing devices based on α-$CsPbI_3$ and $CsPb_{0.96}Bi_{0.04}I_3$. c) PCE evolution as a function of explosion time in air condition for devices based on α-$CsPbI_3$ and $CsPb_{0.96}Bi_{0.04}I_3$. Reproduced with permission.[35] Copyright 2017, American Chemical Society. d) Schematic diagram of roles of $MnCl_2$ in driving crystalline grain growth and passivating surface defects. e) Stability of unencapsulated device based on 2% of $MnCl_2$ stored at 25 °C and 25−35% RH. Reproduced with permission.[60] Copyright 2018, American Chemical Society.

© 2020 Wiley-VCH GmbH

Zn4s-I5p states. After Zn^{2+} doping, improved ambient and thermal stability was testified.

The transition metal manganese (Mn) was attempted to partially substitute Pb in inorganic perovskites.[60,61] The former (0.66 Å) possesses a much smaller radius than the latter (1.20 Å), as shown in Table 1. Liang et al. found that Mn^{2+} can be successfully inserted into the crystal lattice of $CsPbIBr_2$ to form novel Mn-doped $CsPb_{1-x}Mn_xI_{1+2x}Br_{2-2x}$.[61] Improved crystallinity and morphology as well as improved energy-level alignment was achieved upon $x = 0.005$. A promising PCE of 7.36% was obtained for the $CsPb_{0.995}Mn_{0.005}I_{1.01}Br_{1.99}$-based device using CE, which was higher than 6.14% of the reference device. Finally, the encapsulated $CsPb_{0.995}Mn_{0.005}I_{1.01}Br_{1.99}$-based device dropped only 8% of its initial value after ambient exposure for over 300 h. This work highlights the importance of the development of all-inorganic PSCs in achieving long-term stability. Different from the above work, Bai et al. demonstrated that Mn^{2+} lay in the interstices of $CsPbI_2Br$ instead of crystal lattices of Pb through introducing additional $MnCl_2$ into precursor solutions containing equivalent molar amounts of PbI_2 and CsBr.[60] The excellent solid solution between $CsPbI_2Br$ and $MnCl_2$ was formed and the structure of perovskite host was retained, as confirmed by XRD results. Scanning electron microscopy (SEM) results indicated that grain sizes of perovskite films were gradually enlarged with the gradual increase of Mn^{2+}, which was attributed to suppressed crystallization. As shown in Figure 3d, possible mechanisms of $CsPbI_2Br$ formation with and without Mn were proposed. A small amount of Mn^{2+} was incorporated into interstices of $CsPbI_2Br$ lattices and excess Mn^{2+} was aggregated at GBs of perovskite films which can passivate trap states at GBs, leading to the decreased nonradiative recombination losses. By the doping of Mn^{2+}, the PCE increased from 11.88% for the reference device to 13.47% for the device with Mn^{2+}. The device doped by Mn^{2+} slightly degraded to 97% of its initial value at 25 °C under 25−35% RH (Figure **3**e). Except for Mn^{2+}, transition metal Ni^{2+} was utilized to partially substitute Pb^{2+} in $CsPbI_2Br$, and the inverted PSC with a structure of ITO/P3CT/$CsPbI_2Br$ with or without Ni^{2+} doping/PCBM/C_{60}/BCP/Ag was assembled.[85] The best-performing device with $CsPb_{0.98}Ni_{0.02}I_2Br$ yielded a PCE of 13.88%, higher than 11.97% of the reference device, which was attributed to improved crystallinity and reduced trap states and thus suppressed nonradiative recombination reaction. More importantly, ambient and light stabilities were improved for Ni-doped devices as compared with control devices. The earlier research results show that transition metal doping is very promising in stabilizing the black phase and improving film quality, which should receive more attention in future research work.

In the past few years, alkaline earth metals have been developed to stabilize the black phase of inorganic perovskites and improve their optoelectronic properties.[30,31,62,63] Calcium (Ca, 0.99 Å) with a smaller ionic radius was used to partially replace Pb in $CsPbI_3$.[31] The more uniform films with larger grains were obtained due to reduced colloidal sizes in the precursor solution after Ca^{2+} doping, which resulted in improved interface contact between perovskite and hole transport layer (HTL). It was demonstrated that surface defects can be passivated by a Ca-rich oxide layer. The optimized device based on 5% Ca^{2+} substitution delivered a promising PCE of 13.5% in reverse scan (RS). The encapsulated device maintained 85% of its initial PCE after two months. To find out the optimal alkaline earth metal used for doping inorganic perovskites, the effect of alkaline earth metals (including Mg^{2+}, Ca^{2+}, Sr^{2+}, and Ba^{2+}) on $CsPbBr_3$-based all-inorganic PSCs was systematically investigated.[62] It was found that all investigated doping metals can increase the PCE of devices but Sr^{2+} was the most effective. They concluded that the incorporation of divalent hard Lewis acids was beneficial for grain size enlargement along with reduced GB density and thus PCE improvement. In addition, the enhanced formation energy of vacancy defects led to suppressed carrier recombination. Although the effect of different alkaline earth metals on device performance was compared in this work, why the Sr^{2+}-doped device exhibited the highest PCE among all the investigated doping metals is not revealed. Apart from $CsPbBr_3$, Sr^{2+} was also reported to dope the $CsPbI_2Br$ to form $CsPb_{1-x}Sr_xI_2Br$ and the doped device based on the optimal concentration ($x = 0.02$) gave a 11.2% PCE which was much higher than 7.7% of the reference device with pristine $CsPbI_2Br$.[30] It was revealed that Sr^{2+} at the surface of perovskite films can effectively passivate the defects at GBs and/or surface of perovskite films. To further increase the PCE of inorganic PSCs with Sr^{2+} doping, it should be stressed that doping of Sr^{2+} for $CsPbI_3$ is worth attempting due to its more favorable bandgap as compared with $CsPbI_2Br$. Mali et al.[63] developed an effective synergistic strategy that the partial substitution of Pb^{2+} with Ba^{2+} was implemented in typical $CsPbI_2Br$ and the dynamic hot-air (DHA) casting process was used to prepare high-quality inorganic perovskite films in ambient condition. Through this synergistic strategy, the device based on BaI_2:$CsPbI_2Br$ presented a high PCE of 14.85% for a small active area of 0.09 cm^2 and 13.78% for a large area of 1 cm^2, respectively. The DHA casting method provides an opportunity for upscaling all-inorganic perovskite photovoltaics at a wide processing window. Much improved thermal stability was demonstrated for DHA-processed BaI_2:$CsPbI_2Br$-based devices compared with control device without BaI_2 doping.

To maximize the potentials of B-site metal doping, lanthanide metal elements were used to partially substitute Pb in inorganic perovskites.[64,65] Duan et al. investigated the effect of different lanthanide ion doping ($Ln^{3+} = La^{3+}$, Ce^{3+}, Nd^{3+}, Sm^{3+}, Eu^{3+}, Gd^{3+}, Tb^{3+}, Ho^{3+}, Er^{3+}, Yb^{3+}, and Lu^{3+}) on $CsPbBr_3$-based all-inorganic PSCs.[64] They found that some Ln^{3+} ions (e.g., Ce^{3+}, Nd^{3+}, Eu^{3+}, etc.) showed a negative effect on perovskite film quality and thus photovoltaic performance but a positive effect for some other ions (i.e., Sm^{3+}, Tb^{3+}, Ho^{3+}, Er^{3+}, and Yb^{3+}). The lattice constants gradually decreased by obeying an order of Sm^{3+}–$CsPbBr_3 > Tb^{3+}$–$CsPbBr_3 > Ho^{3+}$–$CsPbBr_3 > Er^{3+}$–$CsPbBr_3 > Yb^{3+}$–$CsPbBr_3$, which confirmed the successful incorporation of Ln^{3+} ions into crystal lattices of $CsPbBr_3$ (**Figure 4**a). It was inferred that the improved grain size and crystallinity occurred due to the change in surface energy for crystal growth. Improved crystallization and grain size facilitated charge transfer dynamics and suppressed the carrier nonradiative recombination process. The PCEs of devices were improved after Sm^{3+}, Tb^{3+}, Ho^{3+}, Er^{3+}, or Yb^{3+} doping and the Sm^{3+}-doped device exhibited a much higher PCE of 10.14% than 6.99% for the control device, as shown in Figure 4b. The slightly enhanced thermal stability was observed for the device

© 2020 Wiley-VCH GmbH

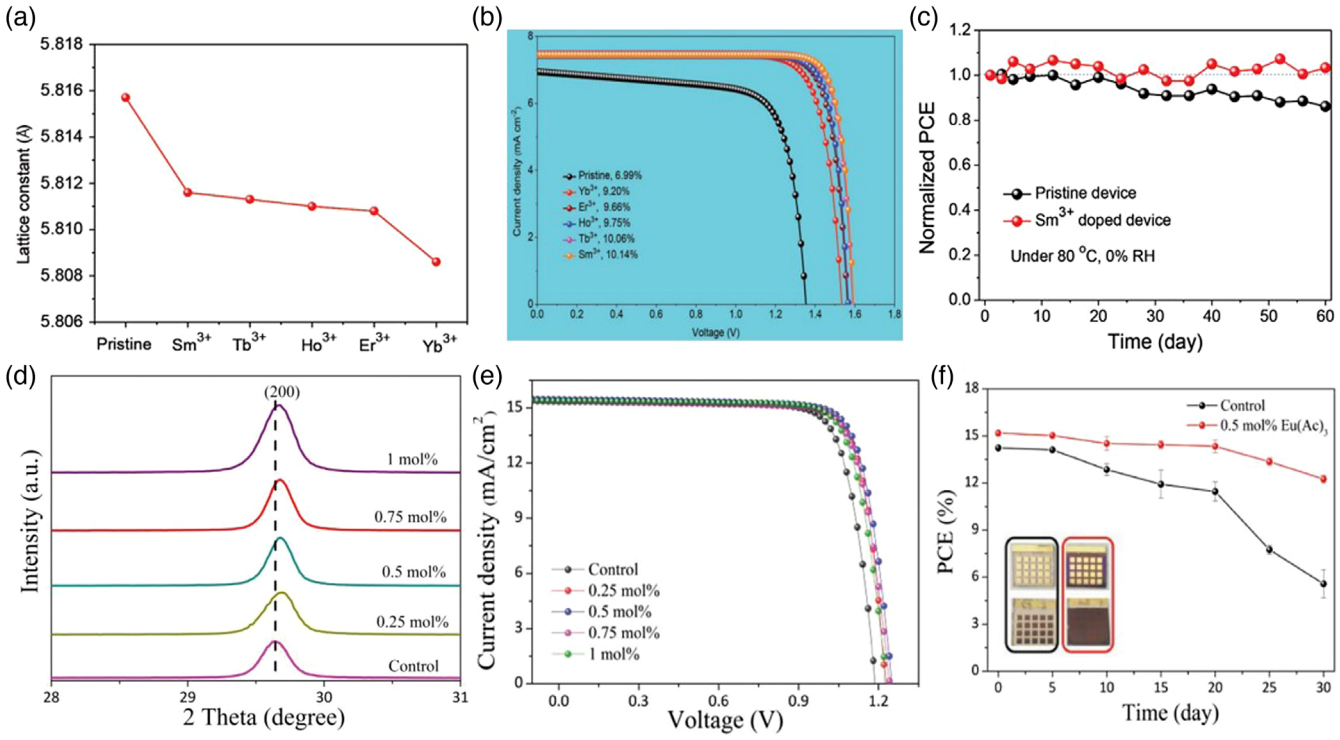


Figure 4. a) The lattice constants of $CsPbBr_3$ crystals doped by different Ln^{3+} ions. b) *J–V* curves of devices based on perovskite absorbers without doping and with doping by different lanthanide ions. c) Long-term stability of unencapsulated devices without and with Sm^{3+} doping at 80 °C and 0% RH. Reproduced with permission.[64] Copyright 2018, Wiley-VCH. d) XRD patterns of $CsPbI_2Br$ perovskite films doped by different concentrations of $Eu(Ac)_3$. e) *J–V* curves of devices based on $CsPbI_2Br$ perovskite films doped with different concentrations of $Eu(Ac)_3$. f) Ambient stability of unencapsulated PSCs without and with 0.5 mol% $Eu(Ac)_3$ doping. Reproduced with permission.[65] Copyright 2019, Wiley-VCH.

with Sm^{3+} doping relative to reference device (Figure 4c). Yang et al.[65] developed a europium and acetate codoping strategy for $CsPbI_2Br$ and found that shift of peaks at 29.5° corresponding to (200) crystal plane of α-phase $CsPbI_2Br$ perovskite was indicative of successful insertion of Eu^{3+} (0.95 Å) and Ac^- (1.62 Å) into crystal lattices of $CsPbI_2Br$, as shown by XRD results in Figure 4d. As shown in Figure 4e, the optimal doping concentration of $Eu(Ac)_3$ was determined to be 0.5 mol% and the optimized device delivered a promising PCE of 15.25%, which was higher than 14.26% of the reference device without doping. Moreover, much improved ambient stability was revealed for the doped device in comparison with the control device (Figure 4f). Improved film quality and phase stability should be responsible for improved PCE and stability. The research works indicate that lanthanide ion doping shows great potentials in stabilizing the black phase of inorganic perovskites and improving film quality, which remain to be explored especially for narrow-bandgap $CsPbI_3$ for the purpose of a higher PCE.

2.2. X-Site Substitution

Apart from B-site doping, X-site doping is an effective approach to stabilize the black phase of $CsPbI_3$ because of increased *t*. Regarding X-site doping, partial or complete substitution of I^- by Br^- was extensively investigated in the past several years. A PCE of 6.5% was reported by 33% replacement of I^- with Br^- in $CsPbI_3$. Improved light, thermal, and phase stabilities were achieved after Br doping.[86] Snaith and coworkers[87] achieved a PCE of 9.8% based on $CsPbI_2Br$ through tuning the substitution ratio of Br in $CsPbI_3$ based on the two-step method. They found that the $CsPbI_2Br$-based device showed excellent structural stability at 85 °C under high 30–40% RH, which was much better than the pure iodide inorganic perovskite-based device. Since then, huge attention has been devoted to investigate $CsPbI_2Br$-based PSCs.[47,67,79,88–91] It is well known that high-quality perovskite films are prerequisites to achieve efficient and stable inorganic PSCs. Chen et al.[67] precisely controlled the crystal growth by developing a synergistic strategy of gradient thermal annealing (GTA) and ATS and demonstrated a PCE as high as 16.07%, accompanied with a stabilized efficiency of 15.75%.

Moisture stability and UV light stabilities were both improved by obeying an order of GTA-based device < GTA–ATS–Tol-based device (Tol: toluene) < GTA–ATS–IPA-based device. The improved stability was ascribed to a much improved film quality. Tian et al.[68] developed an amino-functionalized polymer (PN4N) to modify $SnO_2/CsPbI_2Br$ interface, which resulted in an improved band alignment. It was revealed that the PN4N interface layer can promote the crystal growth of perovskites by tuning the surface wetting property, as reflected by increased grain sizes from SEM results (**Figure 5**a,b) and improved crystallization from XRD results (Figure 5c). Most importantly, it was proved that PN4N and PDCBT can interact strongly with perovskite

© 2020 Wiley-VCH GmbH

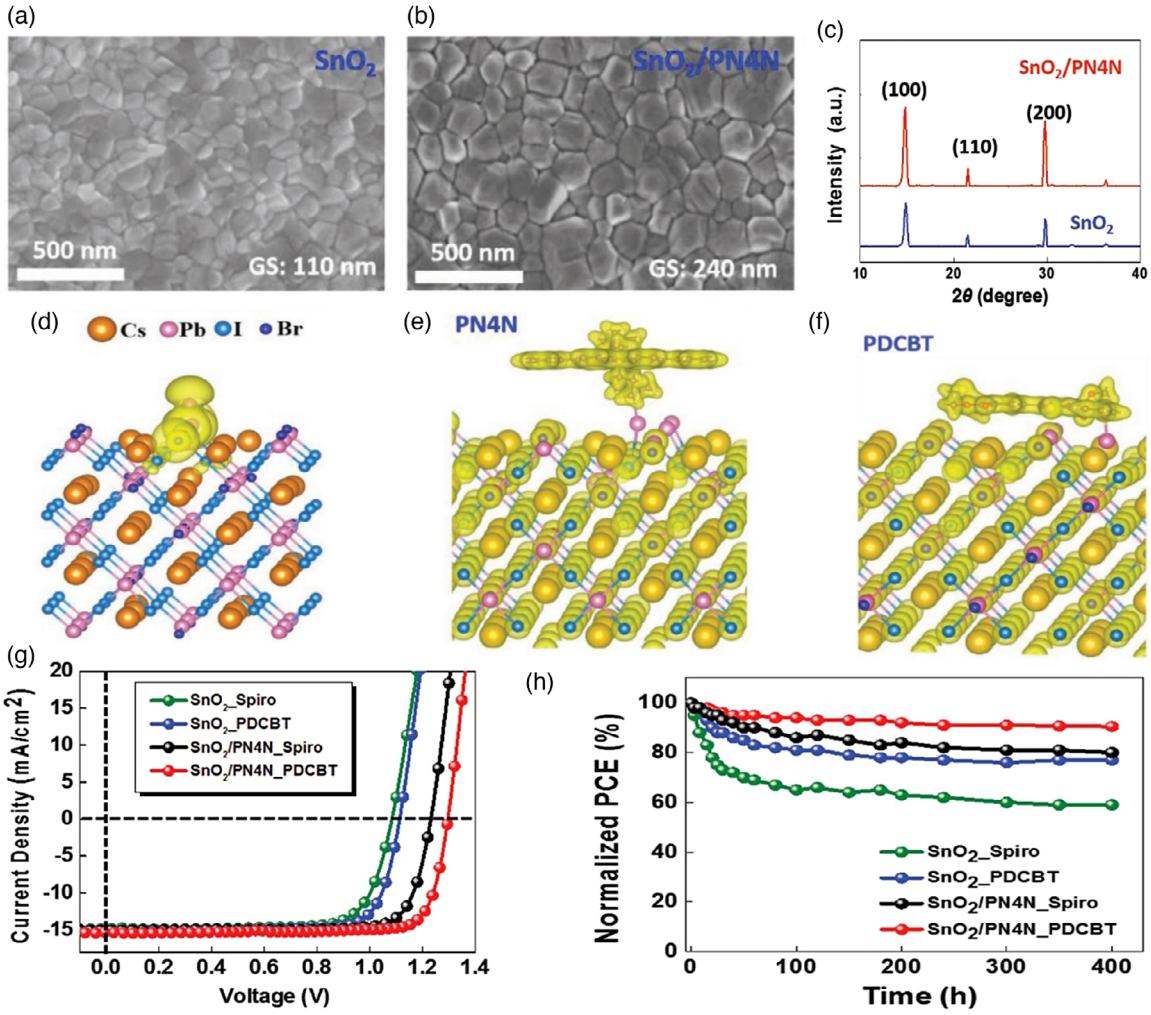


Figure 5. Top-view SEM images of $CsPbI_2Br$ films on a) SnO_2 and b) SnO_2/PN4N. c) XRD patterns of $CsPbI_2Br$ films deposited onto SnO_2 and SnO_2/PN4N substrates. d) Charge density distribution plots of $CsPbI_2Br$ (110) surface possessing an antisite defect. e) Passivation of PN4N for surface antisite defects of $CsPbI_2Br$ (110). f) Passivation of PDCBT for surface antisite defects of $CsPbI_2Br$ (110). g) *J–V* characteristics of devices based on different HTLs and ETLs. h) Stability of PSCs based on different HTLs and ETLs under 1 sun equivalent illumination. Reproduced with permission.[68] Copyright 2019, Wiley-VCH.

crystals and accordingly passivate surface defects as well as suppress photoinduced halide segregation (Figure 5d–f). As shown in Figure 5g, the PCE was increased after modification of PN4N for $SnO_2/CsPbI_2Br$ interface or after substitution of Spiro-OMeTAD by PDCBT. Finally, the optimized device with PN4N interface modification in conjunction with PDCBT as the dopant-free HTM produced a high PCE of 16.2% and showed excellent photostability, which maintained over 90% of its initial value under continuous 1 sun equivalent illumination for 400 h (Figure 5h). Except for $CsPbI_2Br$ (1.92 eV), $CsPbIBr_2$ with a bandgap of 2.05 eV much larger than 1.73 eV of $CsPbI_3$ was believed to be very promising for light-harvesting materials, especially for tandem solar cell applications, due to its much better phase stability in comparison with $CsPbI_3$.[92] Enormous efforts have been made to optimize the PCE of $CsPbIBr_2$-based devices.[93–97] To overcome interfacial nonradiative recombination, ETL/$CsPbIBr_2$ interface modification was implemented by inserting a $SmBr_3$ interfacial layer. It was demonstrated that improved crystallization and morphology of perovskite films were realized after interface modification.[69] In addition, a gradient energy band alignment was achieved, which effectively suppressed the interfacial and bulk nonradiative recombination. The device based on interface modification of $SmBr_3$ demonstrated a PCE of 10.88% under 1 sun illumination, which increased by 30% as compared with its counterpart without modification. To explore potentials of Br substitution for stabilizing the black phase of $CsPbI_3$, $CsPbBr_3$ with a bandgap of 2.3 eV is obtained after thorough replacement of I^- with Br^-. Excellent thermal, light, and moisture stabilities have been demonstrated for $CsPbBr_3$ films and $CsPbBr_3$-based devices especially for all-inorganic PSC based on CE.[37,70–72,98,99] In the recent two years, PCEs of 10.5–11% have been achieved for $CsPbBr_3$-based devices even based on CE.[37,70–72] It is worth noting that a PCE as high as 10.85% was realized for all-inorganic $CsPbBr_3$-based devices

© 2020 Wiley-VCH GmbH

using inorganic materials as HTMs,[71] and a PCE up to 10.91% was demonstrated for $CsPbBr_3$-based devices based on organic Spiro-OMeTAD HTM.[72] Although the very impressive stability has been testified for $CsPbBr_3$-based devices, its low PCE still hinders its further commercial application, mainly originating from insufficient light harvesting due to the wide bandgap of up to 2.3 eV and serious back contact interfacial recombination losses as well as a large energy barrier. Consequently, further minimizing interfacial recombination losses is imperative to maximize the PCE of $CsPbBr_3$-based devices.

In organic–inorganic hybrid perovskites, Cl^- ion is usually introduced into perovskite precursor solution through organic ammonium salt containing Cl^- (like MACl) to prepare high-quality perovskite films with large grain sizes and less defects. A few works have demonstrated that an extremely small amount of Cl^- ion was incorporated into crystal lattices of perovskites.[100,101] Nevertheless, most works indicated that Cl^- ion was not finally incorporated into the crystal lattices of perovskites and it left from films during high-temperature annealing.[102,103] In a word, it still remained unclear whether Cl^- ion was inserted into the crystal lattices. However, it was widely revealed that Cl^- ion can effectively improve perovskite crystallization, increase grain sizes, passivate defects at GBs, and enhance carrier lifetimes.[6,101–103] Learning from hybrid perovskites, incorporation of Cl^- ion was also attempted by several groups to prepare high-quality and phase-stable inorganic perovskite films.[32,33] You and coworkers prepared efficient and stable inorganic $CsPbI_{3-x}Br_x$-based PSCs through interface and compositional engineering simultaneously.[33] As shown in **Figure 6**a, LiF interfacial layer was used to modify SnO_2/perovskite interface. LiF modification upshifted the conduction band minimum (CBM) of SnO_2 from 4.3 to 4.01 eV, which was better matched with the CBM (3.94 eV) of $CsPbI_{3-x}Br_x$ (Figure 6b). In addition, LiF interface layer can effectively passivate interfacial defects. As a result, the PCE of the device was enhanced from 13.54% to 17.08%. In this work, $PbCl_2$ was introduced into perovskite precursor solution to improve further film quality. It was found that the crystallinity of perovskite films was remarkably improved and charge recombination was significantly suppressed after addition of $PbCl_2$. It is worth noting that the black phase stability of $CsPbI_{3-x}Br_x$ dramatically improved after $PbCl_2$ addition. As shown in Figure 6c, the PCE of device was further increased from 16.96% to 18.22%, which was mainly a result of enhanced V_{oc} due to the reduced nonradiative recombination losses. The best-performing device with LiF modification in combination with $PbCl_2$ addition achieved a promising PCE as high as 18.64%. Over 94% of its initial PCE was retained for the $CsPbI_{3-x}Br_x$-based device with interfacial and compositional engineering under continuous 1 sun equivalent illumination for over 1000 h, as shown in Figure 6d. The earlier work highlights the importance of synergistic engineering strategy in realizing efficient and stable inorganic PSCs.

Apart from Br^- and Cl^- doping, acetate anion (Ac^-) was also developed to partially replace I^- in the $CsPbI_2Br$ framework to obtain $CsPbI_{2-x}Br(Ac)_x$.[104] Compared with pristine $CsPbI_2Br$ films, Ac^- doping reduced trap states, increased carrier lifetimes, and improved charge transportation. The device based on $CsPbI_{2-x}Br(Ac)_x$ exhibited excellent reproducibility and a PCE of 15.56%, along with a high V_{oc} of 1.30 V. The much enhanced moisture stability was demonstrated for $CsPbI_{2-x}Br(Ac)_x$-based devices compared with the control device without doping.

2.3. Intermediate with Hydroiodic Acid

To increase the activation energy barrier of phase transition from black phase to yellow phase, the strategy that HI or hydrogen lead iodide ($HPbI_3$) was added into perovskite precursor solution to improve film quality and phase stability was first attempted in 2015.[105] The phase stability was improved due to the formation of small perovskite crystals and generation of lattice strain when a small amount of HI was incorporated. As a result, a PCE of 2.9% was reported for $CsPbI_3$-based PSCs. After that, HI or $HPbI_3$ intermediate strategy has been extensively adopted to prepare high-quality and phase-stable inorganic perovskite films for solar cells. It was reported that the crystallization temperature of α-$CsPbI_3$ was prominently reduced from 330 to 200 °C when $HPbI_3$ was used to take the place of PbI_2. Furthermore, α-$CsPbI_3$ was stabilized for several days in dry air. However, α-$CsPbI_3$ is unstable and would spontaneously convert into yellow phase in ambient condition with over 20% RH. Consequently, α-$CsPbI_3$ film is difficult to fabricate in ambient atmosphere with high RH. Chen and coworkers used $HPbI_3$ to prepare α-$CsPbI_3$ and found that highly stable α-$CsPbI_3$ can be acquired by one-step deposition solution method.[106] Tensile lattice strain led to a reduced bandgap from 1.72 to 1.68 eV. A PCE of 9.5% was achieved for the all-inorganic PSCs based on CE and over 90% of its original value was retained after storage in dry air for 3000 h. To conquer phase instability under relative high humidity, a low novel low-temperature phase transition route was developed by Luo et al.,[107] where the perovskite film that consisted of intermediate Cs_4PbI_6 phase was dipped into the hot IPA solution, annealed at 100 °C for 5 min, and then gradually converted into a dark brown α-$CsPbI_3$ film. The device prepared by this method showed a PCE of 4.13% and almost no degradation in ambient condition with less than 30% RH after 72 h. The present work proves that the fabrication of α-$CsPbI_3$-based PSC in fully open-air conditions with high humidity is feasible if an appropriate approach is adopted. It is worth mentioning that Zhao and coworkers used $HPbI_{3+x}$ ($x = 0.1$–0.15) to prepare precursor solution and used phenyltrimethylammonium bromide (PTABr) to post-treat perovskite films.[73] Based on this method, improved phase stability was realized. Due to improved phase stability and film quality along with effective defect passivation by PTABr, a high PCE of 17.06% was obtained, accompanied by a stable output of 16.3%. You and coworkers achieved an appealing PCE of 18.64% through introducing $PbCl_2$ and using $HPbI_{3+x}$ to prepare perovskite precursor solution in conjunction with adopting LiF interfacial modification.[33]

As we mentioned previously, β-$CsPbI_3$ and γ-$CsPbI_3$ phases are also photoactive appropriate for the absorber of solar cells except for α-$CsPbI_3$. The much lower phase transition temperature (260 °C for β-$CsPbI_3$ and 175 °C for γ-$CsPbI_3$) was reported as compared with 360 °C of α-$CsPbI_3$, which implies that lower-symmetry β-$CsPbI_3$ and γ-$CsPbI_3$ phases could be suitable for fabricating highly stable PSCs.[34] Similar with α-$CsPbI_3$, HI or $HPbI_3$ was also demonstrated to be effective in stabilizing γ-$CsPbI_3$.[76,108] For example, Hu and coworkers introduced a

© 2020 Wiley-VCH GmbH

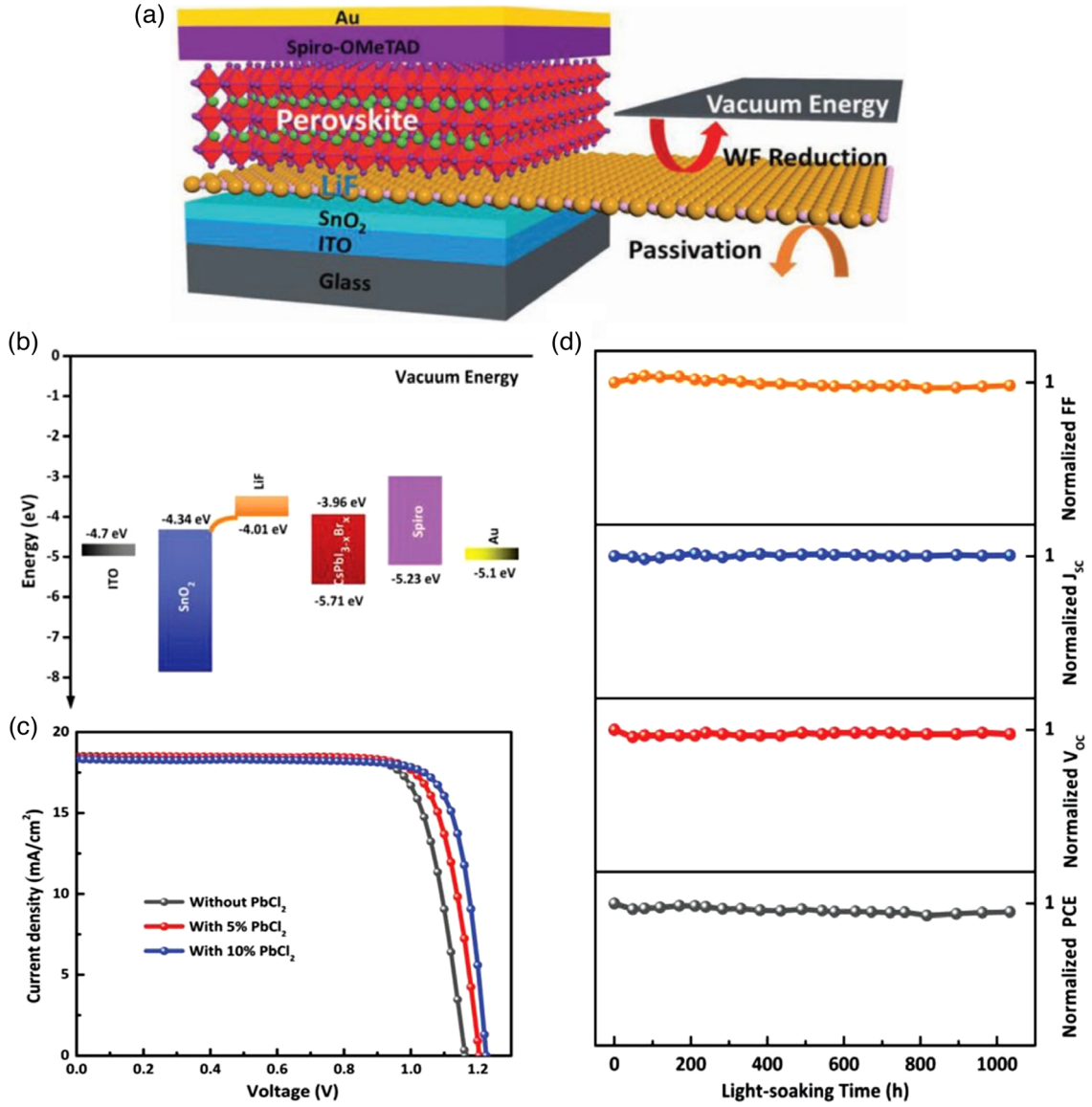


Figure 6. a) The schematically illustrated architecture of inorganic PSC with LiF interface modification. b) Energy band diagram for each layer in inorganic PSC. c) *J*–*V* characteristics for devices with different concentrations of $PbCl_2$. d) Photostability of unencapsulated $CsPbI_{3-x}Br_x$-based device with LiF interlayer and $PbCl_2$ additive measured under continuous white light LED illumination (100 mW cm^{-2}) in a nitrogen glovebox. Reproduced with permission.[33] Copyright 2019, Wiley-VCH.

small amount of H_2O and HI into perovskite precursor solution to stabilize γ-$CsPbI_3$ through a proton transfer reaction and demonstrated a PCE of 11.3%.[108] Theoretical and experimental results revealed that γ-$CsPbI_3$ was thermodynamically preferred in comparison with δ-$CsPbI_3$ due to the much lower surface free energy of the former than the latter. Liberated H^+ and I^- from the ionization of HI from DMF·*x*HI complexes contributed to improved phase stability through reducing the sizes of PbI_2 colloids which were made of lead polyiodide complexes. Then the corner-sharing $[PbI_6]_4^-$ octahedra intercalated by Cs^+ ions was formed and finally was converted into perovskite polymorph with a decreased size after thermal annealing. In addition, phenylethylammonium iodine (PEAI) and HI were incorporated by Liu et al. into $CsPbI_3$ precursor solution. It was found that much better phase stability was realized by the synergistic use of PEAI and HI.[76] The unencapsulated device with PEAI and HI displayed a PCE of 15.07% and exhibited a negligible decay after light illumination for 300 h. A total of 92% of its initial efficiency was maintained after being stored for 2 months under ambient conditions. To further understand the mechanism of stabilizing the black phase of $CsPbI_3$ by HI or $HPbI_3$, Ke et al. revealed that the real intermediate by incorporating HI was $DMAPbI_3$ (DMA = dimethylammonium, $(CH_3)_2NH_2^+$) rather than $HPbI_3$, where DMA was the decomposition product of HI and DMF by acidic hydrolysis.[109] They thought that the final perovskite was α-$Cs_{1-x}DMA_xPbI_3$ (x = 0.2–0.5) cubic perovskite instead of (α, γ)

© 2020 Wiley-VCH GmbH

$CsPbI_3$ phase. However, Zhao and coworkers demonstrated that DMAI completely escaped from the final $CsPbI_3$ perovskite films rather than being incorporated into its crystal lattices, and β-$CsPbI_3$ was obtained by this additive strategy.[22] They proposed that proper humidity was helpful for DMAI removal from final films. The device based on DMAI and phenyltrimethylammonium chloride (PTACl) passivation delivered a record PCE of 19.03%.

2.4. Organic Cations

In the past few years, organic cations were demonstrated to be one of the most effective and feasible approaches to stabilize the black phase of inorganic perovskites. Huang and coworkers stabilized the black phase of $CsPbI_3$ via incorporating sulfobetaine zwitterion into perovskite precursor solution.[32] The mechanisms of $CsPbI_3$ perovskite formation without and with zwitterion molecules were proposed. For the formation of $CsPbI_3$ perovskite without zwitterion molecules, crystallized PbI_2·DMSO colloid was formed through the coordination between PbI_2 Lewis acid in precursor solution (**Figure 7**a) and DMSO Lewis base, and then coordination of I^- ions with Pb^{2+} generated corner-sharing $[PbI_6]^{4-}$ octahedra during spin coating (Figure 7b). Finally, $CsPbI_3$ perovskites were formed by occupying the octahedral sites with Cs^+ (Figure 7c). As for the formation of $CsPbI_3$ perovskites with zwitterion, the layered structure of the colloid PbI_2·DMSO was broken because of electrostatic interaction between zwitterion and PbI_2·DMSO colloids, resulting in a reduced colloid size and amorphous phase in the spun film before annealing (Figure 7d,e). Zwitterion molecules were expelled to GBs and the grain surface during the $CsPbI_3$ grain growth process (Figure 7f). In a word, phase stability was significantly enhanced after the introduction of zwitterion molecules, which was due to prominently suppressed crystallization and reduced grain sizes. As a result, a stabilized PCE of 11.4% was obtained for the devices stabilized by zwitterion.

Inspired by the excellent moisture stability of 2D perovskites demonstrated in hybrid perovskites, dimensional engineering strategy was attempted to stabilize the black phase of inorganic perovskites.[25,74,75,110,111] For instance, Zhao and coworkers first added a small amount of 2D perovskite $EDAPbI_4$ based on bication into $CsPbI_3$ perovskite precursor solution to stabilize the α-phase of $CsPbI_3$.[25] As shown in Figure 7g,h, the

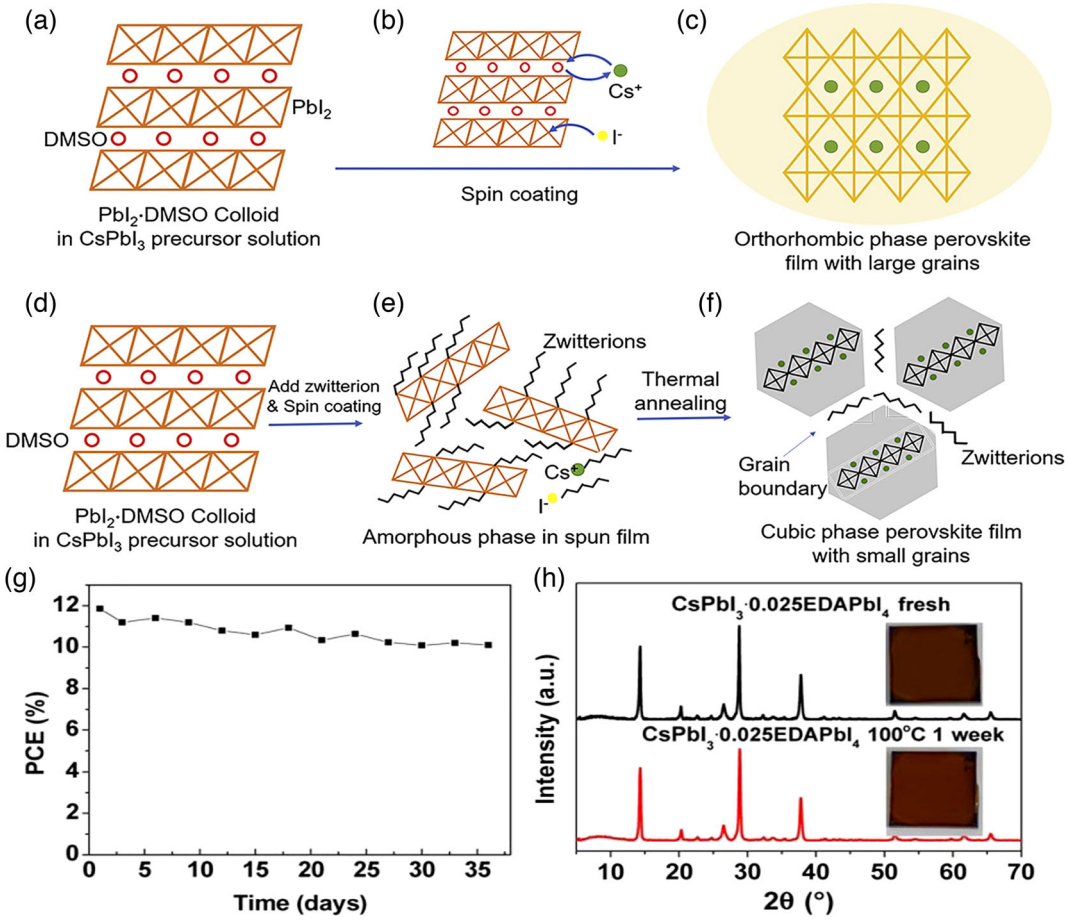


Figure 7. Schematic representation of $CsPbI_3$ crystal formation from precursor solution without a–c) or with d–f) the zwitterion. Reproduced with permission.[32] Copyright 2017, Elsevier Inc. g) Ambient stability of the devices based on $CsPbI_3$·0.025$EDAPbI_4$ in a dark dry box. h) XRD pattern and images of the $CsPbI_3$·0.025$EDAPbI_4$ film before and after aging at 100 °C in a dry box for 1 week. Reproduced with permission.[25] Copyright 2017, American Association for the Advancement of Science (AAAS).

© 2020 Wiley-VCH GmbH

EDAPbI$_4$-based devices delivered a PCE of 11.8% and ambient and thermal stability, which were ascribed to the unique (110) layered structure of 2D perovskite EDAPbI$_4$. In addition, Jiang et al.[74] used commonly used large-sized organic cation PEA$^+$ to fabricate quasi-2D perovskite $PEA_2Cs_{n-1}Pb_nX_{3n+1}$. It was found that the larger n was, smaller the decomposition energy and poorer the phase stability. This suggested that as-prepared quasi-2D perovskites suppressed undesirable phase transition from black phase to yellow phase (**Figure 8**a). The optimized $PEA_2Cs_{59}Pb_{60}X_{181}$-based device showed a 12.4% PCE (Figure 8b) and excellent ambient stability (Figure 8c). Zhu and coworkers[75] developed a spontaneous interfacial manipulation (SIM) method, where 2D GA_2PbI_4 was formed on the surface 3D $CsPbI_xBr_{3-x}$ through adding guanidinium bromide (GABr) into $CsPbI_xBr_{3-x}$ precursor solution. It was revealed that spontaneously formed ultrathin 2D perovskite cannot only effectively passivate interfacial defects but also effectively protect 3D perovskite films from moisture. Finally, the markedly enhanced PCE from 13.64% to 18.06% was demonstrated for the devices with 2D modification as well as improved moisture and phase stability (Figure 8d,e). In addition, Daoud and coworkers[112] also demonstrated that the 2D GA_2PbI_4 interface layer can effectively passivate defects on the surface of $Cs_{(1-x)}Rb_xPbI_2Br$ films and improve device stability. The PSC with 2D interface layer yielded a PCE of 15.6% much higher than 12.9% of the reference device. The remarkably enhanced moisture, thermal, and light stability were demonstrated. Lu and coworkers[113] demonstrated that GA$^+$ doping can stabilize the cubic phase of $CsPbI_2Br$ via releasing the lattice strain and forming strong hydrogen bonds. GA-doped devices produced a PCE as high as 14.34% fabricated at 140 °C without ATS and maintained around 94% of its initial PCE after being stored for 1000 h.

Different from the earlier research results, some groups demonstrated that it was difficult to form 2D or quasi-2D perovskites through incorporating large-sized organic cations into inorganic perovskite precursor solutions or post-treating the surface of inorganic perovskite films.[73,76,114,115] In the case of precursor incorporation, Liu and coworkers[76] achieved a PCE of 15.07% by introducing PEAI into $CsPbI_3$ perovskite precursor solution based on the device configuration of FTO/TiO_2/$CsPbI_3$/PTAA/Au. They found that HI and PEAI can effectively stabilize the black phase of $CsPbI_3$. The mechanism of stabilization of HI and PEAI for the black phase of $CsPbI_3$ was proposed as follows. First, the distorted black-phase $CsPbI_3$ was formed through the reaction between HI and PbI_2 during annealing. Second, PEAI participated in the nucleation and growth of $CsPbI_3$ films, which

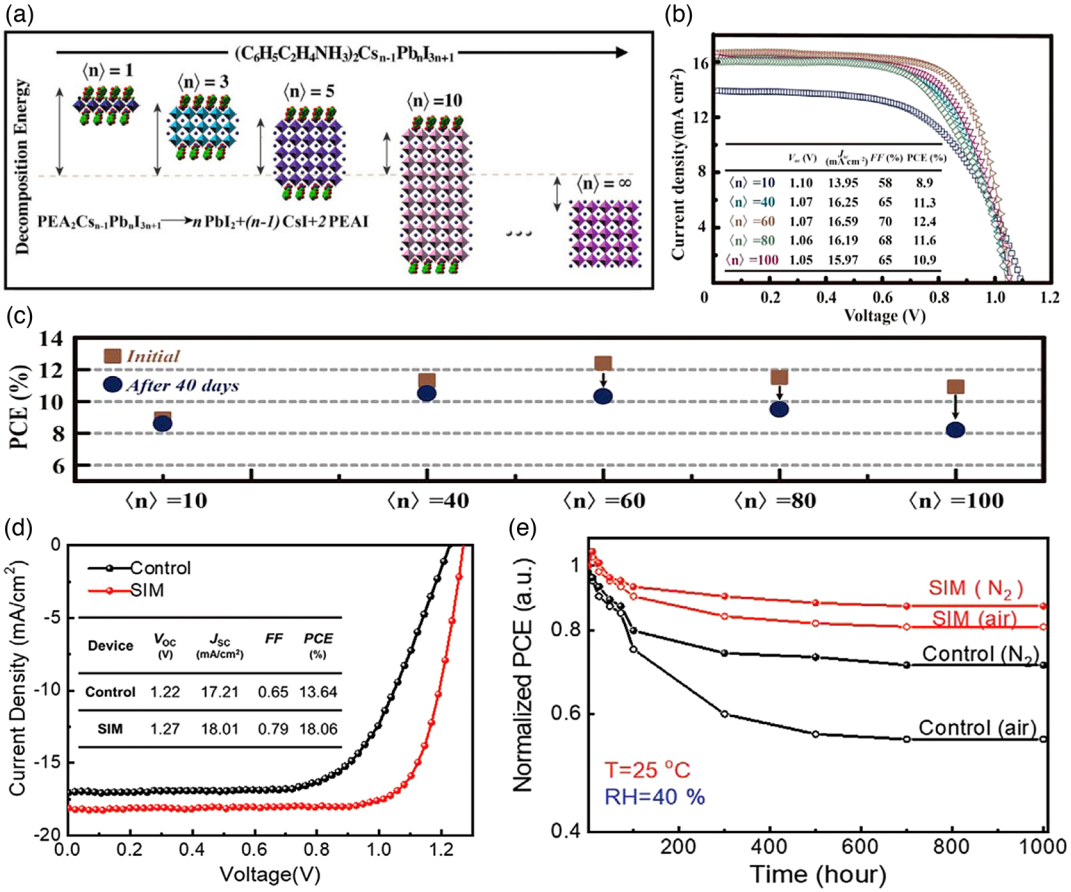


Figure 8. a) Unit cell structure and decomposition energetics of $PEA_2Cs_{n-1}Pb_nX_{3n+1}$ using first-principles density functional theory (DFT). b) *J*–*V* curves of devices based on $PEA_2Cs_{n-1}Pb_nI_{3n+1}$. c) PCE evolution of unsealed devices based on $PEA_2Cs_{n-1}Pb_nI_{3n+1}$ under ambient atmosphere. Reproduced with permission.[74] Copyright 2018, Elsevier Inc. d) *J*–*V* curve of the PSCs with and without SIM. e) Stability of devices based on pure $CsPbI_xBr_{3-x}$ and $CsPbI_xBr_{3-x}$ + 2% v/v GABr in air or N_2 atmosphere. Reproduced with permission.[75] Copyright 2020, Wiley-VCH.

© 2020 Wiley-VCH GmbH

resulted in oriented crystal growth. The electrostatic interaction between PEAI and $CsPbI_3$ crystal as well as steric effect can hinder the phase transition from black phase to yellow phase. The PEAI-based $CsPbI_3$ films maintained black color after being aged at 80 °C for 120 h while yellow spots appeared for the reference films after only 40 h aging. Furthermore, the improved thermal stability was also confirmed by thermogravimetric analysis (TGA) and differential scanning calorimeter (DSC). Compared with precursor incorporation, more attention has been paid to post-treatment of inorganic perovskite films by organic large-sized cations.[12,22,73,114,115] For example, Zhao and coworkers[114] reported a post-treatment of PEAI for inorganic $CsPbI_3$ films and demonstrated a PCE of 14.3% much higher than 11.2% of the reference device, which was ascribed to the effective passivation for defects/trap states at the GBs and/or surface of inorganic $CsPbI_3$ films as reflected from the reduced carrier recombination by transient photovoltage (TPV) decay measurement. As shown in **Figure 9**a, they proposed that PEA^+ and I^- in PEAI salts would passivate Cs^+ and I^- vacancies, respectively. Meanwhile, some Cs^+ ions could be substituted by PEA^+. They thought that 2D PEA_2PbI_4 was difficult to generate but formed PEA^+ functional organic layer can effectively stabilize the black phase of $CsPbI_3$. As shown in Figure 9b, the improved moisture stability of films proved that PEAI post-treatment really can enhance the phase stability of perovskite films. As a result of improved film moisture stability, the device with PEAI post-treatment showed a prominently improved moisture stability as compared with the reference one without post-treatment, as shown in Figure 9c. Through simultaneous judicious design of anion and cation in organic salts, Liu and coworkers post-treated the $CsPbI_2Br$ films with PEACl and demonstrated a much improved moisture stability along with a comparable PCE relative to control device.[115] It was found that the hydrophobic aromatic group PEA^+ was located in edge-on orientation at the surface of $CsPbI_2Br$ films and doping of Cl^- into the $CsPbI_2Br$ crystal lattice led to lattice shrinking. In addition, Zhao and coworkers[73] designed a bifunctional organic large-sized salt phenyltrimethylammonium bromide (PTABr), achieving gradient Br doping and surface passivation. A champion PCE of 17.06% and a stable output of 16.3% were achieved for the devices with PTABr post-treatment. As shown in Figure 9d, no impurity peaks were observed in the PTABr-based $CsPbI_3$ film after being annealed at 80 °C in N_2 glovebox for 72 h whereas $CsPbI_3$ film without surface modification almost completely degraded into yellow δ phase. As shown in Figure 9e, the control $CsPbI_3$ film turned yellow after being exposed to 80 ± 5% RH at ≈35 °C for 0.5 h, whereas the PTABr–$CsPbI_3$ thin film still retained pure black phase under the same condition. The earlier results indicated that moisture and thermal stabilities were enhanced significantly after PTABr surface modification. This work suggests that the simultaneous rational design of anion and cation is of extreme importance for fabricating efficient and stable inorganic PSCs, which deserves more attention. Recently, Liu et al.[116] reported a gradient grain-sized (GGS) $CsPbI_3$ bilayer to stabilize the black phase of $CsPbI_3$ through the upward migration of (adamantan-1-yl) methanammonium (ADMA), together with a hot-casting technique. It was demonstrated that the large grain-sized $CsPbI_3$ layer was located at the bottom site, along with the tiny grain-sized $CsPbI_3$ layer at the surface site. It showed that the

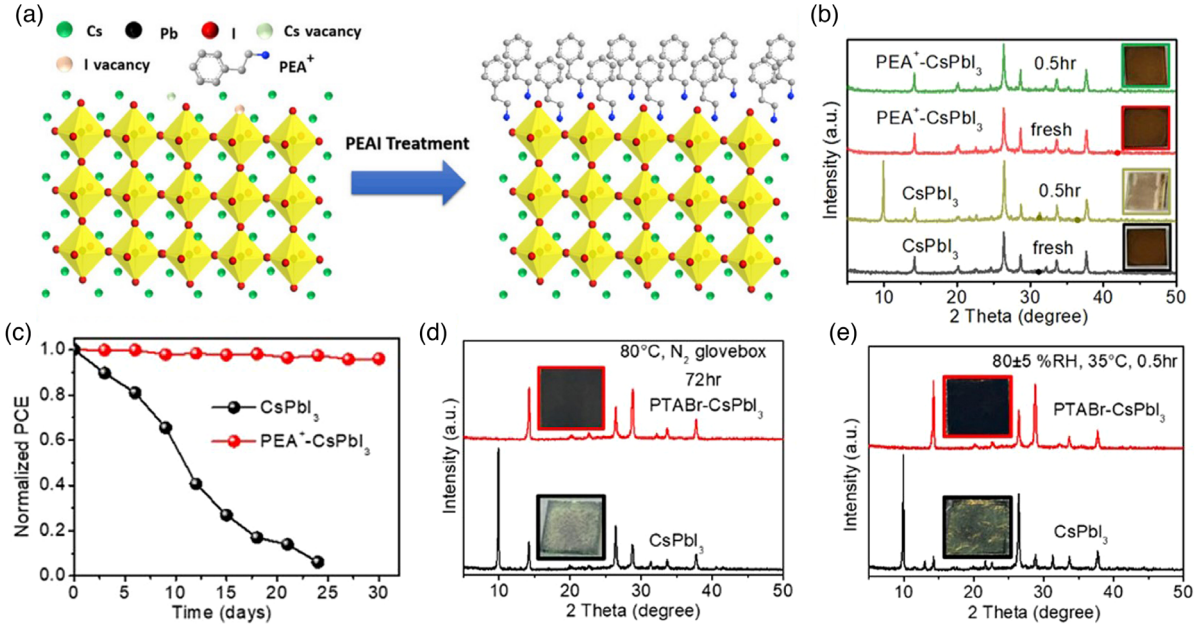


Figure 9. a) Schematic illustration of $CsPbI_3$ modified by PEAI showing that PEA^+ and I^- can passivate the PEA^+ and I^- vacancies, respectively. b) XRD patterns and photographs of $CsPbI_3$ films without and with PEAI modification before and after being exposed to ambient condition with 85–90% RH at RT for 0.5 h. c) PCE as a function of storage time in a dark and dry box with less than 20% RH at RT for the devices without and with PEAI post-treatment. Reproduced with permission.[114] Copyright 2018, Elsevier Inc. XRD patterns of $CsPbI_3$ films without and with PTABr modification before and after d) being heated at 80 °C in a N_2 glovebox for 72 h and e) after being exposed to 80 ± 5% RH at ≈35 °C for 0.5 h. Reproduced with permission.[73] Copyright 2018, American Chemical Society.

© 2020 Wiley-VCH GmbH

large-sized perovskite layer had a high carrier mobility and low trap-state density whereas the small-sized perovskite layer can ameliorate phase stability due to high surface energy. Based on this strategy, a promising PCE of 15.5% was obtained.

Similar to MACl additive commonly used for preparing high-quality hybrid perovskite films, dimethylamine iodide (DMAI) was demonstrated to be very effective in stabilizing the black phase of $CsPbI_3$ and improving film quality in recent two years. As we discussed previously, Ke et al. demonstrated that the intermediate was $DMAPbI_3$ when HI was added into inorganic perovskite precursor solution and found that DMAI has been incorporated into crystal lattices of $CsPbI_3$ to obtain α-$Cs_{1-x}DMA_xPbI_3$ ($x = 0.2$–0.5) cubic perovskite.[109] Similarly, Jin et al. also revealed that high-quality intermediate compounds were $DMAI/DMAPbI_x$ rather than $HPbI_3$ after incorporating HI into precursor solution.[117] It was shown that most of DMA^+ was lost during high-temperature annealing and only an ultrasmall amount of DMA^+ was doped into the crystal lattices of $CsPbI_3$. In addition, they found that excess DMA^+ can form Lewis acid–base adducts with Pb^{2+} at the surface of $CsPbI_3$. Finally, the device with HI delivered a high PCE of 17.3%. As the intermediate phase was $DMAPbI_3$ or $DMAI/DMAPbI_x$ after HI was introduced, Pang and coworkers[77] directly incorporated DMAI into $CsPbI_3$ precursor solution to prepare phase-stable and high-quality perovskite films. As shown in **Figure 10**a, it was revealed that $DMAPbI_3$ and Cs_4PbI_6 were first formed when films were annealed at 100 °C for 10 min and then converted into mixed-cation perovskite phase $DMA_{0.15}Cs_{0.85}PbI_3$ upon annealing at 180 °C for 15 min. $DMA_{0.15}Cs_{0.85}PbI_3$ was thermodynamically stable and possessed a bandgap of 1.67 eV. When the annealing time further extended, $DMA_{0.15}Cs_{0.85}PbI_3$ was directly transformed into γ-$CsPbI_3$ and then was spontaneously converted into δ-$CsPbI_3$. It means that the thermodynamically stable $DMA_{0.15}Cs_{0.85}PbI_3$ was obtained through adopting appropriate annealing temperature and time, as confirmed by XRD results in Figure 10b–d. The corresponding device based on more symmetrical perovskite $DMA_{0.15}Cs_{0.85}PbI_3$ reached a PCE of 15.3%, which was markedly higher than 10.7% of the reference device based on pristine γ-$CsPbI_3$. Wang et al.[[12] also directly introduced DMAI into $CsPbI_3$ perovskite precursor containing a stoichiometric ratio of $CsI:PbI_2:xDMAI$ ($x = 1.1$–1.2). It was found that the bandgap (1.68 eV) of as-prepared $CsPbI_3$ was much narrower than 1.73 eV previously reported. They concluded that β-$CsPbI_3$ instead of (α, γ) $CsPbI_3$ was obtained by the addition of DMAI, which was confirmed by XRD results in Figure 10e. To further improve film quality, choline iodide (CHI) quaternary ammonium salt was used to post-treat as-prepared films. The carrier lifetime of perovskite films was substantially increased after CHI post-treatment, as shown in Figure 10f. Finally, a PCE enhancement from 15.1% to 18.4% was demonstrated after CHI treatment (Figure 10g). Moreover, the excellent photostability was achieved for the device with the synergistic use of CHI and DMAI, which maintained 92% of its original PCE under continuous illumination at the maximum power point (MPP) after 500 h, as shown in Figure 10h. In consideration of the significant role of DMAI in improving film quality and stabilizing black phase of $CsPbI_3$, the same group further investigated the role of DMAI as an additive or dopant.[22] As shown by the crystal phase evolution in Figure 10i, peaks at 11.6° and 12.0° assigned to $DMAPbI_3$ and the possible intermediate phase were found in the precursor film annealed less than 5 min weakened gradually as annealing time increased and thoroughly disappeared in the final film when annealing time was increased to 5 min. As shown in Figure 10j, the growth mechanism was proposed as follows. The intermediate phase between DMAI and PbI_2 was first formed. DMAI would sublimate and Cs^+ would enter the crystal lattice position during the annealing process. They proposed that γ-$CsPbI_3$ was obtained due to fast crystallization when x was equal to 0.5 and 0.7 in PbI_2:xDMAI but a slightly distorted β-$CsPbI_3$ was obtained due to slow crystallization when x was increased to 1.0 and 1.5. Taking XRD, UV absorption, time-of-flight secondary ion mass spectrometry, NMR, and TGA measurements together, it was revealed that DMAI was a volatile additive to $CsPbI_3$ inorganic perovskite crystallization instead of the dopant. Combined with PTACl, the device delivered a remarkably enhanced PCE from 16.62% to 19.03% as compared with the reference device without PTACl post-treatment. They demonstrated that the residue of DMAI was detrimental to device stability. However, the influence mechanism of DMAI residue for device stability was not revealed in this work, which remains investigated deeply in the subsequent research work. Although huge progresses have been achieved on DMAI, inconsistent conclusions were obtained on its role of DMAI as an additive[12,22,117] or dopant,[77,109] which could be ascribed to different annealing temperatures and times along with different amounts of DMAI and preparation condition (e.g., humidity, oxygen, etc.).

2.5. Additive Engineering

It was widely demonstrated that additives play a crucial role in stabilizing the black phase of inorganic perovskites and improving film quality. The nonstoichiometric method is usually adopted to achieve the earlier purposes. For example, excess CsBr was added into $CsPbI_3$ precursor solution.[118] The improved stability of the cubic $CsPbI_3$ phase at a low temperature was demonstrated after introducing excess CsBr, which was put down to produced microstrain in the lattice. The device with excess CsBr yielded a PCE of 10.92%. In addition, Yao and coworkers.[78] also incorporated excess CsBr into $CsPbI_3$ precursor solution and the intermediate product $CsI_{1-y}Br_y/CsPbI_{3-x}Br_x$ was obtained. The moisture treatment led to structural evolution from $CsI_{1-y}Br_y/CsPbI_{3-x}Br_x$ to uniform $CsPbI_{3-z}Br_z$ layer. Due to improved homogeneity of the stoichiometry and crystallinity, the PCE of the device was increased from 10.89% to 13.09% after moisture treatment. Unold and coworkers prepared γ-$CsPbI_3$ films through the coevaporation method.[119] It was found that excess CsI can lead to distorted perovskite $CsPbI_3$ whereas PbI_2-rich growth conditions resulted in nonperovskite yellow phase. A PCE of 12.5% was obtained for the inverted structure of $ITO/PTAA/CsPbI_3/C_{60}/BCP/Cu$ based on perovskite films with excess CsI. The device showed good shelf stability of over 1200 h. Miyasaka and coworkers prepared α-$CsPbI_3$ via introducing Pb(II) propionate additive in the $CsPbI_2Br$ precursor and achieved a 14.58% PCE using dopant-free HTM.[79] It was found that Pb(II) propionate can passivate defects within perovskite films, which was possibly due to the

© 2020 Wiley-VCH GmbH

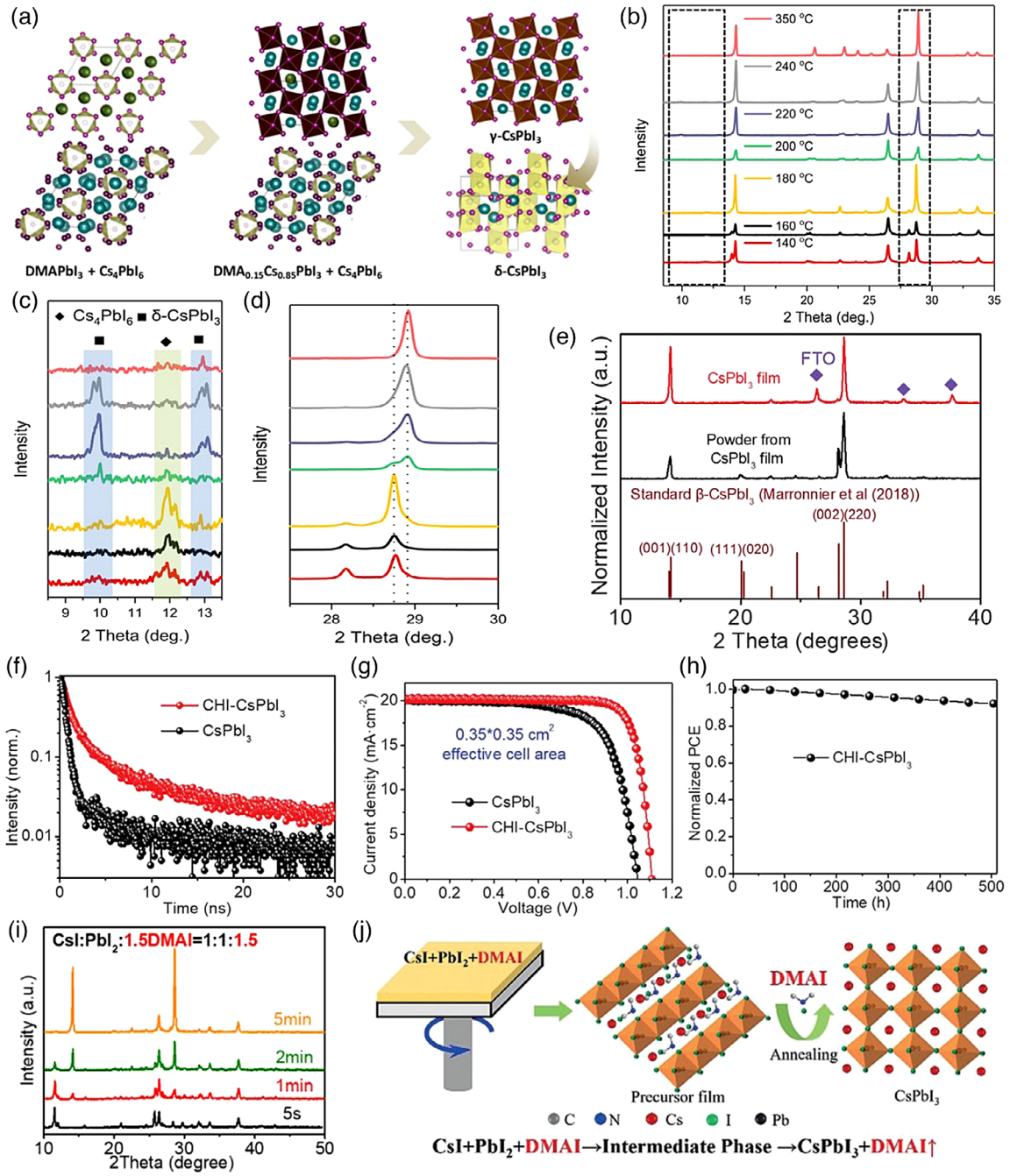


Figure 10. a) Crystal structure and phase evolution during the fabrication of $DMA_{0.15}Cs_{0.85}PbI_3$ film. b–d) XRD patterns of the DMAI/$CsPbI_3$ films annealed at different temperatures. Reproduced with permission.[77] Copyright 2020, American Chemical Society. e) XRD patterns of $CsPbI_3$ thin film and powders scratched from the films. The standard β-$CsPbI_3$ XRD pattern calculated for Cu Kα1 radiation for the tetragonal perovskite structure is given. f) Time-resolved photoluminescence (TRPL) decay curves of $CsPbI_3$ films without and with CHI post-treatment. g) *J–V* characteristics of devices based on $CsPbI_3$ and CHI-$CsPbI_3$ measured under simulated AM 1.5G solar illumination of 100 mW/cm^2 in RS. h) Stability of the unencapsulated CHI–$CsPbI_3$ device under continuous white light LED illumination (100 mW cm^{-2}) at their MPP in N_2 glovebox. Reproduced with permission.[12] Copyright 2019, American Association for the Advancement of Science. (i) XRD patterns of Cs-1.5 DMAI films at different annealing times. j) Schematic mechanism of black-phase $CsPbI_3$ formation with the aid of DMAI additive. Reproduced with permission.[22] Copyright 2019, Wiley-VCH.

coordination between propionate ion and undercoordinated Pb^{2+} at the surface or GB of perovskite films. Pang and coworkers[120] used MA gas to improve the morphology and quality of $CsPbI_2Br$ in conjunction with incorporating a certain amount of MAX (X = I or Br) into the precursor solution. It proved that excess MAX can improve the interconnection

 © 2020 Wiley-VCH GmbH

between the perovskite film and the MA gas. Using this method, the PCE of the device was improved from 10.1% to 13.1%. Han et al.[80] developed a novel strategy where a series of organic molecules with different surface organic terminal groups were incorporated into precursor. It was found that these organic molecules can effectively suppress the octahedral tilting of $[PbI_6]^{4-}$ units in cubic $CsPbI_3$. It was demonstrated that steric hindrance can effectively hinder the lattice distortion and accordingly enhance the energy barrier for phase transition from black phase to yellow phase. Moreover, organic additive molecules can passivate surface defects of perovskite films. Finally, the device with molecular modification gave a PCE of 13.2% and maintained 85% of its initial efficiency value under ambient conditions after 30 days.

2.6. Quantum Dots

It is widely accepted that many physical properties between nanometer-sized materials and bulk crystalline materials are different for the same chemical compound. Luther et al.[23] demonstrated that α-$CsPbI_3$ QD films can be stabilized in ambient air for months. The device based on α-$CsPbI_3$ QD films showed a high V_{oc} of 1.23 V and a PCE of 10.77%. To further improve film quality of $CsPbI_3$ QDs and increase PCE, the same group developed a surface modification strategy where the A-site cation halide salt (AX: FAI, MAI, FABr, MABr, and CsI) was used to treat $CsPbI_3$ QD films.[24] **Figure 11**a schematically shows the QD film deposition process and AX post-treatment process. $CsPbI_3$ QD films were prepared by the layer-by-layer way by spin

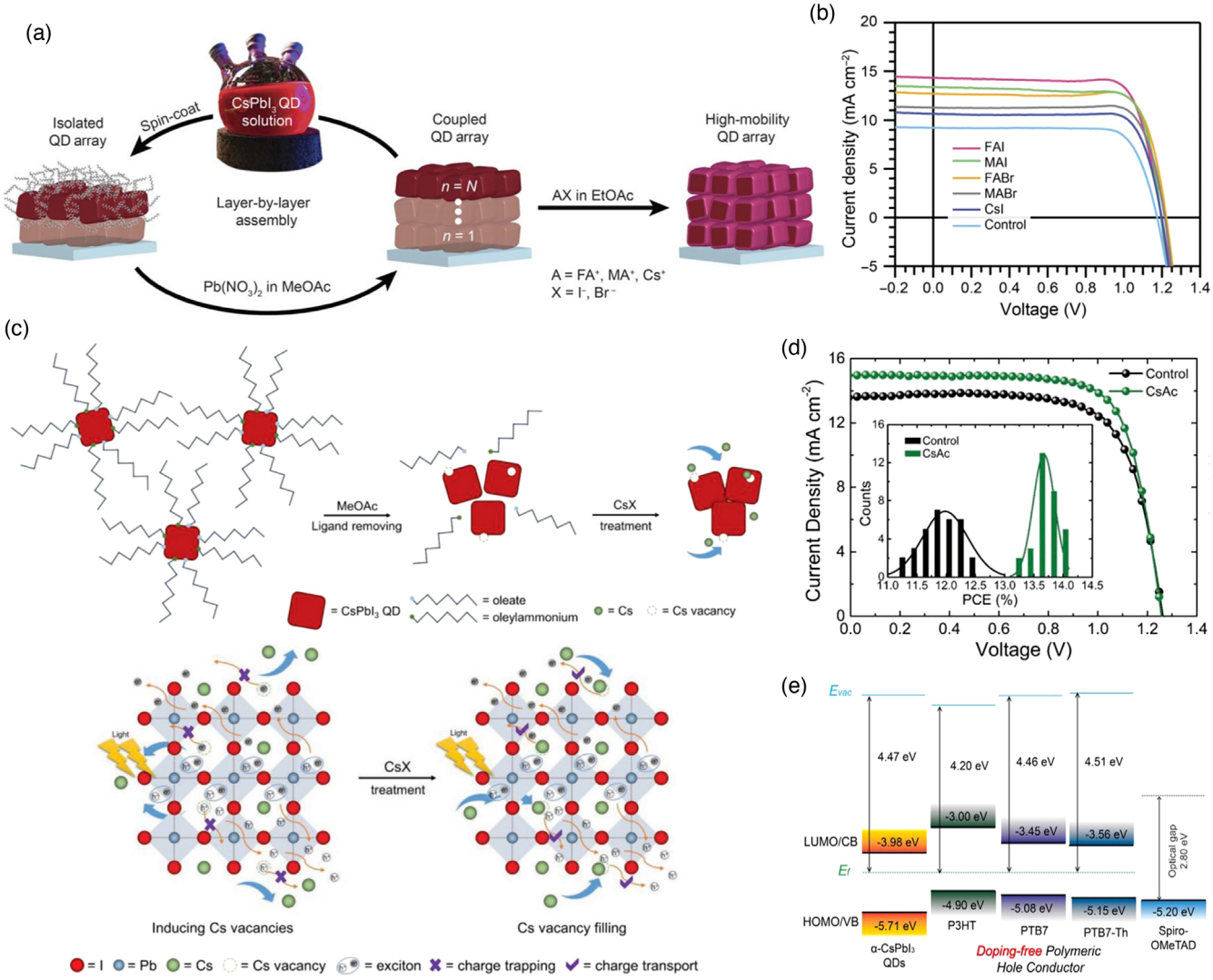


Figure 11. a) Schematic illustration of $CsPbI_3$ QD film preparation process and AX salt post-treatment. b) *J–V* curves of devices based on $CsPbI_3$ QD films post-treated by different AX salts. Reproduced with permission.[24] Copyright 2017, American Association for the Advancement of Science. c) Schematic illustrated diagram of deposition process of $CsPbI_3$ QD film post-treated by CsX (upper part) and filling Cs vacancies by CsX salts and thus defect passivation (bottom part). d) *J–V* curves of the champion PSCs based on $CsPbI_3$ QD films without and with CsAc post-treatment. Reproduced with permission.[82] Copyright 2019, Wiley-VCH. e) Energy-level diagram of MeOAc-treated $CsPbI_3$ QDs and dopant-free polymeric HTMs. Reproduced with permission.[81] Copyright 2018, Elsevier Inc.

© 2020 Wiley-VCH GmbH

coating as-synthesized $CsPbI_3$ QDs in octane. The QD films were immersed into a saturated lead(II) nitrate [$Pb(NO_3)_2$] solution in methyl acetate (MeOAc) after each QD layer to further deposit the next layer. Finally, as-prepared QD films with sufficient thicknesses were treated by immersing them into a saturated AX salt solution in ethyl acetate (EtOAc) for around 10 s. As shown in Figure 11b, the FA-treated device showed the highest PCE of 13.4% among all the investigated devices, which outperformed 8.5% of the control device treated by only neat EtOAc. The improved PCE was attributed to significantly increased carrier mobility and thus carrier transport of $CsPbI_3$ QD film after FAI post-treatment. The AX treatment strategy reported in this work provides an effective method for tuning the electronic properties of $CsPbI_3$ QD films. Apart from organic cation halide salts, Ma et al.[82] developed an efficient surface passivation strategy where a variety of inorganic cesium salts (cesium acetate [CsAc], cesium carbonate [Cs_2CO_3], cesium nitrate [$CsNO_3$], and cesium iodide [CsI]) were used to treat the surface of $CsPbI_3$ QD films. It was found that all the Cs salts can increase device performance. In the present work, CsAc was chosen to investigate the effect of surface treatment on device performance because of its highest performance. The corresponding schematically illustrated diagram of CsAc post-treatment is shown in Figure 11c. First, $CsPbI_3$ QD films with long native insulating ligands were obtained by the spin-coating process. Subsequently, MeOAc orthogonal solvent was used to wash the film to prepare conductive films by removing insulating capping ligands. Finally, as-prepared QD films were treated by saturated CsAc and residual organic ligands were further removed. It was proposed that Cs cations can fill the Cs vacancies and effectively passivate the surface trap states of $CsPbI_3$ QD films. After CsAc treatment, the V_{oc} loss ($E_g - qV_{oc}$) was reduced from 0.525 to 0.505 eV, indicating a successful defect passivation by CsAc. Moreover, the free carrier lifetimes, mobility, and diffusion lengths of QD films were enhanced simultaneously. In a word, the PCE of the device was enhanced from 12.59% to 14.10% after CsAc treatment, which was mainly as a result of improved J_{sc} along with a slightly increased FF, as shown in Figure 11d. To improve the quality of inorganic perovskite nanocrystals (NCs), surface ligand modulation was implemented by a facile hexane/ethyl acetate (MeOAc) solvent treatment method.[121] It was demonstrated that the quality and electric properties of the films were significantly improved by this surface ligand management strategy. As a result, a PCE of 12.2% was delivered for the device based on perovskite $CsPbI_2Br$ NCs treated by hexane/MeOAc. More recently, Ma and coworkers demonstrated a PCE of 14.90% through surface ligand modulation and management.[83] It was found that the secondary amine (di-*n*-propylamine [DPA]) was the optimal among the investigated primary, secondary, and tertiary amine ligands. To overcome the poor carrier transport properties of inorganic perovskite QDs, Liu and coworkers[122] used micrometer-sized graphene (μGR) sheets with a high mobility ($800\,cm^2\,V^{-1}\,s^{-1}$) to crosslink the $CsPbI_3$ QDs (denoted as $CsPbI_3$ QDs-μGR) for normal PSCs using PTAA as HTM. The resultant $CsPbI_3$ QDs-μGR films showed not only improved carrier transport but also enhanced stability (including moisture and thermal stability). The device based on $CsPbI_3$ QDs-μGR exhibited an improved PCE of 11.40% compared with 10.41% of the control device and maintained over 98% of its original PCE after storage in N_2 for 1 month. Apart from enhancing quality of QD films, the PCE of the device based on QD films was increased by the rational energy-level alignment modulation strategy where different polymeric dopant-free HTMs (including P3HT, PTB7, and PTB7-Th) were used to modulate band alignment with inorganic perovskite QDs.[81] The device based on PTB7 HTM achieved a PCE of 12.55% along with an extremely low V_{oc} loss up to 0.45 eV.

3. Deposition and Growth Techniques of Inorganic Perovskite Films

Similar to organic inorganic hybrid perovskites, inorganic perovskite films are fabricated by either solution processing or vacuum processing techniques. Regarding solution deposition technique, one-step or two-step solution deposition method is usually adopted. It is well known that proper deposition techniques are key to fabricate large-sized, defect-less, and compact high-quality inorganic perovskite films.

3.1. Solution Deposition Techniques

One-step solution deposition has been extensively used to prepare inorganic perovskite films for solar cells.[12,22,33] For the one-step approach, perovskite precursor solution is prepared by dissolving the stoichiometric amount of precursor compositions (PbX_2 and CsX) into polar organic solvents (e.g., dimethylformamide [DMF] or dimethyl sulfoxide [DMSO]). Perovskite films were prepared through spin coating the as-prepared precursor solution on the substrates and annealing as-prepared wet films. For the purpose of fabrication of high-quality perovskite films, fabrication conditions (humidity, spin-coating conditions, annealing temperature, substrate temperature, etc.) should be optimized. Compared with one-step deposition method, two-step solution deposition method has received much less attention. As for the two-step method, the first step is to prepare PbX_2 films by spin coating the solution of PbX_2 in DMF or DMSO and the wet films are annealed at an appropriate temperature. In the second step, as-prepared PbX_2 films are dipped into the solution of CsX in poorly polar solvents or the solution of CsX is spin coated on the as-prepared PbX_2 films, which is followed by an additional annealing process to obtain phase-pure highly crystalline inorganic perovskite films. Compared with the one-step deposition method, the thickness of perovskite films is easy to increase to harvest sufficient light to guarantee high J_{sc} for the two-step method. Currently, the two-step deposition approach was usually used for preparing $CsPbIBr_2$ and $CsPbBr_3$ films due to the extremely limited solubility of $PbBr_2$ and CsBr.[123–125]

3.2. Vacuum Deposition Technique

Vacuum deposition makes it possible to precisely control the thickness of inorganic perovskite films according to our requirement. This technique can improve reproducibility of devices by removing artificial uncertain factors. Generally, several vacuum deposition methods have been attempted to prepare inorganic perovskite films, such as sequential evaporation,[126]

© 2020 Wiley-VCH GmbH

coevaporation,[119,127–129] double-layer evaporation,[130] alternative evaporation,[130] etc. Li et al.[126] prepared $CsPbBr_3$ films through sequential evaporation for solar cells and demonstrated a PCE of 8.34% by incorporating $CsPb_2Br_5$ at the interface of $CsPbBr_3$ crystals. It was revealed that the derivative phase can increase the grain size, passivate grain defects, and reduce carrier recombination. Superior stability was reported for the device without any degradation. In the past few years, more efforts have been contributed to optimize the coevaporation approach as compared with other vacuum deposition methods. For example, Troshin and coworkers obtained a PCE of 10.5% based on PSCs with $CsPbI_3$ films prepared by the coevaporation of CsI and PbI_2, which was comparable with 12.1% of $MAPbI_3$ counterpart.[128] Unold and coworkers[119] fabricated γ-$CsPbI_3$ films by means of the coevaporation method and achieved a PCE of 12.5% based on inverted PSCs. Lin and coworkers[129] prepared all-vacuum-deposited $CsPbI_3$ and $CsPbI_2Br$ solar cells and achieved a PCE of 9.4% and 11.8% by combining these films with vacuum-sublimed ETL and HTL, respectively. Taima and coworkers[130] developed an alternate vacuum deposition method of two double layers to prepare $CsPbI_3$ films and demonstrated a PCE of 6.79%. It proved that alternating vacuum deposition can promote the intercalation control of inorganic $CsPbI_3$ films and accordingly improve reproducibility of devices.

3.3. Solvent-Controlled Growth Technique

Nucleation and growth of inorganic perovskites play a critical role in preparation of high-quality inorganic perovskite films and thus efficient and stable solar cells. Rational engineering of precursor solvents and ATSs is key to effectively modulate the nucleation and growth of inorganic perovskites. Regarding precursor solvents, strongly polar solvents (DFM and DMSO) are usually chosen to dissolve the precursor compositions. Poor film quality and small grain size are usually obtained for adoption of pure DMF because easy volatilization of DMF and weak interaction between DMF and Pb^{2+} result in fast crystallization. It was reported in hybrid perovskites that a certain amount of DMSO was usually added into DMF-based perovskite precursor solution to slow down the crystallization of perovskites due to the formation of Lewis acid–base adduct PbI_2·DMSO and high boiling point (189 °C).[131,132] Chen and coworkers[133] investigated the effect of the volume ratio of DMF and DMSO on the morphology and crystallinity of $CsPbI_2Br$ film and accordingly the corresponding device performance. The intermediate phase of CsI–PbX_2–DMSO was demonstrated to be formed during the spin-coating process, which slowed down the perovskite crystallization process. When excess DMSO was used, the quality of as-prepared films was very poor, which was due to large surface tension and significant volume shrinkage during annealing. It indicated that an appropriate amount of DMF was helpful for adjusting the surface energy of the precursor solution and volume change. After optimization, 2:1 of DMF to DMSO was found to be optimal for film quality and device performance. They also revealed that a part of DMSO was beneficial for mass transport. It was proposed that mass transport in the direction perpendicular to the substrate was remarkably affected by solvent evaporation. Considering the prominent effect of spin-coating time on mass transport parallel to the substrate, the effect of spin-coating time on film and device performance was also studied and then the optimal spin-coating time was found to be 120 s. The optimized device with a ratio of DMF and DMSO and 120 s spin-coating time produced a PCE of 14.30%, which maintained 90.33% of its initial PCE after continuous illumination for 500 h and retained 83.58% of its original PCE after heating at 85 °C for 500 h. In addition, You and coworkers[134] adopted the solvent engineering strategy to prepare high-quality and stable α-$CsPbI_3$ films and applied it into solar cells, which achieved a 15.7% PCE and withstood continuous light soaking for over 500 h without any decay. Yang and coworkers found that uniform and [100]-oriented $CsPbI_2Br$ films with large grain sizes can be obtained through the synergistic effect of H_2O and DMSO.[135] It was demonstrated that H_2O molecules were beneficial for desorbing the DMSO molecules and thus the formation of the cubic phase. Finally, the optimized champion device yielded a PCE of 16.47% as well as excellent stability. Except for precursor solvents, ATSs are of great importance to modulate the perovskite crystallization process. It is well known that ATSs can affect nucleation and growth of perovskites through influencing the evaporation rate of DMSO and the appropriate interaction strengths between precursor compositions and ATSs. To date, several ATSs have been developed to prepare inorganic perovskite films, including diethyl ether, chlorobenzene (CB), anisole, ethyl acetate (EtOAc), methyl acetate (MeOAc), toluene, and IPA. Song and coworkers[136] reported a 9.17% PCE based on the $CsPbIBr_2$-based device through the synergistic adoption of ATS (diethyl ether) and organic ion (guanidinium: GA^+) surface passivation strategies. High-quality inorganic perovskite $CsPbIBr_2$ films with an average size of 950 nm were obtained, which showed few GBs and high hydrophobic properties. Excellent moisture and thermal stability were achieved for the devices, which maintained 100% of its original PCE after aging at 100 °C for 100 h. To reduce the toxicity of ATSs and improve further film quality, Dong et al.[137] used a green solvent EtOAc to prepare high-quality $CsPbI_2Br$ films with large grain size and improved surface morphology. All-inorganic PSCs were fabricated through using low-cost stable CEs in combination with removal of unstable and expensive organic HTM, achieving a PCE of 10.0% and an outstanding long-term stability. This work provides an effective strategy for preparing efficient and stable all-inorganic PSCs by low-cost materials and green manufacturing procedures. Chen et al. developed a precise crystal growth control strategy were GTA and ATS were synergistically used to precisely control the crystal growth of $CsPbI_2Br$.[67] This strategy led to a uniform and high-quality $CsPbI_2Br$ films. As shown in **Figure 12**a, a plausible mechanism of the synergistic effect of GTA and ATS was proposed. The transparent films were acquired after spin coating. Without ATS in the spin-coating step, the evaporation rate of DMSO was very slow, resulting in severe nucleation aggregation, solvent edge effects across the entire film, and irregular crystals and stripes along the edge. In contrast, the use of ATS would lead to uniform $CsPbI_2Br$ films because of fast evaporation of DMSO during spin coating. GTA was favorable for obtaining phase-pure α-$CsPbI_2Br$ films. In a word, synergistic use of GTA and ATS was crucial to fabricate high-quality, compact, and large-sized $CsPbI_2Br$ films. The PCE of the device based on GTA was increased from 12.65% to

© 2020 Wiley-VCH GmbH

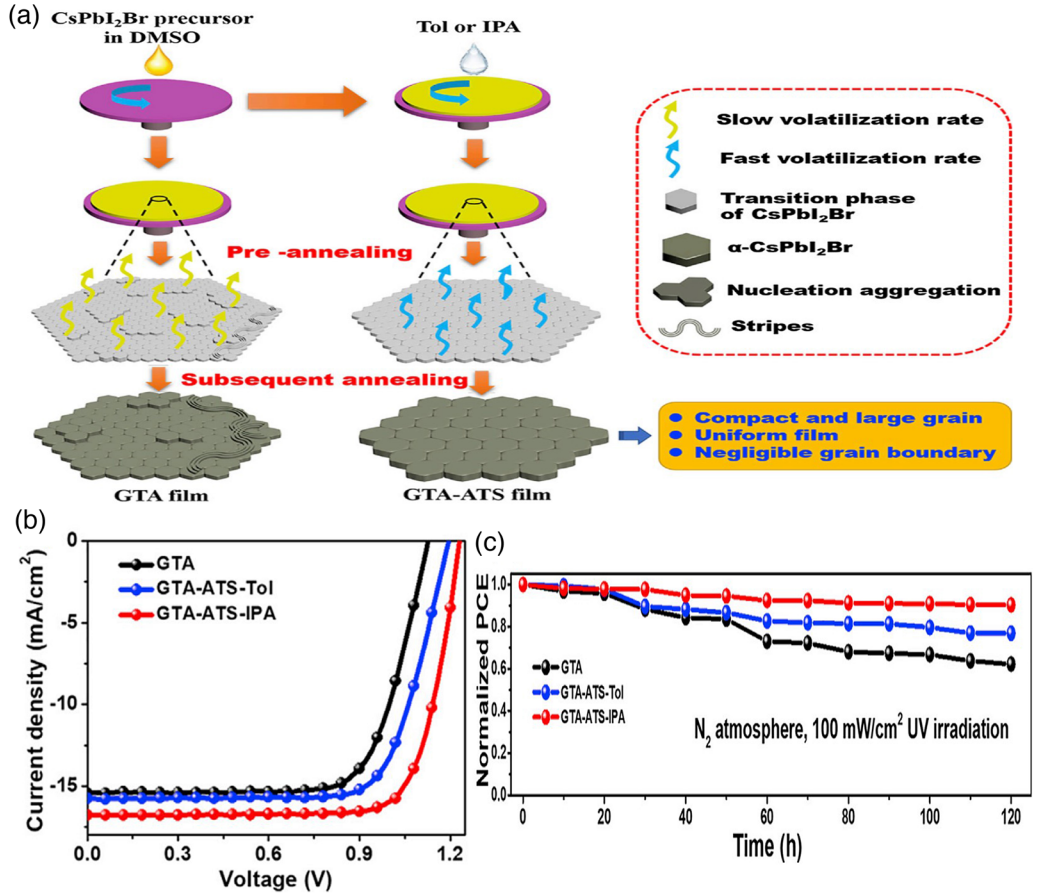


Figure 12. a) Schematically illustrated diagram of $CsPbI_2Br$ perovskite crystallization process based on GTA or GTA–ATS processing. b) *J–V* curves of devices based on the GTA, GTA–ATS–Tol, and GTA–ATS–IPA. c) UV stability of unencapsulated PSCs based on the GTA, GTA–ATS–Tol, and GTA–ATS–IPA perovskite films in N_2 atmosphere. Reproduced with permission.[67] Copyright 2019, Elsevier Inc.

13.82% for the device with GTA–ATS–toluene and 16.07% for the device with GTA–ATS–IPA, as shown in Figure 12b. As shown in Figure 12c, the GTA–ATS–IPA device retained 90% of its original value after UV light irradiation for 120 h whereas 63% and 77% of their original PCEs were maintained for GTA and GTA–ATS–toluene devices, respectively. Zhang et al. developed a mediator–ATS strategy where MAI was introduced into $CsPbI_3$ precursor solution and PCBM was added into CB ATS.[138] It was shown that the incorporation of PCBM in ATS can stabilize the black phase of $CsPbI_3$ by reducing grain sizes. In addition, the added MAI improved the quality of $CsPbI_3$ films through acting as the mediator. Finally, the device based on this strategy exhibited a PCE of 16.04%, which retained 95% of its initial PCE after 1000 h of aging. Moot et al.[139] investigated the effect of different ATSs (including CB, toluene, diethyl ether, anisole, EtOAc, and MeOAc) on the photovoltaic performance of the devices based on $CsPbI_3$. The large difference in PCE was observed for the devices based on different ATSs. The adoption of MeOAc was demonstrated to be the most beneficial for the fabrication of high-quality $CsPbI_3$ films, which was ascribed to the strongest interaction between CsI and MeOAc as compared with the other investigated ATSs. As a result, the best-performing device showed a PCE of 14.4%. This work suggests that interactions not only between perovskite components and precursor solvents but also between perovskite components and ATSs play key roles in perovskite nucleation and crystallization. Consequently, it is highly desirable to fabricate high-quality inorganic perovskite films via the synergistic engineering of precursor solvents and ATSs.

4. Effective Inorganic HTMs in Normal All-Inorganic PSCs

Although the current record PCE was achieved by normal PSCs, the device was fabricated based on organic HTMs. First, the typically used high-performance HTMs (e.g., Spiro-OMeTAD and PTAA) are much more expensive than inorganic HTMs (e.g., CuSCN, NiO_x, CuI, MnS, etc.). Second, organic HTMs themselves were difficult to withstand high temperature ($\geq$ 85 °C).[140] Finally, hygroscopic dopants (e.g., LiTFSI and *t*-BP), which were used to increase the conductivity of organic HTMs, endowed the corresponding PSCs poor moisture stability. Consequently, high cost, poor thermal, and moisture stability induced by use of organic HTMs impede their commercial application. It is important to develop low-cost stable inorganic

© 2020 Wiley-VCH GmbH

HTMs with high hole mobility and well-matched energy levels with perovskite layers to fabricate efficient and stable normal all-inorganic PSCs. To date, a variety of inorganic HTMs have been developed for organic–inorganic hybrid PSCs but their applications in all-inorganic PSCs were extremely scarce.[141] In the past several years, some inorganic HTMs were developed and applied for normal all-inorganic PSCs, such as CuI, Cu_2ZnSnS_4 QDs, $CuInS_2$/ZnS QDs, Cu(Cr,M)O_2 NCs, Co_3O_4, MnS, PbS, PEI–CNT, Ti_3C_2–MXene, etc. The normal all-inorganic PSCs based on different inorganic HTMs are shown in **Table 3**. Zhang and coworkers[35] prepared normal all-inorganic PSCs based on CuI HTM and $CsPb_{0.96}Bi_{0.04}I_3$ absorber (**Figure 13**a), achieving a PCE of 13.21% along with good ambient stability. It was found that CuI possessed a well-matched energy band alignment with perovskites and Au electrode (Figure 13b). In this work, mixed solvents of diisopropyl sulfide and CB were utilized to dissolve CuI to avoid destroying pure diisopropyl sulfide underneath perovskite films. Cu_2ZnSnS_4 (CZTS) widely used for light harvesting materials in thin-film photovoltaics is promising as an alternative HTM due to its high-hole-mobility, low-cost, Earth-abundant, and nontoxic elemental constituents. Wu and coworkers[36] prepared CZTS QDs and USED it as HTM in normal all-inorganic PSCs using $CsPbBr_3$, realizing a PCE of 4.84%, which was comparable with 5.36% of the device based on Spiro-OMeTAD. The device based on CZTS QDs showed excellent air stability without degradation for even over 2500 h whereas about 80% of its initial PCE was retained for the device with Spiro-OMeTAD after only 800 h under the same condition. However, it should be noted that CBM (−4.1 eV) of CZTS QDs was much lower than −3.3 eV of $CsPbBr_3$, which was not beneficial for suppressing electron back transfer from perovskite to CZTS and thus could result in serious nonradiative recombination. In addition, a large energy offset (up to 0.7 eV) between the CBM (−3.3 eV) of $CsPbBr_3$ and −4.0 eV of TiO_2 was still nonbeneficial for electron injection. Therefore, the imperfect energy-level alignment should be overcome for CZTS QDs by the chemical doping strategy. Compared with CZTS QDs, $CuInS_2$/ZnS QDs with wider bandgaps were synthesized as HTMs in carbon-based all-inorganic PSCs based on $CsPbBr_3$ absorber.[143] Bandgaps of $CuInS_2$/ZnS QDs can be tuned from 1.68 to 1.81 eV by adjusting temperatures. The PCE of the device was improved from 6.01% for the control device to 8.42% for 1.81 eV QDs-based device, 7.79% for 1.71 eV QDs-based device, and 6.66% for 1.68 eV QDs-based device. The 1.81 eV QDs showed a better band alignment with the perovskite layer as compared with 1.71 eV QDs and 1.68 eV QDs, which was consistent with its better photovoltaic performance. In addition, the same group achieved a PCE of 9.43% based on $CsPbBr_3$ and carbon-based all-inorganic PSCs, where graphene quantum dots (GQDs) were utilized to modify the TiO_2/$CsPbBr_3$ interface and $CuInS_2$/ZnS QDs was used as HTM.[144] Although band alignment was improved as compared with CZTS QDs, very close CBM between $CuInS_2$/ZnS QDs and $CsPbBr_3$ still would lead to electron back transfer and thus nonradiative recombination. Therefore, it is highly desirable to develop wider-bandgap inorganic HTMs. To this end, Tang and coworkers[37] prepared M-substituted delafossite materials Cu(Cr, M)O_2 NCs ($M = Ba^{2+}$, Ca^{2+}, or Ni^{2+}) to increase the electrical conductivity of $CuCrO_2$. As shown in Figure 13c, the PCE of devices increased gradually abiding by the order of without $CuCrO_2$ < with $CuCrO_2$ < with Cu(Cr,Ni)O_2 < with Cu(Cr,Ca)O_2 < with Cu(Cr,Ba)O_2, which was opposite to the energy offset between VBM of HTMs and VBM of $CsPbBr_3$ following the order of without $CuCrO_2$ > with $CuCrO_2$ > with Cu(Cr,Ni)O_2 > with Cu(Cr,Ca)O_2 > with Cu(Cr,Ba)O_2 (Figure 13d). This indicated that much improved PCE was ascribed to improved band alignment and electrical conductivity. Based on pure $CsPbBr_3$, the device with Cu(Cr,Ba)O_2 demonstrated a PCE of 10.18%, which was much higher than 7.39% of the control device without HTM. The PCE of device with Cu(Cr,Ba)O_2 was further improved to 10.79% after doping Sm^{3+} in $CsPbBr_3$. As shown in Figure 13e,f, excellent moisture (25 °C and 80% RH) and thermal stability (80 °C and 0% RH) were demonstrated for both control and target device with Cu(Cr,Ba)O_2 as reflected by almost unchanged PCEs. The earlier research results show that wide-bandgap delafossite materials are promising in preparing high-efficiency and highly stable all-inorganic normal PSCs, which should be paid more attention to in future.

Apart from Cu-based inorganic HTMs, Wu and coworkers[38] prepared Co_3O_4 NCs as HTMs for the all-inorganic PSCs of

Table 3. Summary of normal all-inorganic PSCs based on different inorganic HTMs. The CBM, VBM, hole mobility, and processing techniques of inorganic HTMs are also summarized.[141]

Perovskites	Inorganic HTMs	CBM [eV]	VBM [eV]	Hole mobility [$cm^2 V s^{-1}$]	Processing methods	PCE [%]	Stability condition	Ref.
$CsPb_{0.96}Bi_{0.04}I_3$	CuI	−2.1	−5.2	9.3[142]	Spin coating	13.21	Ambient condition	[35]
$CsPbBr_3$	Cu_2ZnSnS_4 QDs	−4.1	−5.4	6–30	Spin coating	4.84	Ambient environment, unencapsulated	[36]
$CsPbBr_3$	$CuInS_2$/ZnS QDs	−3.42	−5.23	–	Spin coating	8.42	80% RH and RT, unencapsulated	[143]
$CsPbBr_3$	$CuInS_2$/ZnS QDs	−3.42	−5.23	–	Spin coating	9.43	80% RH and 25 °C	[144]
$CsPb_{1-x}Sm_xBr_3$	Cu(Cr,Ba)O_2 NCs	−2.11	−5.45	–	Spin coating	10.79	25 °C and 80% RH or 80 °C and 0% RH	[37]
$CsPbI_2Br$	Co_3O_4	−1.5	−5.3	–	Spin coating	11.21	–	[38]
$CsPbBr_3$	MnS	−1.60	−5.25	4.50×10^{-1}	Thermal evaporation	8.16	85 °C and 80% RH	[39]
$CsPbI_3$	PbS QDs	−3.83	−5.10	–	Spin coating	7.07	Dry cabinet	[40]
$CsPbI_3$	PEI-CNT	–	–	–	Spin coating	10.55	70% RH and 80 °C	[145]
$CsPbBr_3$	N-CQDs	–	–	–	Spin coating	10.71	85% RH and RT	[146]

© 2020 Wiley-VCH GmbH

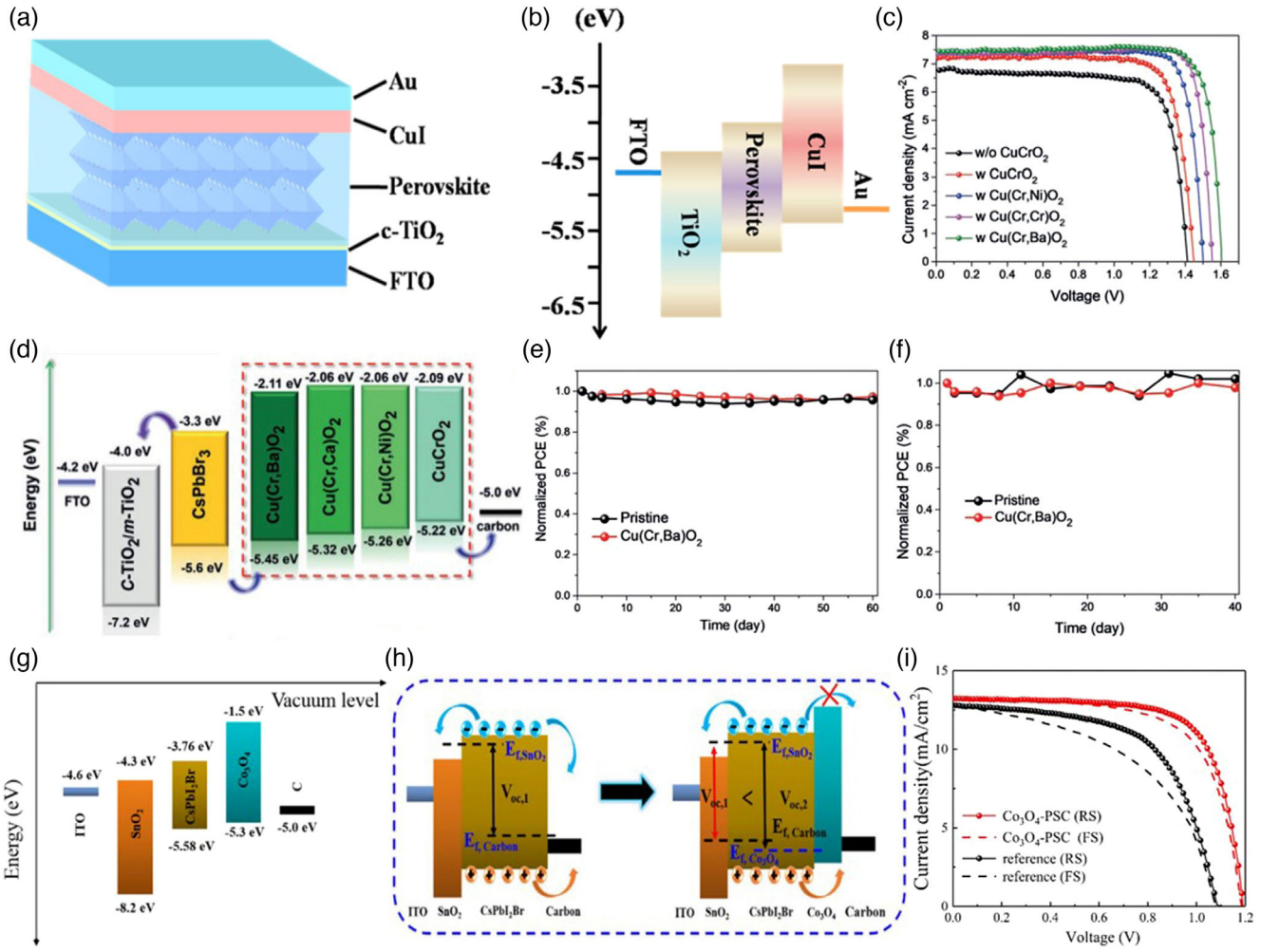


Figure 13. a) The schematically illustrated structure of all-inorganic PSC based on CuI as HTM. b) The schematically illustrated energy-level alignment diagram of all-inorganic PSC based on CuI as HTM. Reproduced with permission.[35] Copyright 2017, American Chemical Society. c) *J*–*V* curves of all-inorganic PSCs without and with different HTMs. d) Schematically illustrated energy band diagram of all-inorganic PSCs showing charge transfer processes. The stability of unencapsulated devices without and with $Cu(Cr,Ba)O_2$ at e) 25 °C and 80% RH and f) thermal stability at 80 °C and 0% RH. Reproduced with permission.[37] Copyright 2019, Wiley-VCH. g) The energy-level diagram of the materials used in all-inorganic PSCs based on Co_3O_4 as HTM. h) Schematically illustrated energy diagram of devices without and with Co_3O_4 HTM showing carrier injection and transfer. Reproduced with permission.[38] Copyright 2019, Wiley-VCH.

ITO/SnO_2/$CsPbI_2Br$/Co_3O_4/carbon. As shown in Figure 13g, the VBM (−5.3 eV) of Co_3O_4 NCs matched well with −5.58 eV of $CsPbI_2Br$ and work function (−5.0 eV) of CE. Meanwhile, the CBM (−1.5 eV) of Co_3O_4 NCs was much higher than −3.76 eV of $CsPbI_2Br$, which can effectively suppress or block back electron transfer. In a word, the relatively perfect band alignment was established after the incorporation of Co_3O_4 NCs HTM between perovskite and CE, which facilitated hole extraction and collection as well as reduced charge recombination at the perovskite/carbon interface. More effective charge separation was confirmed by larger contact potential difference (CPD) both in the dark and under illumination for the $CsPbI_2Br/Co_3O_4$ sample as compared with the $CsPbI_2Br$ sample. As shown in Figure 13h, both electrons and holes can be collected by CEs for HTM-free all-inorganic PSCs. By contrast, only holes can be collected by CEs and the electrons were hindered effectively for all-inorganic PSCs with Co_3O_4 NC HTM. Finally, the device with Co_3O_4 NCs produced a PCE of 11.21%, which was much higher than 9.27% of the control device without Co_3O_4 NC HTM (Figure 13i). Yang and coworkers[39] thermally evaporated a layer of MnS HTM on the $CsPbBr_3$ to fabricate normal all-inorganic PSCs. The VBM (−5.25 eV) of MnS matched well with the VBM (−5.6 eV) of $CsPbBr_3$ and work function (−5.0 eV) of CEs, leading to a cascade band alignment which was favorable for hole extraction and collection. At the same time, the back electron transfer process was effectively suppressed due to a much higher CBM (−1.60 eV) of MnS compared with −3.3 eV of $CsPbBr_3$. They used an evaporation-assisted solution method to fabricate $CsPbBr_3$ films. Namely, $PbBr_2$ layer was prepared by spin coating its solution in DMF and then a different thickness of CsBr was thermally evaporated on the as-prepared $PbBr_2$ films. It was found that CsBr with a thickness of 250 nm gave the best

© 2020 Wiley-VCH GmbH

performance among the investigated thicknesses (100, 150, 200, 250, and 300 nm). The optimized device based on the CE delivered a PCE of 10.45%, which far outperformed 8.16% of the HTM-free device. Moreover, 80% of its initial efficiency was maintained for the device with MnS HTM at 80% RH at 85 °C after 90 days. To reduce the nonradiative recombination at perovskite/carbon interface, Yang et al. developed a polyethyleneimine-functionalized carbon nanotube (PEI/CNT) to modify this interface and demonstrated a PCE of 10.55% outperforming 7.41% of the reference device without the incorporation of PEI/CNT, which was ascribed to enhanced charge extraction and transfer.[145] Moreover, improved stability was demonstrated for the device with PEI/CNT HTM. It was proposed that the coordination interaction between perovskite and PEI molecules probably should be responsible for the increased stability. Dai and coworkers[40] prepared PbS QDs and inserted them between $CsPbI_3$ and Au counter electrode. The VBM (−5.10 eV) of PbS was slightly higher than −5.35 eV of $CsPbI_3$ and was identical to −5.10 eV of Au, which indicated that holes can be extracted by PbS and further collected by Au. The black phase maintained for at least 30 days after introduction of PbS QDs. The device without HTM yielded a PCE of 0.55%. In contrast, a PCE of 7.07% was achieved by the device with PbS as HTM. Compared with Spiro-OMeTAD-based devices, markedly improved moisture stability was demonstrated for PbS-based devices. Although great advancements have been obtained for the development of HTMs available for normal all-inorganic PSCs, the currently obtained PCE is still much lower than that of inorganic PSCs with organic HTMs (e.g., Spiro-OMeTAD and PTAA). Consequently, further efforts should be made to optimize the PCE of normal all-inorganic PSCs based on already-reported inorganic HTMs and develop novel high-performance inorganic HTMs. In addition, in the past, a large amount of attention has been contributed to $CsPbBr_3$-based normal all-inorganic PSCs. However, its efficiency was limited by the wide bandgap (2.3 eV) of $CsPbBr_3$. Consequently, more attention should be devoted to further increase PCE and stability of $CsPbI_3$-based normal all-inorganic PSCs due to its much more appropriate bandgap (1.73 eV). Tang and coworkers[146] prepared monolayer-aligned and large-grained $CsPbBr_3$ perovskite films via precise control of crystallization temperature of $PbBr_2$ films and achieved a PCE of 10.2% based on HTM-free carbon based all-inorganic PSCs. They proposed that residual-stress-induced GBs and defect-induced carrier recombination were minimized due to enlarged lattice volume by 2.18 times. When nitrogen-doped carbon quantum dots (N-CQDs) was inserted between $CsPbBr_3$ layer and carbon counter electrodes, the PCE was further increased from 10.2% to 10.71% with an ultrahigh V_{oc} of 1.622 V, which was attributed to suppressed interfacial nonradiative recombination at perovskite/CE interface. The outstanding long-term moisture stability at 85% RH was demonstrated for the devices with N-CQDs interface modification. The earlier results suggest that carbon-based conductive materials show great potentials in acting as HTMs in normal all-inorganic PSCs. Precise control of chemical interaction between inorganic perovskites and carbon materials is of great importance for further enhancing PCE and stability through chemical doping and functionalization for carbon materials.

5. HTM-free Normal All-Inorganic PSCs

To simplify device fabrication procedure and reduce the device cost, normal HTM-free all-inorganic PSCs based on CEs are fabricated, where absorber materials mainly include $CsPbBr_3$, $CsPbIBr_2$, $CsPbI_2Br$, and $CsPbI_3$. Among them, $CsPbBr_3$ was used the most extensively in HTM-free all-inorganic PSCs based on CEs because of its best stability (**Table 4**). For example, Chen and coworkers fabricated HTM-free all-inorganic PSCs based on $CsPbBr_3$ films, which were prepared by two-step deposition.[147] After the optimization of reaction time and annealing temperature, the device produced a PCE of 5.0%. After 250 h at 80 °C and 30–50% RH, the $CsPbBr_3$-based device degraded by 11.7% whereas the $MAPbI_3$-based device degraded by 59%. Liang et al.[148] also prepared HTM-free all-inorganic PSCs based on CE in conjunction with $CsPbBr_3$ absorber and demonstrated a promising PCE of 6.7%. The holes can be extracted effectively by CEs due to proper energy band alignment, as shown in **Figure 14**a. It was worth noting that no degradation was found for the unencapsulated device based on $CsPbBr_3$ under 90–95% RH for exceeding 90 days whereas both $MAPbI_3$/carbon-based and $MAPbI_3$/Spiro-OMeTAD-based devices degraded to around 10% of their initial PCEs within 30 days and 20 days, respectively (Figure 14b,c). To improve the quality of $CsPbBr_3$ films, Zhong and coworkers[149] developed a novel precursor engineering strategy where cesium acetate (CsAc) and ionic liquid methylammonium acetate (MAAc) were used to increase the concentration of $CsPbBr_3$ precursor solution. Due to the improved light-harvesting capacity and reduced trap states, the champion $CsPbBr_3$-based HTM-free all-inorganic PSC delivered a PCE of 7.37% accompanied by negligible decay upon being attacked by 30–50% RH after 1500 h. Tang and coworkers[125] developed a multi-step solution-processed method to prepare $CsPbBr_3$ films. $CsPb_2Br_5$ ($n \leq 3$), $CsPbBr_3$ ($n = 4$), and Cs_4PbBr_6 ($n \geq 5$) were obtained through tuning the deposition cycle (n) of CsBr solution. The device with $CsPbBr_3$ ($n = 4$) gave the highest PCE of 7.54% among all cycle times. In addition, GQDs were used to modify the TiO_2/perovskite interface, resulting in enhanced electron extraction and reduced charge recombination. The best-performing device achieved a PCE as high as 9.72%. Moreover, 87% and 95% of their initial PCEs were maintained for the HTM-free all-inorganic PSCs after being aged under 90% RH at 25 °C for 130 days and 80 °C at 0% RH for 40 days, respectively. This work implies that the phase purity of inorganic perovskite films plays an important role in the realization of high-efficiency and stable all-inorganic PSCs. Tang and coworkers[150] prepared all CEs (multiwalled carbon nanotubes [MWCNT] and carbon black [CB]) for fabricating all-inorganic PSCs. The highest PCE of up to 7.62% was obtained for the device based on 75:25 wt% of MWCNT : CB as HTM. The device degraded by 5% upon being attacked by 80% RH air atmosphere over 1100 h. The polyaniline/graphite (PANi/G) composites were introduced into CE. It was revealed that improved energy-level alignment and hole extraction resulted in reduced energy loss and charge recombination.[151] After the incorporation of 5 wt% of PANi/G, the work function of CE was lowered from −5.001 to −5.229 eV, which matched well with the VBM (−5.6 eV) of $CsPbBr_3$. As a result, the HTM-free device based on $CsPbBr_3$ yielded a PCE of 8.87%, which was higher than 6.17% of the

© 2020 Wiley-VCH GmbH

Table 4. Summary of HTM-free normal all-inorganic PSCs.

Device configuration	J_{sc} [mA cm^{-2}]	V_{oc} [V]	FF	PCE [%]	Stability condition	Ref.
FTO/c-TiO_2/mp-TiO_2/$CsPbBr_3$/Carbon	5.70	1.29	0.68	5.0	80 °C and 30–50% RH	[147]
FTO/c-TiO_2/mp-TiO_2/$CsPbBr_3$/Carbon	7.40	1.24	0.73	6.7	90–95% RH and 25 °C or 100 °C, unencapsulated	[148]
FTO/c-TiO_2/mp-TiO_2/$CsPbBr_3$/Carbon	7.40	1.22	0.841	7.37	20–25 °C and 30–35% RH	[149]
FTO/c-TiO_2/mp-TiO_2/GQDs/$CsPbBr_3$/Carbon	8.12	1.458	0.821	9.72	90% RH and RT °C or 80 °C and 0% RH	[125]
FTO/c-TiO_2/mp-TiO_2/$CsPbBr_3$/MWCNT/CB	6.84	1.431	0.78	7.62	80% RH and 25 °C	[150]
FTO/c-TiO_2/mp-TiO_2/$CsPbBr_3$/Carbon-PANi/G	6.87	1.59	0.812	8.87	80% RH and 25 °C	[151]
FTO/c-TiO_2/(mp-TiO_2/ZrO_2/Carbon)/$CsPbBr_3$	7.75	1.44	0.735	8.19	–	[152]
FTO/c-TiO_2/mp-TiO_2/$CsPb_{0.97}Sr_{0.03}Br_3$/Carbon	7.71	1.54	0.811	9.63	80% RH and 25 °C	[62]
FTO/c-TiO_2/mp-TiO_2/$CsPb_{0.995}Zn_{0.005}Br_3$/Carbon	7.30	1.560	0.806	9.18	80% RH and 25 °C	[153]
FTO/c-TiO_2/$CsPbIBr_2$/Carbon	9.11	1.142	0.63	6.55	85 °C	[154]
FTO/c-TiO_2/$CsPbIBr_2$/Carbon	10.66	1.245	0.69	9.16	85 °C	[93]
FTO/c-TiO_2/$CsPbIBr_2$/Carbon	11.19	1.253	0.65	9.12	–	[155]
FTO/c-TiO_2/CsBr/$CsPbIBr_2$/Carbon	11.61	1.258	0.62	9.06	–	[156]
FTO/c-TiO_2/$CsPb_{0.995}Mn_{0.005}I_{1.01}Br_{1.99}$/Carbon	13.15	0.99	0.57	7.36	ambient atmosphere, encapsulated	[61]
FTO/c-TiO_2/mp-TiO_2/$CsPb_{0.9}Sn_{0.1}IBr_2$/Carbon	14.30	1.26	0.63	11.33	100 °C, encapsulated	[28]
FTO/ZnO/$CsPbIBr_2$/Carbon	11.60	1.03	0.63	7.60	–	[157]
ITO/SnO_2/$CsPbI_2Br$/Carbon	15.46	1.23	0.64	12.19	100 °C and 45–60% RH, unencapsulated	[43]
ITO/SnO_2/$CsPb_{0.995}Nb_{0.005}I_2Br$/Carbon	12.06	1.20	0.72	10.42	–	[158]
FTO/c-TiO_2/mp-TiO_2/$CsPbI_3$/Carbon	18.5	0.79	0.65	9.5	20–30 °C and 10–20% RH, unencapsulated	[106]
FTO/c-TiO_2/mp-TiO_2/mp-Al_2O_3/$CsPb_{0.96}Sb_{0.04}I_3$/Carbon	14.65	0.73	0.50	5.31	Air atmosphere at RT	[58]
FTO/c-TiO_2/mp-TiO_2/$CsPbI_3$:Br:InI_3/Carbon	15.68	1.20	0.64	12.04	Ambient atmosphere	[42]
FTO/c-TiO_2/mp-TiO_2/$CsPbI_2Br$/CB/Carbon	14.94	1.210	0.73	13.13	–	[44]

control device. Furthermore, the device retained 93.5% of its original efficiency value after being exposed to air with a RH of 80% at 25 °C for more than 50 days. The earlier results show that the modulation of CEs is critical to achieve efficient hole extraction and collection by reducing energy loss. Screen printing technology has widely been used to fabricate fully printable hole-conductor-free triple-layer mesoporous PSC-based CEs, which is appropriate for large-scale commercial production.[53,131] In view of this, Cameron and coworkers[152] fabricated HTM-free all-inorganic PSCs FTO/c-TiO_2/(m-TiO_2/m-ZrO_2/m-carbon)/$CsPbBr_3$ using screen printing technology. The effect of annealing temperatures (100, 200, 300, and 400 °C) of $CsPbBr_3$ films on device performance was systematically investigated. It was found that high annealing temperature was beneficial for the complete conversion from $PbBr_2$ to $CsPbBr_3$ and reducing carrier nonradiative recombination. Finally, the device with 400 °C annealing exhibited the highest PCE of 8.19% among the investigated annealing temperatures. Apart from the optimization of the preparation procedure of $CsPbBr_3$ and CEs, B-site doping of $CsPbBr_3$ was also demonstrated to be effective in improving the photovoltaic performance of $CsPbBr_3$-based HTM-free all-inorganic PSCs. For instance, Tang et al.[62] reported a compositional engineering strategy that divalent hard Lewis acids (Mg^{2+}, Ca^{2+}, Sr^{2+} and Ba^{2+}) were employed to partially substitute the Pb^{2+} in $CsPbBr_3$. It proved that all doping metals can increase PCE but the increase amplitude was different. The authors proposed that improved PCE was due to enlarged grain sizes and inhibited the formation of point defects in perovskite films. The champion $CsPb_{0.97}Sr_{0.03}Br_3$-based device demonstrated a PCE of 9.63%, which was much higher than 7.25% for the control device based on pristine $CsPbBr_3$. Over 95% of its initial PCE was retained for the $CsPb_{0.97}Sr_{0.03}Br_3$-based device under 80% humidity at 25 °C after 800 h. The same group reported a PCE of 9.18% for the all-inorganic $CsPb_{0.995}Zn_{0.005}Br_3$ PSC based on compositional engineering strategy where divalent transition metal ions (Mn^{2+}, Ni^{2+}, Cu^{2+}, and Zn^{2+}) were used to partially replace Pb^{2+} in $CsPbBr_3$.[153] It was demonstrated that enlarged grain sizes and reduced defect density should be responsible for improved PCE.

Except for $CsPbBr_3$, $CsPbIBr_2$ with a wider bandgap is also used as an absorber in HTM-free all-inorganic PSCs, which is expected to obtain higher J_{sc}. Zhang and coworkers[154] demonstrated that the crystallization kinetics of $CsPbIBr_2$ film prepared by the one-step solution deposition method was greatly affected by the aging time of precursor solution. They found that PCE gradually increased from 0 week to 3 weeks. The annealing temperature was reduced from about 300–100 °C. It was proposed that more CsI–$PbBr_2$ clusters can be formed and act as nucleation sites of $CsPbIBr_2$ grains because more DMSO molecules are pushed out from $PbBr_2$ interlayers of CsI–$PbBr_2$–DMSO

© 2020 Wiley-VCH GmbH

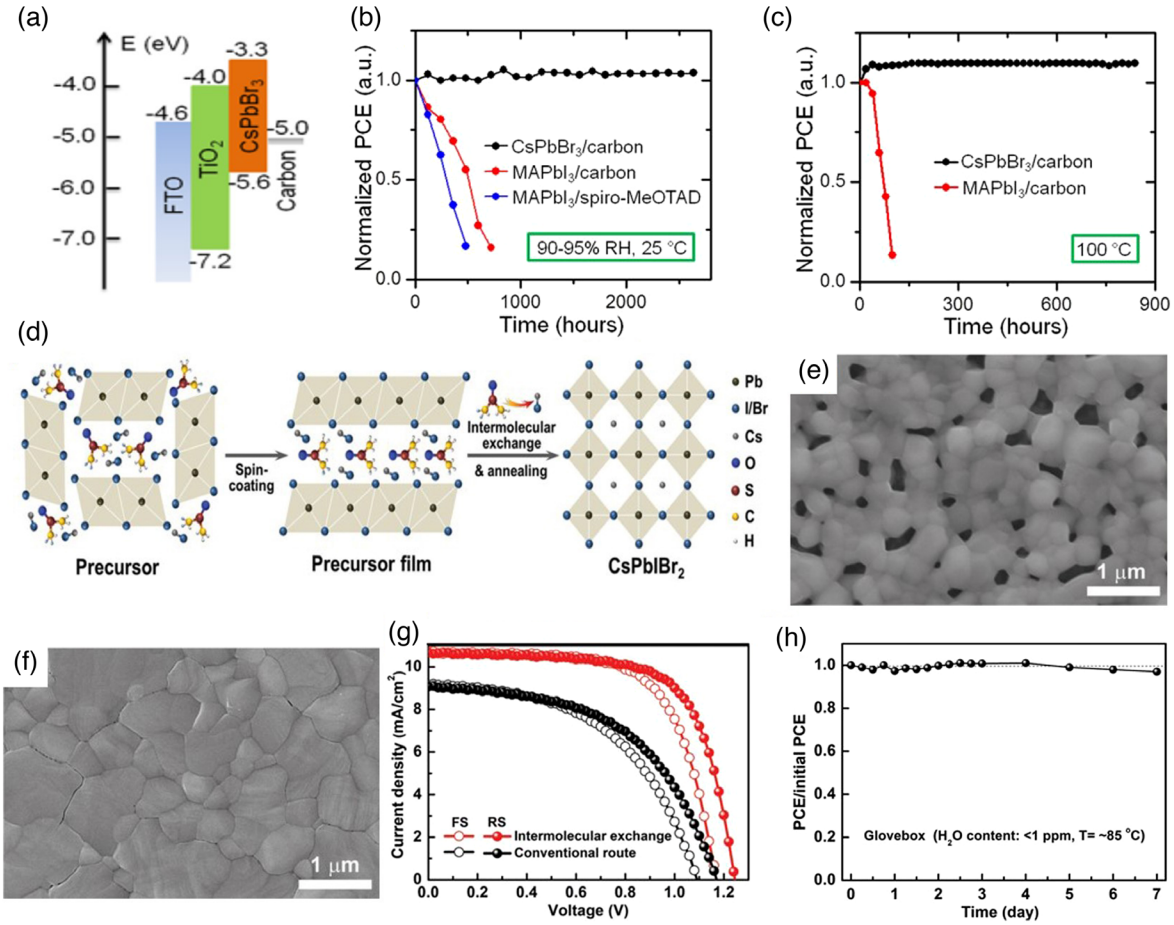


Figure 14. a) Energy-level diagram of the components in the HTM-free all-inorganic PSCs. b) Moisture and c) thermal stability of $CsPbBr_3$/carbon based all-inorganic PSCs, $MAPbI_3$/carbon-based, and $MAPbI_3$/Spiro-OMeTAD-based hybrid PSCs at 90–95% RH at 25 °C and 100 °C, respectively. Reproduced with permission.[148] Copyright 2016, American Chemical Society. d) Schematic illustration of intermolecular exchange strategy in this work. SEM images of $CsPbIBr_2$ film prepared by e) conventional route and f) intermolecular exchange strategy. g) *J–V* curves of devices fabricated through conventional route and intermolecular exchange strategy measured under simulated AM 1.5 G illumination in forward scan (FS) and RS, respectively. h) PCE evolution of the unencapsulated device based on intermolecular exchange strategy upon the persistent attack of around 85 °C. Reproduced with permission.[93] Copyright 2018, Wiley-VCH.

complexes upon prolonging the aging time of precursor solution. The all-inorganic PSC based on $CsPbIBr_2$ film and prepared by precursor solution aged for 3 weeks delivered a PCE of 6.55% along with excellent thermal and moisture stability. To improve quality of $CsPbIBr_2$ films, Zhang and coworkers developed an intermolecular exchange strategy to prepare high-quality $CsPbIBr_2$ films.[93] In this strategy, DMSO in DMSO–$PbBr_2$ can be exchanged by CsI. Figure 14d schematically shows the formation process of $CsPbIBr_2$ films based on the intermolecular exchange strategy. First, the wet films which were composed of CsI–$PbBr_2$–DMSO complexes were obtained by spin-coating precursor solution containing 1 M CsI and 1 M $PbBr_2$ in DMSO. Second, the intermolecular exchange of DMSO by CsI would take place during the spin coating of CsI solution onto as-prepared wet films, which was due to the higher affinity of CsI for $PbBr_2$ than DMSO. Finally, the annealing process at 280 °C for 10 min was required to acquire phase-pure and highly crystalline $CsPbIBr_2$ films. The large voids and poor surface coverage were observed in $CsPbIBr_2$ films with small-sized grains prepared by the conventional route, which was possibly due to extremely slow perovskite crystallization (Figure 14e). In contrast, uniform and compact $CsPbIBr_2$ films with large-sized grains were obtained based on intermolecular exchange strategy (Figure 14f). The significantly improved perovskite crystallinity was found for $CsPbIBr_2$ films prepared by the intermolecular exchange strategy as compared with those by the conventional route, as confirmed by XRD results. As shown in Figure 14g, the device based on the intermolecular exchange strategy presented an improved PCE from 5.49% to 9.16% in comparison with the control device with the conventional route. The device based on the intermolecular exchange strategy presented superior thermal stability because 97% of its original PCE was retained after being thermally aged at 85 °C in a glovebox with water content less than 1 ppm for over 7 days, as shown in Figure 14h. Generally, the pinholes in perovskite films are thought to be detrimental to device performance. However, Zhang and coworkers[156] came to a different conclusion in all-inorganic PSCs based on CE where pinholes were favorable

© 2020 Wiley-VCH GmbH

for suppressing carrier nonradiative recombination through forming desirable crystalline grains, The device based on $CsPbIBr_2$ films with benign pinholes yielded a PCE of 9.06%, which was much higher than 6.19% of the reference device without pinholes. Zhang and coworkers[155] developed a recycle strategy which enabled the simultaneous achievement of PCE enhancement and cost saving. The champion device based on this recycle strategy produced a PCE of 9.12% due to the suppressed halide separation and reduced defects.

$CsPbI_2Br$ with a narrower bandgap as compared with $CsPbIBr_2$ and $CsPbBr_3$ was also attempted in normal all-inorganic PSCs.[43,158] Zhang and coworkers[43] revealed that intermediate CsBr was easy to form in $CsPbI_2Br$ films due to its low solubility, which had a great effect on the crystalline quality of $CsPbI_2Br$ films. They proposed a lead-excess strategy (like excess PbI_2, $PbBr_2$, $PbCl_2$, and $Pb(SCN)_2$) to solve the earlier issue. Based on the nonstoichiometric strategy, significantly improved crystallinity and grain size were obtained compared with the stoichiometric one. In the end, the all-inorganic PSC based on the nonstoichiometric $CsPbI_2Br$ film achieved a PCE of 12.19%, which much outperformed 9.50% of the reference device with the stoichiometric one. Meanwhile, much better long-term stability was also demonstrated for the nonstoichiometric-based device relative to control device. In addition, Ma and coworkers[158] incorporated niobium (Nb^{5+}) into $CsPbI_2Br$ and found that the phase stability of $CsPbI_2Br$ can be remarkably improved by Nb^{5+} incorporation. The device based on $CsPb_{0.995}Nb_{0.005}I_2Br$ films and CE delivered a high PCE of 10.42%, which was much higher than 9.05% of the control device.

$CsPbI_3$ with the most suitable bandgap was also applied into HTM-free all-inorganic PSCs.[42,58,106] Chen and coworkers.[106] stabilized the black phase of $CsPbI_3$ through the adoption of $HPbI_3$ as precursor composition instead of PbI_2. The bandgap of $CsPbI_3$ prepared by $HPbI_3$ was reduced from 1.72 eV for $CsPbI_3$ processed by PbI_2 to 1.68 eV, which was due to the existence of tensile lattice strain. As shown in **Figure 15**a, a PCE of 9.5% was achieved for the device based on $CsPbI_3$ prepared by $HPbI_3$, which retained over 90% of its initial PCE after being stored in dry air for 3000 h. In contrast, the very poor stability was observed for reference device based on PbI_2 under the same conditions, as shown in Figure 15b. Apart from the use of $HPbI_3$,

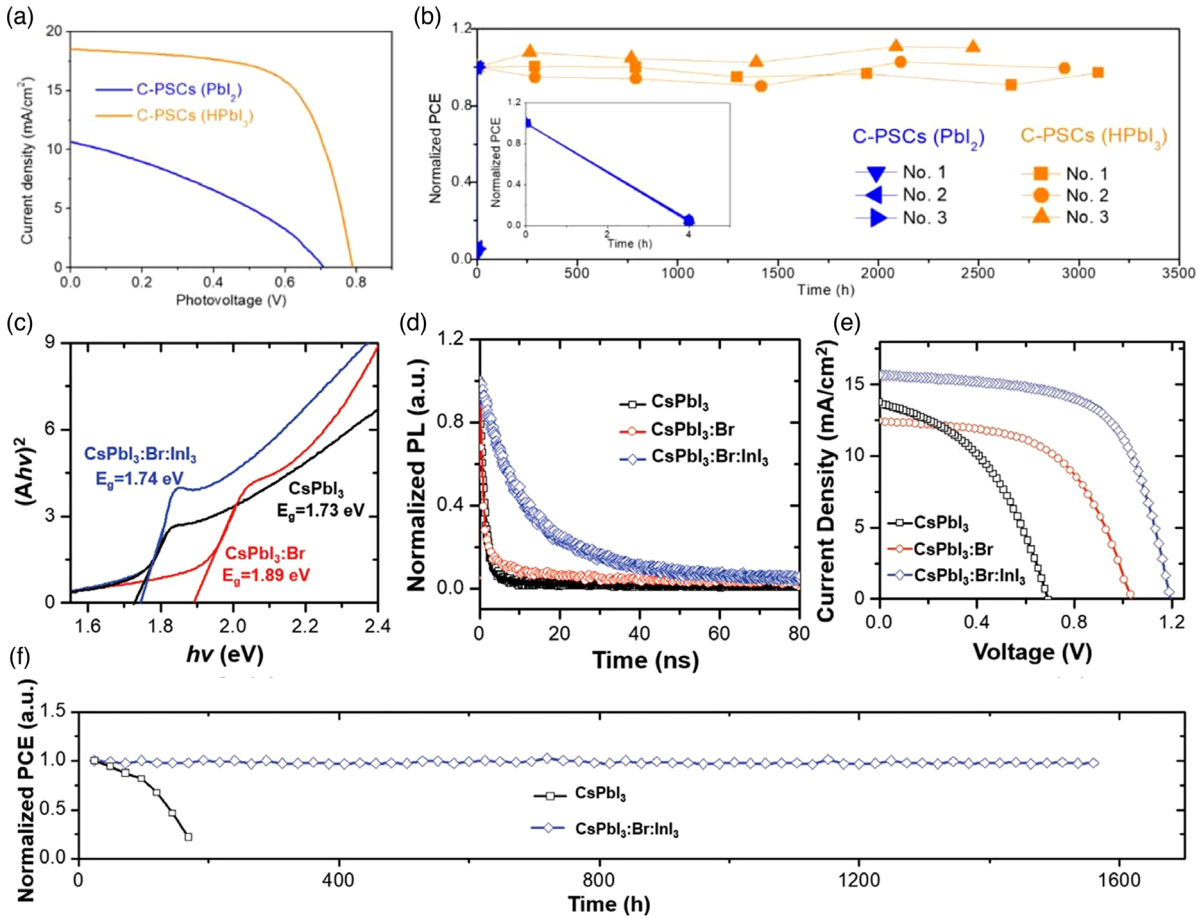


Figure 15. a) $J-V$ curves of the devices based on PbI_2 and $HPbI_3$. b) PCE as a function of aging time for the devices based on PbI_2 and $HPbI_3$ when being exposed to dry air with RH of 10–20% at 20–30 °C. Reproduced with permission.[106] Copyright 2018, American Chemical Society. c) $(Ah\nu)^2$ versus $h\nu$ curves and d) TRPL decay of $CsPbI_3$, $CsPbI_3$:Br, and $CsPbI_3$:Br:InI_3 films. e) $J-V$ characteristics of the devices based on $CsPbI_3$, $CsPbI_3$:Br, and $CsPbI_3$:Br:InI_3 films. f) Normalized PCEs of the devices based on $CsPbI_3$ and $CsPbI_3$:Br:InI_3 depending on aging time in ambient conditions. Reproduced with permission.[42] Copyright 2019, Wiley-VCH.

© 2020 Wiley-VCH GmbH

compositional engineering was also implemented for $CsPbI_3$ to improve phase stability and film quality. Chen and coworkers[58] conducted doping of Sb^{3+} for $CsPbI_3$ and phase stability along with film morphology were improved. As a result, the normal HTM-free all-inorganic PSCs based on $CsPb_{0.96}Sb_{0.04}I_3$ produced a PCE of 5.18% coupled with a nonstoichiometric strategy and maintained 93% of its original PCE after storage in air conditions for 37 days. In addition, Lou and coworkers[42] developed a defect engineering strategy where Br and InI_3 were simultaneously incorporated into $CsPbI_3$ to obtain $CsPbI_3$:Br:InI_3. As shown in Figure 15c, the bandgap of perovskite films was increased from 1.73 eV for pristine $CsPbI_3$ to 1.89 eV for $CsPbI_3$:Br and to 1.74 eV for $CsPbI_3$:Br:InI_3, which was indicative of the effective balance of bandgap after the simultaneous introduction of Br and InI_3. After incorporation of Br and InI_3, carrier nonradiative recombination was markedly suppressed as revealed by prominently increased carrier lifetimes for both fast decay lifetime and slow decay lifetime (Figure 15d). As shown in Figure 15e, the PCE of the device was increased from 4.12% for the control device to 7.22% as a result of much increased V_{oc} along with slightly reduced J_{sc} for the device with Br and further to 12.04% as a consequence of the significantly enhanced V_{oc} and J_{sc} for the device with Br and InI_3. More importantly, remarkably, improved ambient stability was demonstrated for the device incorporating Br^- and In^{3+} in comparison with the control device (Figure 15e). Yang et al. achieved a high PCE of up to 13.13% through incorporating CB at perovskite/CE interface. It was revealed that CB-$CsPbI_2Br$ bulk heterojunction was formed after its diffusion from CB or CE layer to the perovskite layer, which facilitated hole extraction.

As discussed earlier, narrow-bandgap $CsPbI_3$ and $CsPbI_2Br$ can achieve slightly higher PCEs because of higher J_{sc} as compared with wide-bandgap $CsPbIBr_2$ and $CsPbBr_3$, as shown in Table 4. Nevertheless, a much worse stability was demonstrated for the HTM-free inorganic devices based on $CsPbI_3$ and $CsPbI_2Br$ compared with $CsPbIBr_2$ and $CsPbBr_3$, which was ascribed to the very poor phase stability of the former. Consequently, improving phase stability of $CsPbI_3$ and $CsPbI_2Br$ is key to maximize the potentials of J_{sc} and thereby maximize the potentials of PCE as well as stability. Considering their preferable bandgaps, it is an important research direction to further increase the PCE of $CsPbI_3$ and $CsPbI_2Br$-based HTM-free all-inorganic PSCs through stabilizing the black phase and improving film quality via defect passivation. Finally, it should be pointed out that inorganic HTMs are probably needed to improve hole extraction, overcome large energy barrier at perovskite/CE interface, and suppress interfacial nonradiative recombination.

6. Effective Inorganic ETMs in Inverted All-Inorganic PSCs

To fabricate NiO_x-based inverted all-inorganic PSCs, the organic functional layers (PCBM ETL and BCP cathode interlayer) in typical NiO_x-based inverted PSCs should be removed. In this device structure, the development of available inorganic ETMs is critical to achieve efficient and stable NiO_x-based inverted all-inorganic PSCs. For this purpose, some inorganic ETMs have been developed and attempted in NiO_x-based inverted all-inorganic PSCs, as shown in **Table 5**. Mai and coworkers[45] prepared inverted ETL-free all-inorganic PSCs with a structure of FTO/NiO_x/$CsPbIBr_2$/Au, achieving a low PCE of 1.3%, which was considered to be due to poor interface contact between perovskite layers and Au electrodes. To address the poor contact issue, MoO_x buffer layer was inserted between perovskite layers and Au electrodes. It was proposed that $CsPbIBr_2$/Au Schottky barrier hindered the electron extraction. The incorporation of the proper thickness of MoO_x buffer layer can improve electron extraction and increase built-in electric field. As a result of the reduced interfacial nonradiative recombination, the best-performing device exhibited a significant PCE enhancement up to 5.52% as compared with the device without ETL. However, a large hysteresis was observed for the device with MoO_x buffer layer. Yuan and coworkers[50] developed a wide-bandgap CeO_x ETL for inverted NiO_x-based inverted all-inorganic PSCs. The energy band alignment and accordingly electron extraction were improved after using CeO_x ETL in comparison with the commonly used PCBM ETL. A PCE of 5.60% was demonstrated for the device with CeO_x ETL. Apart from MoO_x and CeO_x,

Table 5. Summary of inverted all-inorganic PSCs based on various inorganic ETMs. The CBM, VBM, electron mobility, and processing techniques of inorganic ETMs are also summarized.

Perovskites	ETMs	CBM (eV)	VBM (eV)	Electron mobility [$cm^2 V s^{-1}$]	Processing methods	PCE (%)	Stability condition	Ref.
$CsPbIBr_2$	MoO_x	−4.0	−7.8	–	Thermal evaporation	5.52	160 °C and 30–40% RH	[45]
$CsPbIBr_2$	CeO_x	−4.02	−7.52	–	Spin coating	5.60	40–45 °C and 45–50% RH	[50]
$CsPbI_2Br$	C-TiO_2	−3.63	−7.25	–	Spin coating	14.0	One sun, 45 °C and N_2, encapsulated	[51]
$CsPbI_2Br$	C_{60}	−4.5[159]	−6.2[159]	–	Thermal evaporative	10.4	–	[46]
$CsPbI_2Br$	ZnO@C_{60}	–	–	–	Spin coating	13.74	60 °C and ≈50% RH	[47]
$CsPbI_2Br$	ZnO@C_{60}	–	–	–	Spin coating	13.3	85 °C in N_2	[48]
$CsPbI_2Br$	ZnO@C_{60}	–	–	–	Spin coating	15.19	60 °C in N_2	[160]
$CsPbI_2Br$	ZnO@C_{60}	–	–	–	Spin coating	12.6	–	[161]
$CsPbI_{2.8}Br_{0.2}$	ZnO@C_{60}	−4.25[a)]	−7.41[a)]	–	Spin coating	16.10	–	[49]

[a)]The CBM and VBM are from pure ZnO instead of ZnO@C_{60}.

© 2020 Wiley-VCH GmbH

Chen and coworkers prepared carbide-metal oxides (C-MOXs: C-TiO_2, C-In_2O_3, C-SnO_2, and C-ZnO) and applied them into inverted NiMgLiO-based inverted all-inorganic PSCs with a structure of FTO/NiMgLiO/$CsPbI_2Br$/C-MOX/Bi/Ag.[51] It was found that C-ZnO can destroy the $CsPbI_2Br$ layer via the reaction between C-ZnO and $CsPbI_2Br$ layer. The devices delivered an average PCE of 13.71% for C-TiO_2, 11.34% for C-SnO_2, 10.67% for C-In_2O_3, and 6.24% for C-ZnO. The champion device based on C-TiO_2 gave the highest PCE of 14.0%, which was attributed to its optimal band alignment and appropriate conductivity. Furthermore, the C-TiO_2-based device demonstrated an excellent thermal and light stability, which maintained 92.1% and 95.1% of their initial PCEs after aging at 85 °C in N_2 or under 1 sun and 45 °C in N_2 for 1000 h, respectively. Bian and coworkers[46] developed a RT solvent (DMSO) annealing treatment method to prepare $CsPbI_2Br$ for the inverted structure of ITO/NiO_x/RT-$CsPbI_2Br$/C_{60}/BCP/Ag. As a result, PCEs of 6.4% and 10.4% were achieved for the devices based on $CsPbI_2Br$ films prepared at RT and 120 °C, respectively. Finally, the flexible $CsPbI_2Br$-based device was fabricated and a PCE of 7.3% was realized.

In the past few years, ZnO@C_{60} bilayer ETL was demonstrated to be the most effective in inverted all-inorganic PSCs. For example, Mai and coworkers[48] fabricated an inverted all-inorganic PSC with a device configuration of FTO/NiO_x/$CsPbI_2Br$/ZnO@C_{60}/Ag, where ZnO@C_{60} bilayer acted as effective ETL. The device showed a champion PCE as high as 13.3% and a stabilized power output of about 12%. The unencapsulated device retained 80% of its initial value after being heated at 85 °C for 360 h. Subsequently, the same group developed an effective strategy to stabilize the black phase of $CsPbI_2Br$ by inhibiting the formation of yellow-phase (δ-phase) perovskite.[47] They demonstrated that the improved phase stability was ascribed to the structural reconstruction of $CsPbI_2Br$ perovskite induced by codoping of In^{3+} and Cl^-. Taking a novel thermal radiation heating method together, the best device yielded a PCE of 13.74% for an active area of 0.09 $cm^2$and 11.4% for an active area of 1.0 cm^2. The device with codoping of In^{3+} and Cl^- presented improved moisture and thermal stability compared with the control device. The same group developed a codoping strategy where tris(pentafluorophenyl)borane (TPFPB) and nonhygroscopic lithium salt ($LiClO_4$) were introduced to dope C_{60} ETL.[160] First, the effect of TPFPB concentrations on device performance was investigated. The device based on 4 wt% of TPFPB doping produced a PCE of 15.0%, much higher than that of control device without doping, which was mainly as a result of significantly increased V_{oc} (**Figure 16**a). The improved PCE was largely due to improved electron extraction after TPFPB doping, as shown in Figure 16b. Upon the further doping of $LiClO_4$, the champion device achieved a promising PCE of 15.19% along with slight hysteresis (Figure 16c) and exhibited excellent ambient stability, which maintained about 91.8% of its original PCE after storage in nitrogen environment. A PCE of 12.6% was achieved for the all-inorganic $CsPbI_2Br$ PSCs with a configuration of FTO/NiO_x/$CsPbI_2Br$/ZnO@C_{60}/Ag, where the NiO_x layer was prepared by direct current (DC) reactive magnetron sputtering.[161] Jen and coworkers[49] prepared high-quality $CsPbBr_xI_{3-x}$ films based on a defect passivation strategy where 6TIC-4F Lewis base molecules were incorporated into ATS CB. The electrons can be allowed to transfer from perovskite to ZnO through 6TIC-4F because of favorable energy band alignment. It was proposed that C–N groups in 6TIC-4F molecules were expected to interact with undercoordinated Pb^{2+} (halide vacancies), which can effectively reduce defect density of perovskite films and thereby suppress nonradiative recombination. As a result, the PCE was increased from 13.90% for the control device to 16.10% for the device with 6TIC-4F passivation. It has to be highlighted that long-term stability data were not given in this work. Although a much higher PCE was achieved based on $CsPbI_{2.8}Br_{0.2}$ with low Br content as compared with $CsPbI_2Br$ or $CsPbIBr_2$ with high Br content, the poor device stability resulting from poor phase stability still hinders the further development of the corresponding all-inorganic PSCs based on $CsPbBr_xI_{3-x}$ containing a low content of Br. Except for the poor phase stability of perovskites, the unavoidable chemical reaction between perovskite and ZnO is possibly one of the important reasons of poor device stability although all-inorganic PSCs were fabricated.[49] Consequently, the phase stability of $CsPbBr_xI_{3-x}$ containing a low content of Br and unexpected interfacial chemical reaction of perovskite and ZnO should be addressed urgently in future research work to achieve highly efficient and stable inverted all-inorganic PSCs.

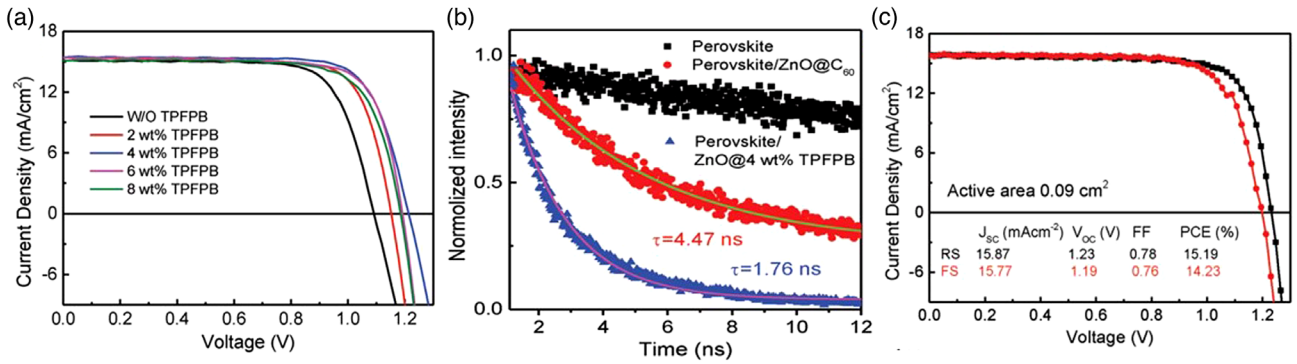


Figure 16. a) *J–V* curves of the devices based on different concentrations of TPFPB dopant. b) TRPL spectra of the perovskite films when were contacted with different ETLs. c) *J–V* curves of the champion all-inorganic PSC based on C_{60} doped by 4 wt% TPFPB and 0.01 wt% $LiClO_4$. Reproduced with permission.[160] Copyright 2020, Wiley-VCH.

© 2020 Wiley-VCH GmbH

7. Interface Engineering for Optimizing Efficiency of All-Inorganic PSCs

Interfaces in all-inorganic PSCs are closely associated with PCE and stability.[54] Rational interface engineering can effectively passivate interfacial defects, modulate interfacial energy-level alignment, and suppress interfacial reactions and/or ion migration, finally contributing to further improvement of both PCE and stability. For example, Ma and coworkers[162] passivated the SnO_2 ETL by spin coating $SnCl_2$ solution onto as-prepared SnO_2 films. Improved electron extraction and suppressed interfacial nonradiative recombination were demonstrated after $SnCl_2$ treatment. The PCE was increased from 4.73% to 7.00% after $SnCl_2$ treatment. Moreover, the unencapsulated all-inorganic PSCs based on $CsPbIBr_2$ maintained 95.5% of its initial efficiency after aging at 90 °C. In addition, Zhang and coworkers used a thin layer of TiO_2 to modify $CsPbIBr_2/SnO_2$ interface, where TiO_2 layer was prepared by atomic layer deposition (ALD).[94] After the interface modification by TiO_2 layer, crystallization and morphology of perovskite films were improved. The CBM (−4.00 eV) of TiO_2 was located between the CBM (−4.43 eV) of SnO_2 and the CBM (−3.49 eV) of $CsPbIBr_2$, which indicated that cascade band alignment was established after the incorporation of TiO_2 layer. Improved band alignment should be responsible for enhanced electron extraction. Finally, the carbon-based all-inorganic PSCs with TiO_2 layer modification showed a remarkable PCE improvement from 6.11% to 9.31% as compared with the reference device. Deng et al. introduced KOH to improve the $SnO_2/CsPbI_2Br$ interface, which can enable the fabrication of high-quality perovskite films and carbon-based all-inorganic PSCs.[163] The work function (−4.25 eV) of SnO_2 was reduced to −4.16 eV after KOH modification, leading to a reduced interfacial energy barrier, which was beneficial for interfacial charge extraction. The authors proposed that halide ion migration and vacancy defect formation were effectively suppressed via forming KBr compounds. As a result, the all-inorganic PSCs with KOH modification delivered a high PCE of 11.78% for an active area of 0.09 cm^2 and 9.34% for an active area of 1.0 cm^2, which dramatically outperformed 9.36% of the control device. Tang and coworkers[164] synthesized a series of $CsPbI_{3-x}Br_x$ NCs to modify $CsPbBr_3$/carbon interface. It was found that the PCE was improved for all $CsPbI_{3-x}Br_x$ NCs regardless of the ratio of I with Br, but the best performance was obtained for $CsPbI_3$ NCs without Br. The all-inorganic PSC with $CsPbI_3$ NCs achieved a champion PCE of 9.45%, which was prominently higher than 5.26% of the control device without any modification.

Compared with the optimization of phase stability of inorganic perovskites and development of inorganic charge transport materials (CTMs), extremely less attention was devoted to increasing device performance through interface engineering in all-inorganic PSCs on whether normal or inverted structures. Considering the high annealing temperature of inorganic perovskite films, it is still a huge challenge to engineer the perovskite/ETL interface for normal devices and perovskite/HTL interface for inverted devices through incorporating organic molecules. Regarding this, inorganic interfacial modifiers could be preferred. However, organic interfacial modifiers are allowed for up interface. Anyway, multifunctional interfacial modifiers should be developed to simultaneously achieve multiple functions, such as defect passivation, energy band alignment modulation, interfacial reactions ion migration suppression, etc. In a word, interface engineering should receive significant attention in the future research work to maximize the potentials of PCE and stability of all-inorganic PSCs through minimizing interfacial nonradiative recombination losses.

8. Large-Area All-Inorganic PSCs

Although huge progresses have been made on small-area all-inorganic PSCs in the past few years, works on large-area all-inorganic PSCs are extremely limited. Liu and coworkers have attempted to fabricate large-area all-inorganic PSCs.[47,160] They demonstrated a PCE of 11.4% based on inverted all-inorganic $InCl_3$:$CsPbI_2Br$ PSCs with an active area of 1.00 cm^2.[47] The same group achieved a PCE of 14.44% (1.00 cm^2) and 12.19% (10.92 cm^2) based on the inverted structure of $FTO/NiO_x/CsPbI_2Br/ZnO@C_{60}/Ag$ via a codoping strategy.[160] In the future, great attention should be focused on developing procedures and technologies of all-inorganic PSCs to speed up the commercialization of PSCs. The accumulated successful experiences in large-area hybrid PSCs should be directly transferred to facilitate the development of large-area all-inorganic PSCs.

9. Conclusion and Outlook

Although a certified record PCE as high as 25.2% has been achieved, the PSCs based on organic inorganic hybrid perovskites in combination with organic HTMs still suffer from poor long-term operational stability, which is expected to be overcome by the development of all-inorganic PSCs. In the past several years, great efforts have been made to increase the PCE and stability of all-inorganic PSCs. To this end, the phase instability of inorganic perovskites should be addressed first. It is well known that either increasing Goldschmidt tolerance factor value or enhancing the activation energy barrier of phase transition (from black phase to yellow phase) can effectively stabilize the black phases of inorganic perovskites.

To date, various strategies have been explored to stabilize the black phase of inorganic perovskites, such as B-site substitution, X-site substitution, intermediate with hydroiodic acid, organic cations, additive engineering, QDs, etc. Regarding B-site substitution, various metals have been attempted to partially substitute Pb^{2+} in organic perovskites, such as Sn^{2+}, Ge^{2+}, Bi^{3+}, Sb^{3+}, Zn^{2+}, Mn^{2+}, Ca^{2+}, Sr^{3+}, Ba^{2+}, Sm^{3+}, Eu^{3+}, etc. Although doping of these metals led to improved PCE and phase stability in different publications, universal doping metal remains to be explored based on theoretical and experimental techniques. Moreover, a deep investigation is needed to gain insights into the mechanisms of improved phase stability through the above metal doping. As for X-site substitution, the incorporation of Br is beneficial for stabilizing black phase but it also can enlarge bandgap accompanying the sacrifice of J_{sc}. Consequently, an appropriate amount of Br should be introduced into inorganic perovskites considering the balance between phase stability

© 2020 Wiley-VCH GmbH

and light-harvesting ability. In addition, the incorporation of Cl was demonstrated to be able to improve carrier lifetimes, grain size, and diffusion length of perovskite films whereas bandgap can be maintained because of the incorporation of an extremely small amount of Cl or thorough evaporation of Cl. For intermediate with hydroiodic acid, mechanisms for stabilizing black phase of $CsPbI_3$ by HI or $HPbI_3$ should be investigated further and deeply. With respect to organic cation strategy, large-sized organic cations (such as PTABr, PTACl, CHI, and PEAI), which were either incorporated into perovskite films or used to post-treat inorganic perovskite films, have been demonstrated to be very effective in stabilizing the black phase of inorganic perovskites. Synergistic engineering of bulk and surface of inorganic perovskite films should be implemented by incorporating large-sized organic ammonium salts to minimize bulk and surface nonradiative recombination losses and stabilize black phase. It is worth noting that DMAI has shown huge potentials in stabilizing the black phase of $CsPbI_3$ and improving its film quality. However, whether DMAI is incorporated into perovskite crystal lattice and the mechanism of the stabilizing phase of $CsPbI_3$ by DMAI remains to be investigated further. More effective organic ammonium salts should be designed and developed to further increase the PCE and phase stability. Some advancements have been obtained on additive and QD strategies but more attention should be paid to both strategies. In a word, as high PCE as 19.03% has been achieved for the device based on $CsPbI_3$ as absorber and Spiro-OMeTAD as HTM. However, the use of Spiro-OMeTAD as HTM leads to poor moisture and thermal stability of the corresponding devices, which hinders their further commercial application. Therefore, it is imperative to develop all-inorganic PSCs completely based on inorganic materials.

All-inorganic PSCs can be classified into normal and inverted all-inorganic PSCs. Normal all-inorganic PSCs can be further classified into normal all-inorganic PSCs containing HTMs and normal HTM-free all-inorganic PSCs. Regarding normal all-inorganic PSCs containing HTMs, the development of effective inorganic HTMs is key to achieve high efficiency and excellent stability. Up to now, several inorganic HTMs have been developed to fabricate normal all-inorganic PSCs containing HTMs, such as CuI, Cu_2ZnSnS_4 QDs, $CuInS_2$/ZnS QDs, $Cu(Cr,M)O_2$ NCs, Co_3O_4, MnS, PbS, PEI-CNT, N-CQDs, etc. From the perspective of energy band alignment, wide-bandgap CuI, $Cu(Cr,M)O_2$ NCs, Co_3O_4, and MnS seem to be more promising in the realization of high efficiency. As far as we know, the highest PCE of up to 13.21% was realized for normal all-inorganic PSCs based on CuI HTM, which is still much lower than 19.03% of PSCs based on Spiro-OMeTAD. Consequently, it is highly desirable to further enhance the PCE of normal all-inorganic PSCs through developing more effective inorganic HTMs. In addition, normal carbon-based HTM-free all-inorganic PSCs have captured significant attention in the past few years and enormous progresses have been made. To date, the highest PCE of up to 12.19% was obtained for carbon-based HTM-free all-inorganic PSCs. Nevertheless, a large energy barrier at the perovskite/carbon interface poses an immense challenge for hole extraction and collection. Therefore, the unexpected energy barrier should be removed via modulating perovskite/carbon interface. Considering the low cost, excellent stability, and easy large-scale production of CEs, carbon-based HTM-free all-inorganic PSCs are still very promising for final commercial applications. As for inverted all-inorganic PSCs, the development of effective inorganic ETMs plays a crucial role in achieving efficient and stable devices. To date, extremely limited inorganic HTMs have been developed to fabricate inverted all-inorganic PSCs, such as MoO_x, CeO_x, C-TiO_2, ZnO@C_{60} bilayer, etc. ZnO@C_{60} bilayer HTM engineering seems to be very effective and a high PCE of 16.10% was demonstrated for inverted all-inorganic PSCs based on ZnO@C_{60} bilayer HTM. However, the device stability is not very attractive in this work probably due to poor phase stability and unavoidable chemical reaction between perovskite and ZnO. Consequently, the phase stability of inorganic perovskites and chemical stability of ETMs should be considered simultaneously and modulated reasonably.

In view of the importance of interface in achieving efficient and stable all-inorganic PSCs, it is highly necessary to further increase the PCE and stability. Compared with the optimization of phase stability of inorganic perovskites and the development of inorganic CTMs, extremely limited work was reported on increasing device performance through interface engineering in all-inorganic PSCs. The high annealing temperature of inorganic perovskite films challenges modification of the perovskite/ETL interface for normal devices and perovskite/HTL interface for inverted devices through incorporating organic molecules. The development of inorganic interfacial modifiers is expected to be able to conquer this difficulty. It should be pointed that the multifunctional interfacial modifiers should be developed to simultaneously achieve multiple functions, such as defect passivation, energy band alignment modulation, interfacial reactions, ion migration suppression, etc. In a word, interface engineering should receive significant attention in the future research work to maximize the potentials of PCE and stability of all-inorganic PSCs through minimizing interfacial nonradiative recombination losses.

Although the PCEs of most of all-inorganic PSCs are in the range of 10–16%, currently, we believe that the PCE can be pushed up to a promising value exceeding 20% in the near future through systematic optimization (development of strategies for stabilizing black phase of inorganic perovskites, development of effective inorganic CTMs, and interface engineering).

Acknowledgements

This work was financially supported by equipment fund and seed fund (grant nos. 2019157209 and 201811159147), from the University Grant Council of the University of Hong Kong as well as the General Research Fund (grant nos. 17201819, 17200518, and 17204117) and Collaborative Research Fund (C5037-18G) from the Research Grants Council and ECF 64/2018 from Environment and Conservation Fund, Hong Kong Special Administrative Region, China, and research start-up fund from Chongqing University (grant no. 02100011044126), the Fundamental Research Funds for the Central Universities (grant no. 2020CDJQY-A028), and Henan Ed Era New Energy Science & technology Co., ltd (grant no. H20200282).

Conflict of Interest

The authors declare no conflict of interest.

© 2020 Wiley-VCH GmbH

Keywords

all-inorganic perovskite solar cells, inorganic electron transport materials, inorganic hole transport materials, interface engineering, phase stabilities

Received: July 24, 2020
Revised: September 8, 2020
Published online:

[1] A. Kojima, K. Teshima, Y. Shirai, T. Miyasaka, *J. Am. Chem. Soc.* **2009**, *131*, 6050.
[2] H. S. Kim, C. R. Lee, J. H. Im, K. B. Lee, T. Moehl, A. Marchioro, S. J. Moon, R. Humphry-Baker, J. H. Yum, J. E. Moser, *Sci. Rep.* **2012**, *2*, 591.
[3] Q. Jiang, Y. Zhao, X. Zhang, X. Yang, Y. Chen, Z. Chu, Q. Ye, X. Li, Z. Yin, J. You, *Nat. Photonics* **2019**, *13*, 460.
[4] E. H. Jung, N. J. Jeon, E. Y. Park, C. S. Moon, T. J. Shin, T.-Y. Yang, J. H. Noh, J. Seo, *Nature* **2019**, *567*, 511.
[5] H. Min, M. Kim, S.-U. Lee, H. Kim, G. Kim, K. Choi, J. H. Lee, S. I. Seok, *Science* **2019**, *366*, 749.
[6] M. Kim, G.-H. Kim, T. K. Lee, I. W. Choi, H. W. Choi, Y. Jo, Y. J. Yoon, J. W. Kim, J. Lee, D. Huh, *Joule* **2019**, *3*, 2179.
[7] L. Wang, H. Zhou, J. Hu, B. Huang, M. Sun, B. Dong, G. Zheng, Y. Huang, Y. Chen, L. Li, *Science* **2019**, *363*, 265.
[8] Y. Wang, T. Wu, J. Barbaud, W. Kong, D. Cui, H. Chen, X. Yang, L. Han, *Science* **2019**, *365*, 687.
[9] S. Yang, S. Chen, E. Mosconi, Y. Fang, X. Xiao, C. Wang, Y. Zhou, Z. Yu, J. Zhao, Y. Gao, *Science* **2019**, *365*, 473.
[10] Y. Hou, E. Aydin, M. De Bastiani, C. Xiao, F. H. Isikgor, D.-J. Xue, B. Chen, H. Chen, B. Bahrami, A. H. Chowdhury, A. Johnston, S.-W. Baek, Z. Huang, M. Wei, Y. Dong, J. Troughton, R. Jalmood, A. J. Mirabelli, T. G. Allen, E. Van Kerschaver, M. I. Saidaminov, D. Baran, Q. Qiao, K. Zhu, S. De Wolf, E. H. Sargent, *Science* **2020**, *367*, 1135.
[11] D. Kim, H. J. Jung, I. J. Park, B. W. Larson, S. P. Dunfield, C. Xiao, J. Kim, J. Tong, P. Boonmongkolras, S. G. Ji, F. Zhang, S. R. Pae, M. Kim, S. B. Kang, V. Dravid, J. J. Berry, J. Y. Kim, K. Zhu, D. H. Kim, B. Shin, *Science* **2020**, *368*, 155.
[12] Y. Wang, M. I. Dar, L. K. Ono, T. Zhang, M. Kan, Y. Li, L. Zhang, X. Wang, Y. Yang, X. Gao, *Science* **2019**, *365*, 591.
[13] M. A. Green, E. D. Dunlop, D. H. Levi, J. Hohl-Ebinger, M. Yoshita, A. W. Ho-Baillie, *Prog. Photovolt. Res. Appl.* **2019**, *27*, 565.
[14] W. Xiang, W. Tress, *Adv. Mater.* **2019**, *31*, 1902851.
[15] N. A. N. Ouedraogo, Y. C. Chen, Y. Y. Xiao, Q. Meng, C. B. Han, H. Yan, Y. Z. Zhang, *Nano Energy* **2020**, *67*, 20.
[16] E. J. Juarez-Perez, L. K. Ono, M. Maeda, Y. Jiang, Z. Hawash, Y. Qi, *J. Mater. Chem. A* **2018**, *6*, 9604.
[17] J.-W. Lee, D.-H. Kim, H.-S. Kim, S.-W. Seo, S. M. Cho, N.-G. Park, *Adv. Energy Mater.* **2015**, *5*, 1501310.
[18] C. Yi, J. Luo, S. Meloni, A. Boziki, N. Ashari-Astani, C. Graetzel, S. M. Zakeeruddin, U. Roethlisberger, M. Graetzel, *Energy Environ. Sci.* **2016**, *9*, 656.
[19] M. Saliba, T. Matsui, J.-Y. Seo, K. Domanski, J.-P. Correa-Baena, M. K. Nazeeruddin, S. M. Zakeeruddin, W. Tress, A. Abate, A. Hagfeldt, M. Gratzel, *Energy Environ. Sci.* **2016**, *9*, 1989.
[20] M. Saliba, T. Matsui, K. Domanski, J.-Y. Seo, A. Ummadisingu, S. M. Zakeeruddin, J.-P. Correa-Baena, W. R. Tress, A. Abate, A. Hagfeldt, M. Gratzel, *Science* **2016**, *354*, 206.
[21] M. B. Faheem, B. Khan, C. Feng, M. U. Farooq, F. Raziq, Y. Xiao, Y. Li, *ACS Energy Lett.* **2020**, *5*, 290.
[22] Y. Wang, X. Liu, T. Zhang, X. Wang, M. Kan, J. Shi, Y. Zhao, *Angew. Chem. Int. Ed.* **2019**, *58*, 16691.
[23] A. Swarnkar, A. R. Marshall, E. M. Sanehira, B. D. Chernomordik, D. T. Moore, J. A. Christians, T. Chakrabarti, J. M. Luther, *Science* **2016**, *354*, 92.
[24] E. M. Sanehira, A. R. Marshall, J. A. Christians, S. P. Harvey, P. N. Ciesielski, L. M. Wheeler, P. Schulz, L. Y. Lin, M. C. Beard, J. M. Luther, *Sci. Adv.* **2017**, *3*, eaao4204.
[25] T. Zhang, M. I. Dar, G. Li, F. Xu, N. Guo, M. Gratzel, Y. Zhao, *Sci. Adv.* **2017**, *3*, e1700841.
[26] Y. Li, J. Duan, H. Yuan, Y. Zhao, B. He, Q. Tang, *Sol. RRL* **2018**, *2*, 1800164.
[27] J. K. Nam, S. U. Chai, W. Cha, Y. J. Choi, W. Kim, M. S. Jung, J. Kwon, D. Kim, J. H. Park, *Nano Lett.* **2017**, *17*, 2028.
[28] J. Liang, P. Zhao, C. Wang, Y. Wang, Y. Hu, G. Zhu, L. Ma, J. Liu, Z. Jin, *J. Am. Chem. Soc.* **2017**, *139*, 14009.
[29] F. Yang, D. Hirotani, G. Kapil, M. A. Kamarudin, C. H. Ng, Y. Zhang, Q. Shen, S. Hayase, *Angew. Chem. Int. Ed.* **2018**, *57*, 12745.
[30] C. F. J. Lau, M. Zhang, X. Deng, J. Zheng, J. Bing, Q. Ma, J. Kim, L. Hu, M. A. Green, S. Huang, A. Ho-Baillie, *ACS Energy Lett.* **2017**, *2*, 2319.
[31] C. F. J. Lau, X. Deng, J. Zheng, J. Kim, Z. Zhang, M. Zhang, J. Bing, B. Wilkinson, L. Hu, R. Patterson, S. Huang, A. Ho-Baillie, *J. Mater. Chem. A* **2018**, *6*, 5580.
[32] Q. Wang, X. P. Zheng, Y. H. Deng, J. J. Zhao, Z. L. Chen, J. S. Huang, *Joule* **2017**, *1*, 371.
[33] Q. Ye, Y. Zhao, S. Mu, F. Ma, F. Gao, Z. Chu, Z. Yin, P. Gao, X. Zhang, J. You, *Adv. Mater.* **2019**, *31*, 1905143.
[34] Z. Qiu, N. Li, Z. Huang, Q. Chen, H. Zhou, *Small Methods* **2020**, *4*, 1900877.
[35] Y. Hu, F. Bai, X. Liu, Q. Ji, X. Miao, T. Qiu, S. Zhang, *ACS Energy Lett.* **2017**, *2*, 2219.
[36] Z.-J. Zhou, Y.-Q. Deng, P.-P. Zhang, D.-X. Kou, W.-H. Zhou, Y.-N. Meng, S.-J. Yuan, S.-X. Wu, *Sol. RRL* **2019**, *3*, 1800354.
[37] J. Duan, Y. Zhao, Y. Wang, X. Yang, Q. Tang, *Angew. Chem. Int. Ed.* **2019**, *58*, 16147.
[38] Y. Zhou, X. Zhang, X. Lu, X. Gao, J. Gao, L. Shui, S. Wu, J.-M. Liu, *Sol. RRL* **2019**, *3*, 1800315.
[39] X. Li, Y. Tan, H. Lai, S. Li, Y. Chen, S. Li, P. Xu, J. Yang, *ACS Appl. Mater. Interfaces* **2019**, *11*, 29746.
[40] X. Ding, M. Cai, X. Liu, Y. Ding, X. Liu, Y. Wu, T. Hayat, A. Alsaedi, S. Dai, *Chem. Select* **2019**, *4*, 13143.
[41] X. Liu, J. Li, Z. Liu, X. Tan, B. Sun, S. Xi, T. Shi, Z. Tang, G. Liao, *Electrochim. Acta* **2020**, *330*, 135266.
[42] J. Liang, X. Han, J.-H. Yang, B. Zhang, Q. Fang, J. Zhang, Q. Ai, M. M. Ogle, T. Terlier, A. A. Marti, J. Lou, *Adv. Mater.* **2019**, *31*, 1903448.
[43] C. Liu, M. Wu, Y. Wu, D. Wang, T. Zhang, *J. Power. Sources* **2020**, *447*, 227389.
[44] S. Gong, H. Li, Z. Chen, C. Shou, M. Huang, S. Yang, *ACS Appl. Mater. Interfaces* **2020**, *12*, 34882.
[45] C. Liu, W. Li, J. Chen, J. Fan, Y. Mai, R. E. I. Schropp, *Nano Energy* **2017**, *41*, 75.
[46] H. Rao, S. Ye, F. Gu, Z. Zhao, Z. Liu, Z. Bian, C. Huang, *Adv. Energy Mater.* **2018**, *8*, 1800758.
[47] C. Liu, W. Li, H. Li, H. Wang, C. Zhang, Y. Yang, X. Gao, Q. Xue, H.-L. Yip, J. Fan, R. E. I. Schropp, Y. Mai, *Adv. Energy Mater.* **2019**, *9*, 1803572.
[48] C. Liu, W. Li, C. Zhang, Y. Ma, J. Fan, Y. Mai, *J. Am. Chem. Soc.* **2018**, *140*, 3825.
[49] J. Wang, J. Zhang, Y. Zhou, H. Liu, Q. Xue, X. Li, C.-C. Chueh, H.-L. Yip, Z. Zhu, A. K. Y. Jen, *Nat. Commun.* **2020**, *11*, 177.
[50] J. Yang, Q. Zhang, J. Xu, H. Liu, R. Qin, H. Zhai, S. Chen, M. Yuan, *Nanomaterials* **2019**, *9*, 1666.
[51] S. Zhang, W. Chen, S. Wu, R. Chen, Y. Huang, Z. Yang, J. Li, L. Han, W. Chen, *J. Mater. Chem. A* **2019**, *7*, 18603.

© 2020 Wiley-VCH GmbH

[52] A. Marronnier, G. Roma, S. Boyer-Richard, L. Pedesseau, J.-M. Jancu, Y. Bonnassieux, C. Katan, C. C. Stoumpos, M. G. Kanatzidis, J. Even, *ACS Nano* **2018**, *12*, 3477.
[53] J. Chen, Y. Rong, A. Mei, Y. Xiong, T. Liu, Y. Sheng, P. Jiang, L. Hong, Y. Guan, X. Zhu, *Adv. Energy Mater.* **2016**, *6*, 1502009.
[54] J. Chen, N. G. Park, *Adv. Mater.* **2019**, *31*, 1803019.
[55] Q. Ye, Y. Zhao, S. Mu, P. Gao, X. Zhang, J. You, *Sci. China Chem.* **2019**, *62*, 810.
[56] N. Li, Z. Zhu, J. Li, A. K. Y. Jen, L. Wang, *Adv. Energy Mater.* **2018**, *8*, 1800525.
[57] J. Huang, D. Zhang, L. Ding, F. Zhang, *Adv. Mater. Interfaces* **2019**, *6*, 1900517.
[58] S. Xiang, W. Li, Y. Wei, J. Liu, H. Liu, L. Zhu, H. Chen, *Nanoscale* **2018**, *10*, 9996.
[59] H. R. Sun, J. Zhang, X. L. Gan, L. T. Yu, H. B. Yuan, M. H. Shang, C. J. Lu, D. G. Hou, Z. Y. Hu, Y. J. Zhu, L. Y. Han, *Adv. Energy Mater.* **2019**, *9*, 1900896.
[60] D. Bai, J. Zhang, Z. Jin, H. Bian, K. Wang, H. Wang, L. Liang, Q. Wang, S. F. Liu, *ACS Energy Lett.* **2018**, *3*, 970.
[61] J. Liang, Z. Liu, L. Qiu, Z. Hawash, L. Meng, Z. Wu, Y. Jiang, L. K. Ono, Y. Qi, *Adv. Energy Mater.* **2018**, *8*, 1800504.
[62] Y. Zhao, Y. Wang, J. Duan, X. Yang, Q. Tang, *J. Mater. Chem. A* **2019**, *7*, 6877.
[63] S. S. Mali, J. V. Patil, C. K. Hong, *Nano Lett.* **2019**, *19*, 6213.
[64] J. Duan, Y. Zhao, X. Yang, Y. Wang, B. He, Q. Tang, *Adv. Energy Mater.* **2018**, *8*, 1802346.
[65] S. Yang, H. Zhao, Y. Han, C. Duan, Z. Liu, S. Liu, *Small* **2019**, *15*, 1904387.
[66] W. Xiang, Z. Wang, D. J. Kubicki, W. Tress, J. Luo, D. Prochowicz, S. Akin, L. Emsley, J. Zhou, G. Dietler, M. Graetzel, A. Hagfeldt, *Joule* **2019**, *3*, 205.
[67] W. Chen, H. Chen, G. Xu, R. Xue, S. Wang, Y. Li, Y. Li, *Joule* **2019**, *3*, 191.
[68] J. Tian, Q. Xue, X. Tang, Y. Chen, N. Li, Z. Hu, T. Shi, X. Wang, F. Huang, C. J. Brabec, H.-L. Yip, Y. Cao, *Adv. Mater.* **2019**, *31*, 1901152.
[69] W. S. Subhani, K. Wang, M. Du, X. Wang, S. Liu, *Adv. Energy Mater.* **2019**, *9*, 1803785.
[70] Y. Zhao, J. Duan, H. Yuan, Y. Wang, X. Yang, B. He, Q. Tang, *Sol. RRL* **2019**, *3*, 1800284.
[71] J. Duan, Y. Wang, X. Yang, Q. Tang, *Angew. Chem. Int. Ed.* **2020**, *59*, 4391.
[72] G. Tong, T. Chen, H. Li, L. Qiu, Z. Liu, Y. Dang, W. Song, L. K. Ono, Y. Jiang, Y. Qi, *Nano Energy* **2019**, *65*, 104015.
[73] Y. Wang, T. Zhang, M. Kan, Y. Zhao, *J. Am. Chem. Soc.* **2018**, *140*, 12345.
[74] Y. Jiang, J. Yuan, Y. Ni, J. Yang, Y. Wang, T. Jiu, M. Yuan, J. Chen, *Joule* **2018**, *2*, 1356.
[75] Y. Zheng, X. Yang, R. Su, P. Wu, Q. Gong, R. Zhu, *Adv. Funct. Mater.* **2020**, 2000457.
[76] K. Wang, Z. Jin, L. Liang, H. Bian, D. Bai, H. Wang, J. Zhang, Q. Wang, S. Liu, *Nat. Commun.* **2018**, *9*, 4544.
[77] H. Meng, Z. Shao, L. Wang, Z. Li, R. Liu, Y. Fan, G. Cui, S. Pang, *ACS Energy Lett.* **2020**, *5*, 263.
[78] Z. Li, X. Liu, J. Xu, Y. Liao, H. Zhao, B. Zhang, S. F. Liu, J. Yao, *J. Phys. Chem. Lett.* **2019**, *10*, 4587.
[79] S. Oz, A. K. Jena, A. Kulkarni, K. Mouri, T. Yokoyama, I. Takei, F. Uenlue, S. Mathur, T. Miyasaka, *ACS Energy Lett.* **2020**, *5*, 1292.
[80] T. Wu, Y. Wang, Z. Dai, D. Cui, T. Wang, X. Meng, E. Bi, X. Yang, L. Han, *Adv. Mater.* **2019**, *31*, 1900605.
[81] J. Yuan, X. Ling, D. Yang, F. Li, S. Zhou, J. Shi, Y. Qian, J. Hu, Y. Sun, Y. Yang, X. Gao, S. Duhm, Q. Zhang, W. Ma, *Joule* **2018**, *2*, 2450.
[82] X. Ling, S. Zhou, J. Yuan, J. Shi, Y. Qian, B. W. Larson, Q. Zhao, C. Qin, F. Li, G. Shi, C. Stewart, J. Hu, X. Zhang, J. M. Luther, S. Duhm, W. Ma, *Adv. Energy Mater.* **2019**, *9*, 1900721.
[83] Y. Wang, J. Yuan, X. Zhang, X. Ling, B. W. Larson, Q. Zhao, Y. Yang, Y. Shi, J. M. Luther, W. Ma, *Adv. Mater.* **2020**, *32*, 2000449.
[84] T. Wang, F. Yan, *Chem. Asian J.* **2020**, *15*, 1524.
[85] L. Chen, L. Wan, X. Li, W. Zhang, S. Fu, Y. Wang, S. Li, H.-Q. Wang, W. Song, J. Fang, *Chem. Mater.* **2019**, *31*, 9032.
[86] R. E. Beal, D. J. Slotcavage, T. Leijtens, A. R. Bowring, R. A. Belisle, W. H. Nguyen, G. F. Burkhard, E. T. Hoke, M. D. McGehee, *J. Phys. Chem. Lett.* **2016**, *7*, 746.
[87] R. J. Sutton, G. E. Eperon, L. Miranda, E. S. Parrott, B. A. Kamino, J. B. Patel, M. T. Horantner, M. B. Johnston, A. A. Haghighirad, D. T. Moore, H. J. Snaith, *Adv. Energy Mater.* **2016**, *6*, 1502458.
[88] G. Yin, H. Zhao, H. Jiang, S. Yuan, T. Niu, K. Zhao, Z. Liu, S. Liu, *Adv. Funct. Mater.* **2018**, *28*, 1803269.
[89] K.-L. Wang, R. Wang, Z.-K. Wang, M. Li, Y. Zhang, H. Ma, L.-S. Liao, Y. Yang, *Nano Lett.* **2019**, *19*, 5176.
[90] W. Xu, F. He, M. Zhang, P. Nie, S. Zhang, C. Zhao, R. Luo, J. Li, X. Zhang, S. Zhao, W.-D. Li, F. Kang, C.-W. Nan, G. Wei, *ACS Energy Lett.* **2019**, *4*, 2491.
[91] S.-C. Liu, Z. Li, Y. Yang, X. Wang, Y.-X. Chen, D.-J. Xue, J.-S. Hu, *J. Am. Chem. Soc.* **2019**, *141*, 18075.
[92] B. Li, L. Fu, S. Li, H. Li, L. Pan, L. Wang, B. Chang, L. Yin, *J. Mater. Chem. A* **2019**, *7*, 20494.
[93] W. Zhu, Q. Zhang, D. Chen, Z. Zhang, Z. Lin, J. Chang, J. Zhang, C. Zhang, Y. Hao, *Adv. Energy Mater.* **2018**, *8*, 1802080.
[94] W. Zhu, W. Chai, Z. Zhang, D. Chen, J. Chang, S. Liu, J. Zhang, C. Zhang, Y. Hao, *Org. Electron.* **2019**, *74*, 103.
[95] Y. Guo, X. Yin, J. Liu, W. Que, *J. Mater. Chem. A* **2019**, *7*, 19008.
[96] Z. Xu, L. Wang, Q. Han, Y. Kamata, T. Ma, *ACS Appl. Mater. Interfaces* **2020**, *12*, 12867.
[97] S. Yang, L. Wang, L. Gao, J. Cao, Q. Han, F. Yu, Y. Kamata, C. Zhang, M. Fan, G. Wei, T. Ma, *ACS Appl. Mater. Interfaces* **2020**, *12*, 13931.
[98] P. Luo, Y. Zhou, S. Zhou, Y. Lu, C. Xu, W. Xia, L. Sun, *Chem. Eng. J.* **2018**, *343*, 146.
[99] K. C. Tang, P. You, F. Yan, *Sol. RRL* **2018**, *2*, 1800075.
[100] D. E. Starr, G. Sadoughi, E. Handick, R. G. Wilks, J. H. Alsmeier, L. Koehler, M. Gorgoi, H. J. Snaith, M. Baer, *Energy Environ. Sci.* **2015**, *8*, 1609.
[101] S. Colella, E. Mosconi, P. Fedeli, A. Listorti, F. Gazza, F. Orlandi, P. Ferro, T. Besagni, A. Rizzo, G. Calestani, G. Gigli, F. De Angelis, R. Mosca, *Chem. Mater.* **2013**, *25*, 4613.
[102] H. Yu, F. Wang, F. Xie, W. Li, J. Chen, N. Zhao, *Adv. Funct. Mater.* **2014**, *24*, 7102.
[103] Y. Tidhar, E. Edri, H. Weissman, D. Zohar, G. Hodes, D. Cahen, B. Rybtchinski, S. Kirmayer, *J. Am. Chem. Soc.* **2014**, *136*, 13249.
[104] H. Zhao, Y. Han, Z. Xu, C. Duan, S. Yang, S. Yuan, Z. Yang, Z. Liu, S. Liu, *Adv. Energy Mater.* **2019**, *9*, 1902279.
[105] G. E. Eperon, G. M. Paterno, R. J. Sutton, A. Zampetti, A. A. Haghighirad, F. Cacialli, H. J. Snaith, *J. Mater. Chem. A* **2015**, *3*, 19688.
[106] S. Xiang, Z. Fu, W. Li, Y. Wei, J. Liu, H. Liu, L. Zhu, R. Zhang, H. Chen, *ACS Energy Lett.* **2018**, *3*, 1824.
[107] P. Luo, W. Xia, S. Zhou, L. Sun, J. Cheng, C. Xu, Y. Lu, *J. Phys. Chem. Lett.* **2016**, *7*, 3603.
[108] B. Zhao, S.-F. Jin, S. Huang, N. Liu, J.-Y. Ma, D.-J. Xue, Q. Han, J. Ding, Q.-Q. Ge, Y. Feng, J.-S. Hu, *J. Am. Chem. Soc.* **2018**, *140*, 11716.
[109] W. Ke, I. Spanopoulos, C. C. Stoumpos, M. G. Kanatzidis, *Nat. Commun.* **2018**, *9*, 4785.
[110] F. Li, Y. Pei, F. Xiao, T. Zeng, Z. Yang, J. Xu, J. Sun, B. Peng, M. Liu, *Nanoscale* **2018**, *10*, 6318.

© 2020 Wiley-VCH GmbH

[111] J.-F. Liao, H.-S. Rao, B.-X. Chen, D.-B. Kuang, C.-Y. Su, *J. Mater. Chem. A* **2017**, *5*, 2066.
[112] W. Zhang, J. Xiong, J. Li, W. A. Daoud, *Sol. RRL* **2020**, *4*, 2000112.
[113] J. Ma, M. Qin, Y. Li, T. Zhang, J. Xu, G. Fang, X. Lu, *J. Mater. Chem. A* **2019**, *7*, 27640.
[114] Y. Wang, T. Zhang, M. Kan, Y. Li, T. Wang, Y. Zhao, *Joule* **2018**, *2*, 2065.
[115] H. Wang, H. Bian, Z. Jin, L. Liang, D. Bai, Q. Wang, S. F. Liu, *Sol. RRL* **2018**, *2*, 1800216.
[116] C. Liu, Y. Yang, O. A. Syzgantseva, Y. Ding, M. A. Syzgantseva, X. Zhang, A. M. Asiri, S. Dai, M. K. Nazeeruddin, *Adv. Mater.* **2020**, 2002632.
[117] H. Bian, H. Wang, Z. Li, F. Zhou, Y. Xu, H. Zhang, Q. Wang, L. Ding, S. Liu, Z. Jin, *Adv. Sci.* **2020**, *7*, 1902868.
[118] Z. Li, J. Xu, S. Zhou, B. Zhang, X. Liu, S. Dai, J. Yao, *ACS Appl. Mater. Interfaces* **2018**, *10*, 38183.
[119] P. Becker, J. A. Marquez, J. Just, A. Al-Ashouri, C. Hages, H. Hempel, M. Jost, S. Albrecht, R. Frahm, T. Unold, *Adv. Energy Mater.* **2019**, *9*, 1900555.
[120] Z. Shao, Z. Wang, Z. Li, Y. Fan, H. Meng, R. Liu, Y. Wang, A. Hagfeldt, G. Cui, S. Pang, *Angew. Chem. Int. Ed.* **2019**, *58*, 5587.
[121] C. Liu, Q. Zeng, Y. Zhao, Y. Yu, M. Yang, H. Gao, H. Wei, B. Yang, *Sol. RRL* **2020**, *4*, 2000102.
[122] Q. Wang, Z. Jin, D. Chen, D. Bai, H. Bian, J. Sun, G. Zhu, G. Wang, S. Liu, *Adv. Energy Mater.* **2018**, *8*, 1800007.
[123] C. F. J. Lau, X. Deng, Q. Ma, J. Zheng, J. S. Yun, M. A. Green, S. Huang, A. W. Y. Ho-Baillie, *ACS Energy Lett.* **2016**, *1*, 573.
[124] P. Teng, X. Han, J. Li, Y. Xu, L. Kang, Y. Wang, Y. Yang, T. Yu, *ACS Appl. Mater. Interfaces* **2018**, *10*, 9541.
[125] J. Duan, Y. Zhao, B. He, Q. Tang, *Angew. Chem. Int. Ed.* **2018**, *57*, 3787.
[126] H. Li, G. Tong, T. Chen, H. Zhu, G. Li, Y. Chang, L. Wang, Y. Jiang, *J. Mater. Chem. A* **2018**, *6*, 14255.
[127] M. Khazaee, K. Sardashti, C.-C. Chung, J.-P. Sun, H. Zhou, E. Bergmann, W. A. Dunlap-Shohl, Q. Han, I. G. Hill, J. Jones, D. C. Lupascu, D. B. Mitzi, *J. Mater. Chem. A* **2019**, *7*, 2095.
[128] L. A. Frolova, D. V. Anokhin, A. A. Piryazev, S. Y. Luchkin, N. N. Dremova, K. J. Stevenson, P. A. Troshin, *J. Phys. Chem. Lett.* **2017**, *8*, 67.
[129] C.-Y. Chen, H.-Y. Lin, K.-M. Chiang, W.-L. Tsai, Y.-C. Huang, C.-S. Tsao, H.-W. Lin, *Adv. Mater.* **2017**, *29*, 1605290.
[130] M. Shahiduzzaman, K. Yonezawa, K. Yamamoto, T. S. Ripolles, M. Karakawa, T. Kuwabara, K. Takahashi, S. Hayase, T. Taima, *ACS Omega* **2017**, *2*, 4464.
[131] J. Chen, Y. Xiong, Y. Rong, A. Mei, Y. Sheng, P. Jiang, Y. Hu, X. Li, H. Han, *Nano Energy* **2016**, *27*, 130.
[132] N. Ahn, D.-Y. Son, I.-H. Jang, S. M. Kang, M. Choi, N.-G. Park, *J. Am. Chem. Soc.* **2015**, *137*, 8696.
[133] H. Zai, D. Zhang, L. Li, C. Zhu, S. Ma, Y. Zhao, Z. Zhao, C. Chen, H. Zhou, Y. Li, Q. Chen, *J. Mater. Chem. A* **2018**, *6*, 23602.
[134] P. Wang, X. Zhang, Y. Zhou, Q. Jiang, Q. Ye, Z. Chu, X. Li, X. Yang, Z. Yin, J. You, *Nat. Commun.* **2018**, *9*, 2225.
[135] Z. Q. Lin, H. W. Qiao, Z. R. Zhou, Y. Hou, X.-L. Li, H. Yang, S. Yang, *J. Mater. Chem. A* **2020**, *8*, 17670.
[136] B. Zhang, W. Bi, Y. Wu, C. Chen, H. Li, Z. Song, Q. Dai, L. Xu, H. Song, *ACS Appl. Mater. Interfaces* **2019**, *11*, 33868.
[137] C. Dong, X. Han, Y. Zhao, J. Li, L. Chang, W. Zhao, *Sol. RRL* **2018**, *2*, 1800139.
[138] T. Zhang, F. Wang, H. Chen, L. Ji, Y. Wang, C. Li, M. B. Raschke, S. Li, *ACS Energy Lett.* **2020**, *5*, 1619.
[139] T. Moot, A. R. Marshall, L. M. Wheeler, S. N. Habisreutinger, T. H. Schloemer, C. C. Boyd, D. R. Dikova, G. F. Pach, A. Hazarika, M. D. McGehee, *Adv. Energy Mater.* **2020**, *10*, 1903365.
[140] X. Zhao, H.-S. Kim, J.-Y. Seo, N.-G. Park, *ACS Appl. Mater. Interfaces* **2017**, *9*, 7148.
[141] J. Chen, N.-G. Park, *J. Phys. Chem. C* **2018**, *122*, 14039.
[142] P. Nazari, F. Ansari, B. Abdollahi Nejand, V. Ahmadi, M. Payandeh, M. Salavati-Niasari, *J. Phys. Chem. C* **2017**, *121*, 21935.
[143] J. Ding, J. Duan, C. Guo, Q. Tang, *J. Mater. Chem. A* **2018**, *6*, 21999.
[144] J. Duan, T. Hu, Y. Zhao, B. He, Q. Tang, *Angew. Chem. Int. Ed.* **2018**, *57*, 5746.
[145] Y. Yang, H. Chen, C. Hu, S. Yang, *J. Mater. Chem. A* **2019**, *7*, 22005.
[146] Y. Zhao, J. Duan, Y. Wang, X. Yang, Q. Tang, *Nano Energy* **2020**, *67*, 104286.
[147] X. Chang, W. Li, L. Zhu, H. Liu, H. Geng, S. Xiang, J. Liu, H. Chen, *ACS Appl. Mater. Interfaces* **2016**, *8*, 33649.
[148] J. Liang, C. Wang, Y. Wang, Z. Xu, Z. Lu, Y. Ma, H. Zhu, Y. Hu, C. Xiao, X. Yi, *J. Am. Chem. Soc.* **2016**, *138*, 15829.
[149] D. Huang, P. Xie, Z. Pan, H. Rao, X. Zhong, *J. Mater. Chem. A* **2019**, *7*, 22420.
[150] G. Liao, Y. Zhao, J. Duan, H. Yuan, Y. Wang, X. Yang, B. He, Q. Tang, *Dalton Trans.* **2018**, *47*, 15283.
[151] F. Bu, B. He, Y. Ding, X. Li, X. Sun, J. Duan, Y. Zhao, H. Chen, Q. Tang, *Sol. Energy Mater. Sol. Cells* **2020**, *205*, 110267.
[152] I. Poli, J. Baker, J. McGettrick, F. De Rossi, S. Eslava, T. Watson, P. J. Cameron, *J. Mater. Chem. A* **2018**, *6*, 18677.
[153] M. Tang, B. He, D. Dou, Y. Liu, J. Duan, Y. Zhao, H. Chen, Q. Tang, *Chem. Eng. J.* **2019**, *375*, 121930.
[154] W. Zhu, Q. Zhang, C. Zhang, Z. Zhang, D. Chen, Z. Lin, J. Chang, J. Zhang, Y. Hao, *ACS Appl. Energy Mater.* **2018**, *1*, 4991.
[155] W. Zhu, W. Chai, D. Chen, H. Xi, D. Chen, J. Chang, J. Zhang, C. Zhang, Y. Hao, *ACS Appl. Mater. Interfaces* **2020**, *12*, 4549.
[156] W. Zhu, Z. Zhang, W. Chai, D. Chen, H. Xi, J. Chang, J. Zhang, C. Zhang, Y. Hao, *ACS Appl. Energy Mater.* **2019**, *2*, 5254.
[157] C. Wang, J. Zhang, L. Jiang, L. Gong, H. Xie, Y. Gao, H. He, Z. Fang, J. Fan, Z. Chao, *J. Alloys Compd.* **2020**, *817*, 152768.
[158] Z. Guo, S. Zhao, A. Liu, Y. Kamata, S. Teo, S. Yang, Z. Xu, S. Hayase, T. Ma, *ACS Appl. Mater. Interfaces* **2019**, *11*, 19994.
[159] A. Rajagopal, K. Yao, A. K. Y. Jen, *Adv. Mater.* **2018**, *30*, 1800455.
[160] C. Liu, Y. Yang, C. Zhang, S. Wu, L. Wei, F. Guo, G. M. Arumugam, J. Hu, X. Liu, J. Lin, *Adv. Mater.* **2020**, 1907361.
[161] L. Pan, C. Liu, H. Zhu, M. Wan, Y. Li, Y. Mai, *Sol. Energy* **2020**, *196*, 521.
[162] Z. Guo, S. Teo, Z. Xu, C. Zhang, Y. Kamata, S. Hayase, T. Ma, *J. Mater. Chem. A* **2019**, *7*, 1227.
[163] F. Deng, X. Li, X.-D. Lv, J. Zhou, Y. Chen, X. Sun, Y.-Z. Zheng, X. Tao, J.-F. Chen, *ACS Appl. Energy Mater.* **2019**, *3*, 401.
[164] G. Su, B. He, Z. Gong, Y. Ding, J. Duan, Y. Zhao, H. Chen, Q. Tang, *Electrochim. Acta* **2019**, *328*, 135102.

© 2020 Wiley-VCH GmbH



Jiangzhao Chen is a professor at College of Optoelectronic Engineering in Chongqing University. He received Ph.D. degree from Huazhong University of Science and Technology and worked as a postdoctoral researcher at Sungkyunkwan University and at the University of Hong Kong, respectively. His current research interests focus on perovskite solar cells.



Wallace C. H. Choy received his Ph.D. in electronic engineering from the University of Surrey, UK, in 1999. He is now a Professor in Department of EEE, HKU. His research interests cover organic/inorganic optoelectronic devices, plasmonic structures, metal oxides, and nanomaterial devices.

© 2020 Wiley-VCH GmbH